LUNAR INTERACTIONS

ABSTRACTS OF PAPERS PRESENTED AT THE CONFERENCE ON

INTERACTIONS OF THE INTERPLANETARY PLASMA

with the

MODERN AND ANCIENT MOON

ORGANIZED BY THE
LUNAR SCIENCE INSTITUTE
AND THE
SPACE PHYSICS DEPARTMENT
RICE UNIVERSITY
sponsored by the
NATIONAL AERONAUTICS
AND
SPACE ADMINISTRATION
AND THE
NATIONAL SCIENCE FOUNDATION

Edited by

DAVID R. CRISWELL

and

JOHN W. FREEMAN

Conference held at

George Williams College

Lake Geneva Campus

Williams Bay, Wisconsin

30 September - 4 October 1974

Compiled by and available

from

The Lunar Science Institute
3303 Nasa Road 1
Houston, Texas 77058

PREFACE

The field of lunar science has essentially completed a period of exponential growth promoted by the national efforts of the 1960's to land on the moon. As normally happens in a diverse scientific community, the interpretations of specialized lunar data have reflected the precepts in the various specialized fields. Constant promotion of the broadest overviews between these diverse fields is appropriate to identify processes or phenomenon recognized in one avenue of investigation which may have great importance in explaining the data of other specialities.

This Conference is directed toward reviewing the active mechanisms relating the moon to its environment and to exploring the linkage between these mechanisms and their records in the lunar sample and geophysical data. Broad topics to be considered include:

- *Observations and theories of the large scale plasma (solar wind and magnetospheric) interactions with the moon and non-magnetic planets.*
- *Ancient and present day lunar surface magnetic and electric fields - their production and effects.*
- *Dynamics and evolution of the lunar atmosphere.*
- *Evolution of the solar plasma: astrophysical expectation - astronomical observations.*
- *Lunar record of solar radiations.*
- *Non-meteoritic and meteoritic disturbance and transport of lunar surface materials.*
- *Future lunar exploration.*

Guided by this philosophy this Conference brings together not only scientists who have been directly involved in various aspects of lunar geophysics and sample analysis but also specialists in plasma physics, astrophysics, astronomy, and material science who provide new views on the many interdisciplinary aspects of current studies of the moon. The Conference format is planned to be informal, with ample time for questions and discussions. This abstracts volume is conceived to provide a working document during the Conference and a source for future reference.

Sincere appreciation is extended to the members of the advisory panel, Dr. R. Vondrak - Stanford Research Institute, and the staff members of the Lunar Science Institute - Mrs. J. Shack, L. Mager, E. Gutierrez and C. Watkins - who participated in the organization of the Conference and this abstracts volume.

ADVISORY PANEL

Professor J. Geiss
University of Bern

Dr. R. R. Hodges
University of Texas at Dallas

Dr. F. Hörz
NASA Johnson Space Center

Dr. R. Manka
National Science Foundation

Dr. K. Papadopoulos
Naval Research Laboratory

Dr. J. A. Philpotts
NASA Goddard Space Flight Center

Dr. C. T. Russell
University of California-Los Angeles

Professor R. M. Walker
Washington University

SPONSORS

Foreign and domestic travel funds and organizational expenses were provided by the National Science Foundation through grant number DES 75-01266 to the Space Physics Department of Rice University and by the National Aeronautics and Space Administration through contract number NSR 09-051-001 to the Lunar Science Institute.

John W. Freeman, Jr.
Department of Space Physics
and Astronomy
Rice University

David R. Criswell
Lunar Science Institute

TEST CASES

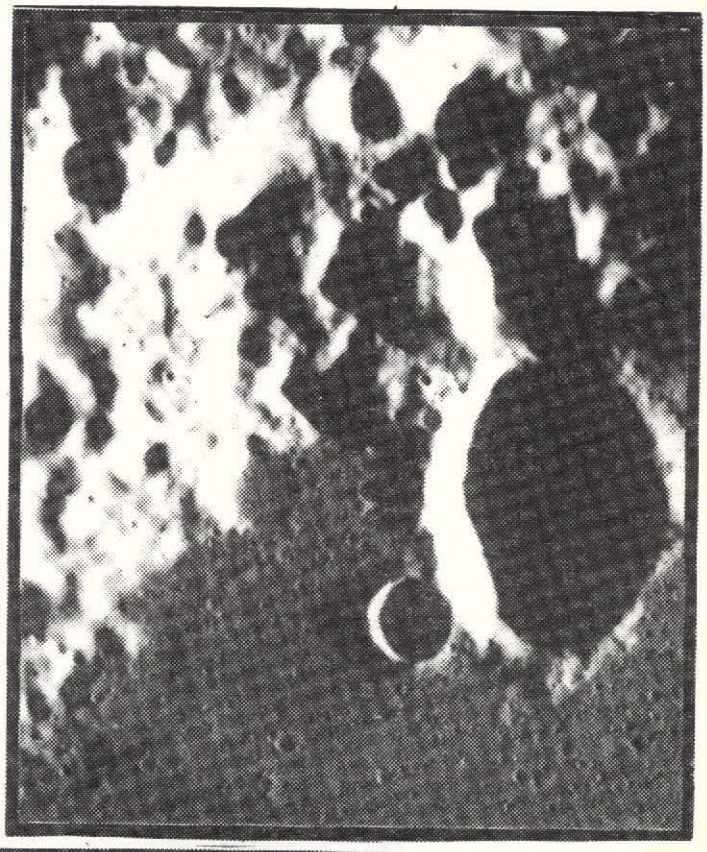

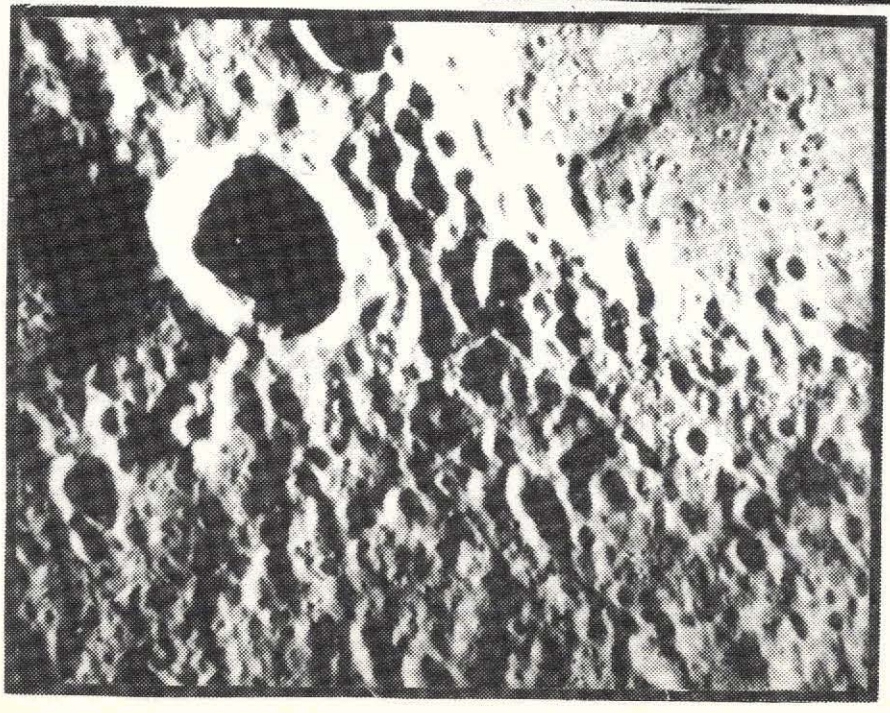

TABLE OF CONTENTS

This publication is Lunar Science Institute Contribution number 195.

THE LUNAR IONOSPHERE, Richard R. Vondrak* and John W. Freeman, Department of Space Physics and Astronomy, Rice University, Houston, Texas, 77001 (*now at Stanford Research Institute, Menlo Park, California 94025).

Extensive investigations of the lunar plasma environment made during the Apollo program have shown that, like the Earth, the moon is surrounded by a region of ionized plasma. However, unlike the terrestrial ionosphere, the lunar ionosphere is directly coupled to the solar wind by the interplanetary electric field. As a result the lunar atmospheric ion fluxes are both directional and variable and the ions have a non-thermal energy distribution. Collisions within the ionosphere are unimportant and interactions with the lunar surface control the ionospheric chemistry. In addition to this plasma of lunar origin, the region surrounding the moon is permeated by the interplanetary and magnetospheric plasmas.

The lowest part of the lunar ionosphere consists of a thin, dense sheath surrounding the moon as a result of the electric potential of the lunar surface. Measurements by SIDE (1) and CPLEE (2) have demonstrated that the surface potential is positive on the dayside. There the sheath consists of a photoelectron layer with an electron density at the surface of about $10^4/cm^3$ and an altitude extent of about 100 meters (2). Near the terminators and on the nightside the lunar surface potential becomes negative (1,3,4).

The most extensive part of the lunar ionosphere consists of ions produced from the lunar atmosphere. The two sources of the gases in the lunar atmosphere are material released or weathered from the lunar surface and the solar wind. Solar wind ions impact the lunar surface, are thermalized and perhaps chemically altered there, and then re-emitted as neutral atoms or molecules which travel along collision-free ballistic trajectories between impacts with the surface. The neutral atmospheric gases are ionized by the solar ultraviolet and corpuscular radiation in a time of typically 10^6-10^7 sec. These ions are then accelerated by the interplanetary electric field E (typically 1-3 mV/m) and are driven either into space or into the lunar surface. Their initial altitude distribution is exponential according to the neutral gas scale height H (20-100 km for most gases) and have a residence time before impacting the surface of only a few seconds. The resulting energy distribution is strongly non-thermal and the differential energy flux has generally an exponential distribution with a folding energy equal to EH (typically 20-300 eV). The production rate of these atmospheric ions is proportional to the product of neutral number density and ionization rate. Consequently, the density and flux of the atmospheric ions vary, being directly responsive to changes in the solar wind flux and transient outgassing from the lunar surface.

THE LUNAR IONOSPHERE

Vondrak, R. R. and Freeman, J. W.

In addition to the ionospheric plasma of lunar origin (the photoelectron layer and lunar atmospheric ions), the moon is exposed to plasma of extralunar origin (the solar wind, magnetospheric plasma, and cosmic rays). Because the moon lacks shielding by either a strong magnetic field or dense atmosphere, these extralunar plasmas penetrate directly to the surface where they have been regularly observed by SIDE, CPLEE, and the SWS.

The dynamics of the lunar ionosphere are important because ionization and subsequent removal by the interplanetary electric field is the principal loss mechanism for most atmospheric gases. Thus, observations of lunar atmospheric ions can be used to compute the atmospheric loss rate and to set constraints on the identification of the sources of the lunar atmosphere (5). A portion of the atmospheric ions which are driven into the lunar surface have energy sufficient for implantation and are evidently the source of the excess Ar^{40} found in the lunar samples (6). Observations at the lunar surface of ions streaming from an impact-generated gas cloud have provided information about the interaction between the solar wind and neutral gases (7). Finally, observations and study of the lunar ionosphere provide valuable insight into the mechanisms presumably operating when the solar wind interacts with the exospheres of the other planets which lack strong magnetic fields.

REFERENCES

(1) Fenner, M. A., Freeman, J. W., and Hills, H. K. (1973) The electric potential of the lunar surface. Proc. Fourth Lunar Sci. Conf., Geochim. Cosmochim. Acta, Suppl. 4, Vol. 3, p. 2287, Pergamon.

(2) Reasoner, D. L., and Burke, W. J. (1972) Direct observation of the lunar photoelectron layer. Proc. Third Lunar Sci. Conf., Geochim. Cosmochim. Acta, Suppl. 4, Vol. 3, p. 2639, MIT Press.

(3) Lindeman, R. A. (1973) Observation of ions from the lunar atmosphere. Ph.D. thesis, Rice University, Houston, Texas.

(4) Manka, R. H. (1973) Plasma and potential at the lunar surface. Photon and Particle Interactions with Surfaces in Space, R. Grard (ed.), p. 347, D. Reidel.

(5) Vondrak, R. R., Freeman, J. W., and Lindeman, R. A. (1974) Measurements of lunar atmospheric loss rate. Proc. Fifth Lunar Sci. Conf., Geochim. Cosmochim. Acta, Suppl. 4, Vol. 3, in press, Pergamon.

(6) Manka, R. H., and Michel, F. C. (1972) Lunar atmosphere as a source of lunar surface elements. Proc. Second Lunar Sci. Conf., Geochim. Cosmochim. Acta, Suppl. 2, Vol. 2, p. 1717, MIT Press.

(7) Lindeman, R. A., Vondrak, R. R., Freeman, J. W., and Snyder, C. W. (1974) The interaction between an impact-produced neutral gas cloud and the solar wind at the lunar surface, J. Geophys. Res., 79, 2287.

ULTRA-HIGH ENERGY INTERACTIONS IN LUNAR ROCKS

L.G.van Loon ,P.B.534 , Dordrecht , The Netherlands.

A study has been made in lunar rock 12021 samples of ultra-high energy interactions caused by cosmic rays of about 10^{13} - 10^{16} eV energy . When cosmic rays at this energy interact to cause cascades of secondary and tertiary particles (mainly mesons and leptons) , the cascade densities produced within the first few interaction lengths of the primary interaction result in ionization effects which are greater than ionization effects caused by heavy nuclei (1) . At lower energies than 10^{13} to 10^{16} eV , etching of rock samples is necessary to make visible nuclear interactions . However , as illustrated in fig. 1 , at 10^{16} eV (10^4 Tev) the cascades from interactions are already visible on fracture planes in the samples without the necessity of etching . With optical or electron microscopes these marks are easily visible . These effects are determined in publication (2) , and fig.2 illustrates the ionization effects expected from different causes : nuclei , electromagnetic cascades or meson cascades in solid matter such as rock .

In general , these marks are not seen in meteorites , because when meteorites heat up falling in the earth's atmosphere the interactions anneal out at temperatures above about 1000^0 K (1) . Therefore lunar surface rocks (10-20 cmin size) lying under no atmosphere are an ideal medium to study the effects of such cosmic ray interactions . Moreover,by analysing the surface densities of the cascades on the rock faces an idea can be formed of how the cosmic ray flux has varied in past geological or cosmic time . For ultra-high energy cosmic rays sofar no major modulation has been found . The cascade-section themselves have given some interesting conclusions about the nature of the primary cosmic ray particles at 10^4 Tev (3).

(1) Lett.Nuov.Cim. Vol. 2 , No.23 (1971) , p.1179 .
(2) Nuov.Cim. B Vol. 14 ,No.2 (1973) , p.267 .
(3) Bul.Am.Phys.Soc. Ser.11 , Vol.17 , No.4 , p.525 (1972)

ULTRA-HIGH ENERGY INTERACTIONS

L.G.van Loon

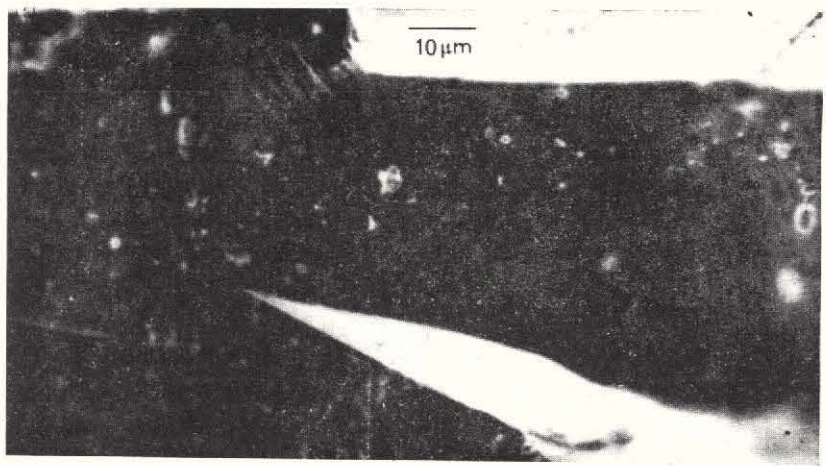

Fig. 1. – Photomicrograph of ultra-high-energy events in lunar minerals on a fracture plane.

Fig.1

Courtesy of *NUOVA CIMENTO*, V. *14B*, No. 2, p. 267, 1973.

ULTRA-HIGH ENERGY INTERACTIONS

L.G.van Loon

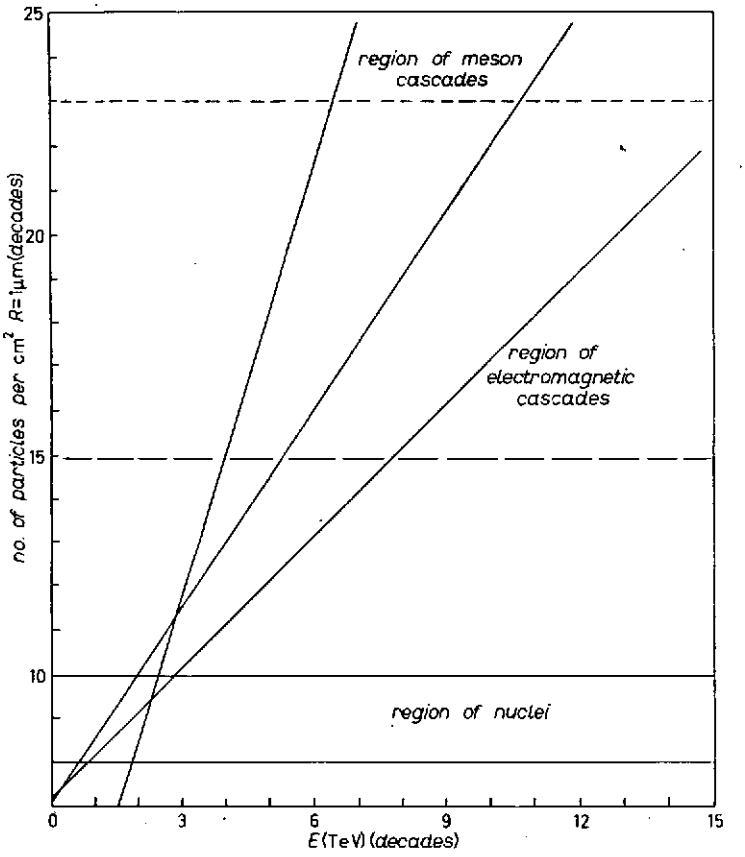

Fig. 5. – Particle density in meson cascades between 10 TeV and 10^8 TeV for a 1 μm radius. ——— surface area (pits), 10^{15} atoms/cm²; — — — bulk volume (holes), 10^{23} atoms/cm².

Fig.2

Courtesy of *NUOVA CIMENTO*, V. *14B*, No. 2, p. 267, 1973.

GEOCHEMICAL EVOLUTION OF THE MOON

S.R. Taylor, Australian National University and Lunar Science Institute.

It is assumed that the Moon accreted from refractory material from which the volatile elements had already been depleted. The accretion was homogeneous since there is (a) a good correlation between volatile/involatile element ratios in both highland and maria samples, and (b) the element distribution in crustal rocks is not governed by volatility differences.

The overall composition of the highland crust can be derived from the orbital Al/Si and Th data and the observed interelemental relationships. The highland REE abundances have a positive Eu anomaly. If the Moon has the same relative pattern as chondrites, the interior has a negative Eu anomaly, with a pattern resembling those of maria basalts, (Fig. 1). The abundances of the refractory trace elements, are about five times those in Type 1 carbonaceous chondrites. In order to account for the high near-surface element abundances, very efficient large scale element fractionation must occur, implying melting of most or all of the Moon.

The following geochemical model is proposed. The center of the Moon (below 1000 km) is primitive unfractionated material, now partially molten due to trapped K, U and Th.

Following accretional melting, the first silicate phase to separate was Mg-rich olivine. As crystallization proceeded, orthopyroxene precipitated. In the low pressure (<50 kbar) environment, most cations except Mg, Fe, Ni, Co and Cr^{2+} were excluded from the olivine and orthopyroxene lattice sites, and migrated upwards. A frozen crust quickly developed, although continually broken up by the declining meteorite bombardment. This frozen surface layer, analogous to a chilled margin retained high concentrations of Mg, Cr etc. in near surface regions. These elements are not derived from chondritic meteorites, which would have contributed high Ni, Ir etc. Because of the refractory nature of the total lunar composition, a Ca-Al rich residuum develops. Increasing crystallization at depth leads to a concentration of these elements, trapped under the frozen surface layer. When the concentration of Al reaches 12-17% Al_2O_3, An-rich plagioclase precipitates, and concentrates beneath the frozen surface, whereas the Mg-Fe phases sink. The Ca-Al rich region incorporates Sr^{2+} and Eu^{2+}.

As crystallization proceeds in both top (crustal Ca-Al) and bottom (mantle Fe-Mg) regions, additional fractionation changes the Mg/Fe ratio, and produces zones of Fe-Ti oxide accumulation. Those elements unable to enter the plagioclase above or the Mg-Fe sites below are trapped between. In this zone, all the

GEOCHEMICAL EVOLUTION OF THE MOON

Taylor, S.R.

remaining elements concentrate. These include K, Ba, Rb, Cs, REE, Th, U, Zr, Nb. Thus following the primordial fractionation, a chemically zoned Moon is produced (Fig. 2).

The crustal zonation established at about 4.5 aeons was changed very quickly. The declining stages of the meteoritic bombardment pulverized the chilled zone and larger impacts mixed in the underlying anorthosite. The high concentration of heat-producing elements K, U and Th (and Zr, Hf, REE etc.) beneath the plagioclase zone provide the high element abundances for the Fra Mauro or KREEP basalts. Possibly this zone did not solidify but the liquids invaded the crust, where impact mixing produced the parent material for the anorthositic gabbro (highland basalt) and the Fra Mauro basalts. This stage continued to 3.9 aeons.

Partial melting next occurred in deeper layers and a succession of maria basalts were erupted. The first of these were the aluminous basalts from shallow depths beneath the KREEP source layer. These overlapped with the later stages of the bombardment, and predate the Imbrium collision in part. Next (3.8 - 3.6 aeons), the Ti-rich Apollo 11 and 17 basalts were erupted from a zone where Fe-Ti oxides accumulated. Finally (3.4 - 3.2 aeons) the Apollo 12 and 15 quartz and olivine normative basalts were extruded.

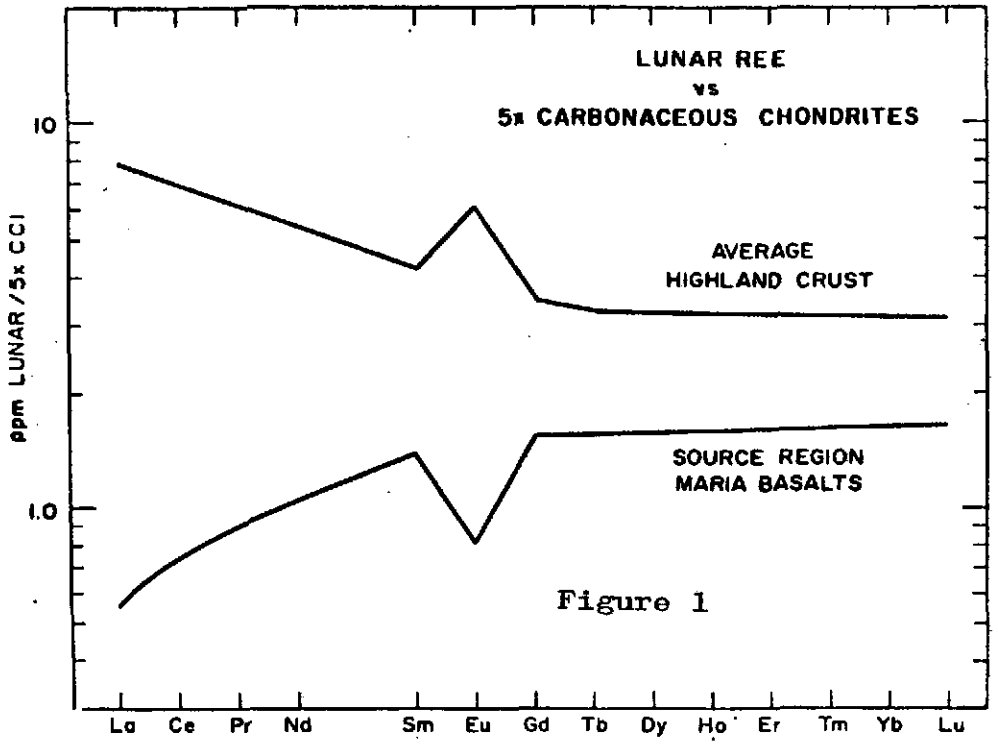

Figure 1

GEOCHEMICAL EVOLUTION OF THE MOON

Taylor, S.R.

Figure 2

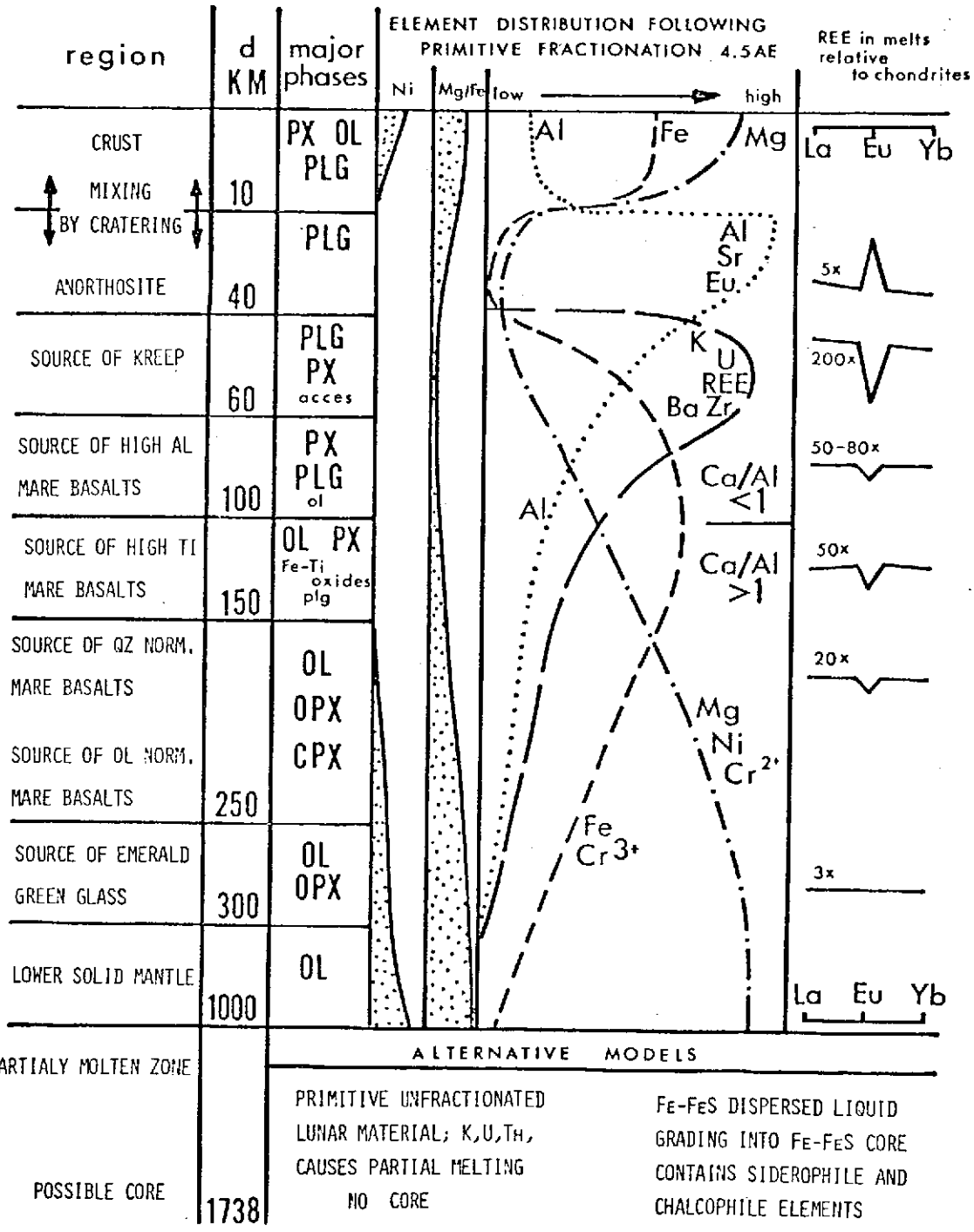

Figs. 1 and 2 Courtesy *Pergamon Press*, Proc. Fifth Lunar Sci. Conf., Vol. 2, p. 1287, 1974.

THEORY OF THE SOLAR WIND INTERACTION WITH THE MOON.
F. C. Michel, Rice U., Houston, Texas. 77001.

The historical development of theoretical models for the interaction of the streaming interplanetary medium with the solid body of the moon is reviewed. The first works date from around early 1960 and are traced to the present. The view that the moon acts mainly to absorb plasma from the flow (rather than present an obstacle to the flow) seems to best describe the data. Moreover, penetration of the flow to the lunar surface is consistent with observed effects on lunar ionospheric particles. Several phenomena remain to be resolved, such as the source of upstream disturbances and the existence of a trailing shock wave.

AMINO ACID PRECURSORS INDIGENOUS TO LUNAR SAMPLES: ACCUMULATED ANALYSES AND EVALUATIONS OF POSSIBLE CONTAMINATIONS.
S. W. Fox, K. Harada, Inst. for Molecular & Cellular Evolution, University of Miami, Coral Gables, FL 33134; and P. E. Hare, Geophysical Laboratory, Carnegie Institution, Washington, D.C. 20008.

The specific question of the presence of amino acids in lunar samples has been examined chemically, primarily through application of the specific amino acid reagent, ninhydrin. Other methods, such as vapor phase, chromatography of volatile derivatives or mass spectrometry, fail either to distinguish from other compounds, or to be sufficiently sensitive for amino acids at the levels that have been found in lunar samples. A profile of five or six proteinous amino acids has been consistently obtained for samples from twelve collections from the six Apollo missions 11 through 17. These results have been obtained mainly, and in some cases solely, by hydrolysis of hot aqueous extracts of the samples. The proportions of total amino acids thus obtained is in the range of 7 to 45 ng/g of sample. The accumulated results are presented in Table I.

Experiments designed to isolate the obligatory aspects of successful analyses for lunar amino acids have identified: extraction by hot water rather than cold, hydrolysis of the aqueous extract instead of direct hydrolysis of the sample, assay by the specific ninhydrin reagent, use of a sufficiently sensitive amino acid analyzer, and numerous precautions to minimize contamination in handling and in reagents.

The values found have tended to be 30-200 times as large as those found from blanks carried through the entire analysis. The possibility of contamination by astronauts or analysts has been examined. Evidence against this possibility has included the regularity of the results and the absence of occasional "spiking," which is characteristic of analyses of contaminated samples. The most conclusive evidence has been the extremely small contribution from blanks, the fact that the profiles closely resemble chemically synthetic products but not those of biotic products, and the fact that some unhydrolyzed samples exhibit no free amino acids at all whereas human fingerprints reveal liberal proportions of 17-19 types of amino acid prior to hydrolysis. The evidence thus does not support the hypothesis that a significant fraction of the amino acids found in our analyses result from human contamination.

The hypothesis that the amino acid precursors are products of the oxidation of jet fuel has been examined by obtaining and analyzing samples proximal to, and distal from, the descent engine on Apollo 15 and 17 (15012 and 72501 at a distance and

AMINO ACID PRECURSORS

Fox, S. W. et al.

15013 and 70011 near to the LM). The values found for the proximal samples are within the range of all samples analyzed but, even so, relatively small amounts of free amino acids may accumulate at the descent engine. For Apollo 15, the distal sample was found to have 7 ng/g of amino acids after hydrolysis of precursors whereas that for Apollo 17 (6.5 km) has 10 ng/g. On the basis of conservative assumptions, the total amount of amino acid precursor calculated to exist in a disc 6.5 km in radius is several orders of magnitude larger than can be accounted for on the basis of the amount of fuel used and conversion values determined, even assuming none of the fuel nor its oxidation products escaped to space during the descent. Accordingly, the hypothesis that the analytical results are explained to a significant degree by human andor chemical contamination is not supported by the evidence.

The significance of the results can be examined in a context of comparative cosmochemistry inasmuch as several meteorites (Murchison, Murray, Allende) have been analyzed by the procedure developed earlier for Apollo 11. The ratios of total amino acids/C content of the samples are comparable for the two extraterrestrial sources. The relative ratios of four or five proteinous amino acids are similar for the two sources and for the samples within either group. These analytical results resemble closely the products of chemical syntheses of amino acids, but not of organisms.

A principal significance of such results is the generalization that the common groundplan of terrestrial organisms emerged from a highly unified cosmochemical carbon chemistry. Another significance is that the pathway of molecular evolution on the Moon was arrested due to lack of water at the stage preceding hydrolysis of the amino acid precursors. The similar analytical results from various lunar samples suggest especially that the amino acid precursors result from implantation of simple molecular species of the interplanetary plasma on the preformed Moon. If this be correct, the lunar analyses for amino acids hold promise in defining and testing concepts of interaction of the Moon with that plasma.

Table I

Analyses of Hydrolyzates of Hot Aqueous Extracts of Lunar Samples
(molar ratios)

Sample	Glycine	Alanine	Glutamic acid	Aspartic acid	Serine	Threonine	Others
10086	50	25	9	5	9	2	0
12033	49	16	27	1	1	1	5
14003	62	20	12	2	4	1	0
14163	47	26	20	2	6	1	0
14240	63	15	6	11	4	0	0
14298	57	7	13	7	10	2	4
15012	61	6	16	6	6	2	3
15013	73	8	3	2	7	2	4
66041	56	6	19	5	8	1	5
72501	70	11	7	7	3	1	0
70011	83	12	0	3	1	0	1

All calculations exclude ammonia and basic amino acids.

LUNAR-SURFACE SOLAR-WIND OBSERVATIONS AT THE APOLLO-12 AND -15 SITES, by D. R. Clay, B. E. Goldstein, M. M. Neugebauer, and C. W. Snyder

Data from Solar Wind Spectrometers at the Apollo-12 and Apollo-15 sites are available for an eleven month simultaneous operation period. Velocity measurements at the Apollo-15 site (6γ local magnetic field) show no substantial differences from simultaneous Vela-3 and -5 measurements in free space. The deviation of the average flow direction from radial flow for solar wind data is at most about 1.5°, and the expected pattern of deflected flow inside the magnetosheath is observed. Previous work has shown that electron observations at Apollo 15 are typical, with certain exceptions, of results expected in the solar wind. Thus, the moon exerts no noticeable influence upon the proton flux observed at the Apollo-15 site.

Plasma data at the Apollo-12 site (38γ local magnetic field) is compared to Apollo-15 data to determine the nature of the interaction at the Apollo-12 site. For the limited periods, primarily during the early lunar afternoon (dawn magnetosheath) when 3-cup angular determinations at both sites are possible, the Apollo-12 plasma had a southward deflection 0° to 10° greater than the Apollo-15 value. Expected deflections during early lunar afternoon due simply to a uniform magnetic field would, however, be small, and cannot account for the pattern of the observations.

To investigate the interaction as a function of plasma direction, twelve orbit averages of hourly averages of plasma velocity, thermal speed, density and flux are computed as a function of the lunar longitude of the solar direction. The plasma velocity at the Apollo-12 site is generally lower than at Apollo 15. The velocity difference increases with changing solar wind direction, averaging 14 km/sec in the lunar morning (dusk magnetosheath), 45 km/sec in the afternoon magnetosheath, and 52 km/sec in the afternoon solar wind. Thermal speeds at the Apollo-12 site are consistently higher. Proton density is 33% lower at Apollo 12 during lunar morning, 5% lower in the afternoon magnetosheath, and 34% higher in the afternoon solar wind.

The interaction also depends upon the solar wind dynamic pressure computed from the velocity component normal to the surface at the Apollo-12 site. At low dynamic pressures the density ratios are greater than average; e.g., the Apollo-12 density is at times only 50% of the Apollo-15 density during lunar morning. At high dynamic pressures, on the other hand, the density ratios approach unity. Velocity differences also decrease with increasing dynamic pressure for morning and afternoon magnetosheath data, but the deceleration for afternoon solar wind data is approximately independent of dynamic pressure.

In general, considerably more fluctuations are observed at the Apollo-12 site than at the Apollo-15 site. Thermal speeds are higher, estimates of alpha particle denisty fluctuate unreasonably, and fits to the Maxwell-Boltzmann model are poorer. Power spectra of plasma velocity show that for frequencies greater than 2×10^{-3} Hz the power at the Apollo-12 site is typically a factor of 2 to 5 times greater than at the Apollo-15 site, with extreme limits of from 1 to 10. At lower frequencies the power at Apollo 12 is from 1 to 2 times greater than at Apollo 15.

LUNAR-SURFACE SOLAR-WIND

Clay, D.R. et al.

These results, and non-thermal 80 to 120 eV electrons observed at the Apollo-12 site, imply a complex interaction involving electric and magnetic fields. Models analogous to the magnetopause are appropriate with the additional consideration that surface charging may greatly alter the interaction. The most likely possibility is a small scale size magnetic field (5km., about a plasma wavelength) that prevents the full magnitude of effects that might be expected for a 38γ magnetic field.

Plasma turbulence, increases and decreases of plasma flux, and deceleration and deflection of the plasma are observed, suggesting that local lunar magnetic fields can cause lunar limb compression waves. The greater plasma density ratio perturbations observed for low solar wind dynamic pressures suggest the more frequent occurence of lunar limb compression waves for low solar-wind dynamic pressures.

SHEATH-LIMITED UNIPOLAR INDUCTION IN THE SOLAR WIND;
Leonard J. Srnka, The Lunar Science Institute, Houston, Texas, 77058.

The collection of charged particles by electrodes in plasmas is controlled by the current-voltage characteristics of the plasma sheath which forms at the electrode surface[1]. This principle is applied to the steady-state electromagnetic interaction of the solar wind with moon-like bodies, or "solid-body" interactions. In some cases the unipolar dynamo response[2,3] of an electrically conducting body in the solar wind motional electric field can be controlled by sheath effects. This occurs for highly conducting bodies when the body radius R is less than a critical value R_C, with the result that no induced bow shock wave can form[4].

The moon and Mercury have $R/R_C \gg 1$, so that sheath effects do not limit their unipolar responses. The asteroids are found to be either too cold or too small to maintain steady-state induced magnetospheres. The Martian satellites, the irregular Jovian satellites, and the outer satellites of Saturn also have $R/R_C \ll 1$. No bow shock waves should be generated by these bodies, unless they are highly magnetized or have large magnetic permeabilities.

Unipolar induction heating of meteorite parent bodies in a primordial enhanced solar wind[5] should not be inhibited by sheath effects, provided $R \geq 50$ meters. Unipolar heating in the ancient moon[6] is therefore also favored, provided the surface temperature was maintained at 300°C or more by a circumstellar obscuration, eddy current (TE mode) heating in the crust[7], or other mechanisms. Mercury may likewise have had an early electrical heating episode in its development.

References

1. Langmuir, I.: 1923, Gen. Electric Rev., 26, 731.
2. Sonett, C. P. and Colburn, D. S.: 1967, Nature, 216, 340.
3. Sonett, C. P. and Colburn, D. S.: 1968, Phys. Earth Planet. Interiors, 1, 326.
4. Srnka, L. J.: 1973, Ph.D. thesis, Univ. Newcastle, England.
5. Sonett, C. P., Colburn, D. S., Schwartz, K. and Keil, K.: 1970, Astrophys. Space Sci., 7, 446.

6. Sonett, C. P., Colburn, D. S. and Schwartz, K.: 1968, Nature, 219, 924.
7. Sonett, C. P., Colburn, D. S. and Schwartz, K.: 1974, Proceedings Fifth Lunar Science Conference, Geochimica et Cosmochimica Acta, Suppl. 5, in press.

MAGNETOCHEMISTRY OF THE APOLLO LANDING SITES

P. J. Wasilewski, NASA, Goddard Space Flight Center, Greenbelt, MD 20771, and M. D. Fuller, University of California, Santa Barbara, CA 93106

A synthesis of relevant magnetic data for samples from all Apollo sites has been completed and the results have been correlated with major element chemistry, petrography, earth-based telescope experiments and the $Al/_{Si}$ ratio. In a series of diagrams the basic magnetochemical aspects of the Apollo sites are summarized. The χ_p (paramagnetic susceptibility) vs I_s (saturation magnetization) data are summarized in Figure 1a, and in Figure 1b a "vector" diagram is presented to show how a given soil may develop in terms of variation of χ_p I_s when components are added or reduction takes place. With a system closed to mixing reduction indicates χ_p decrease and I_s increase. Mixing is clearly evident in a χ_p - I_s plot as will be described and for a given site is further evidenced by comparison of the $Al/_{Si}$ ratio of rocks from the site vs the soil. For mare sites 11 and 12 the ratio increases in the soil, and for highland sites (14 and 16) the opposite is true. The pure highland site (Apollo 16) shows little change i.e., 0.69 for rocks, 0.68 for soil (Rose et al, 1973). The soil groups are clearly defined in a plot of χ_p/I_s vs χ_o/I_s (χ_o is the initial susceptibility). These groups are magnetically distinct, have distinct $Al/_{Si}$ ratios, distinctive telescope reflectivity curves, and distinct FeO and TiO_2 contents (Figure 2). The hysteresis loop squareness ratios R_i (saturation remanence/saturation magnetization) and R_h (remanent coercive force/coercive force) further distinguish soil groups, crystalline rocks, impact melts, breccia samples . The R_h ratio in the soils correlates with the $Al/_{Si}$ ratio indicating that R_h depends on the soil type i.e., mare or highland. This implies that identical processes might produce different metal size distributions in different soils depending on the parent. In Figure 2 it is clear that the range of χ_o/I_s is ~ identical for all groups, χ_p/I_s separates the groups.

Based on surface magnetometer results it is clear that the in situ intensity of magnetization might be related to the type of terrain, i.e., A16 > A14 > A12 (highland > mare). This is not apparent in the subsatellite measurements, but this is only a consideration of scale size. A large scale magnetization coherence is required for subsatellite detection. If the highland > mare contrast is real then a mapping of large scale magnetic patterns correlated with surface morphology, the $Al/_{Si}$ geochemical experiments, and telescope reflectivity curves could provide a dynamic time sequence picture of lunar magnetization.

MAGNETOCHEMISTRY OF THE APOLLO LANDING SITES

Wasilewski, P. J. and Fuller, M. D.

FIGURE 1a

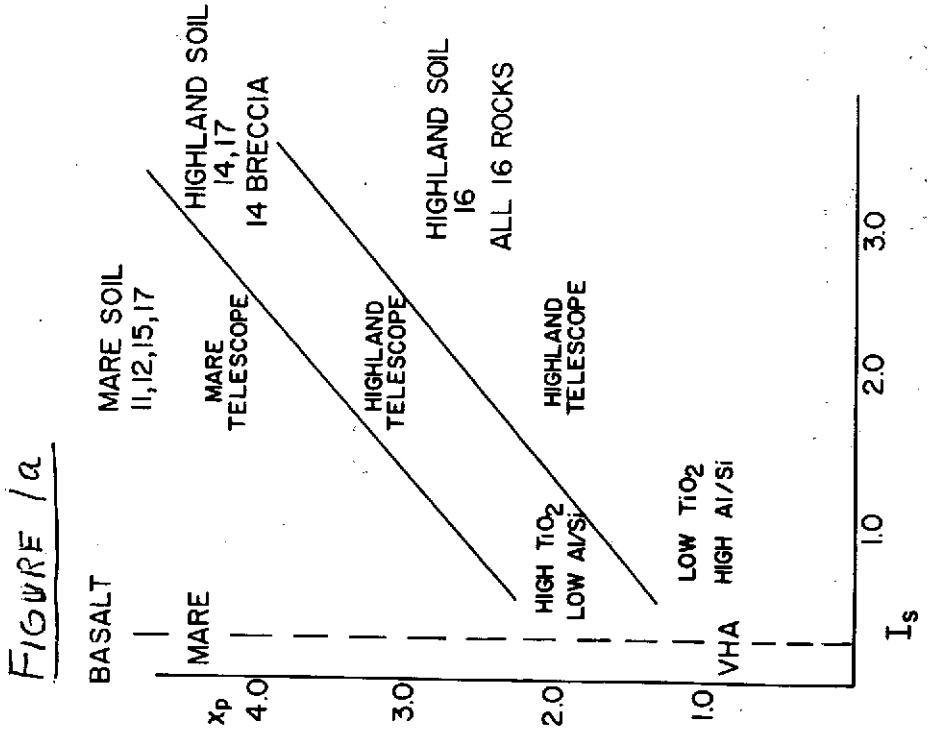

FIGURE 1b

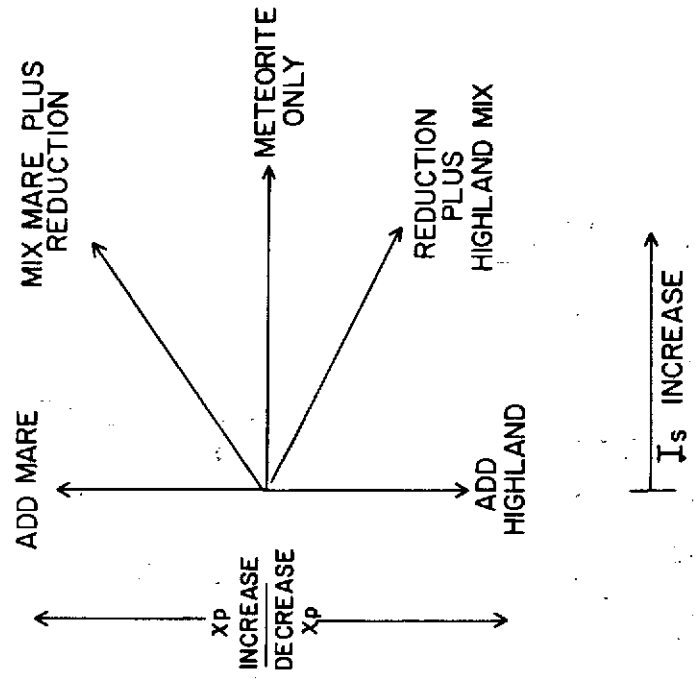

MAGNETOCHEMISTRY OF THE APOLLO LANDING SITES

Wasilewski, P. J. and Fuller, M. D.

FIGURE 2

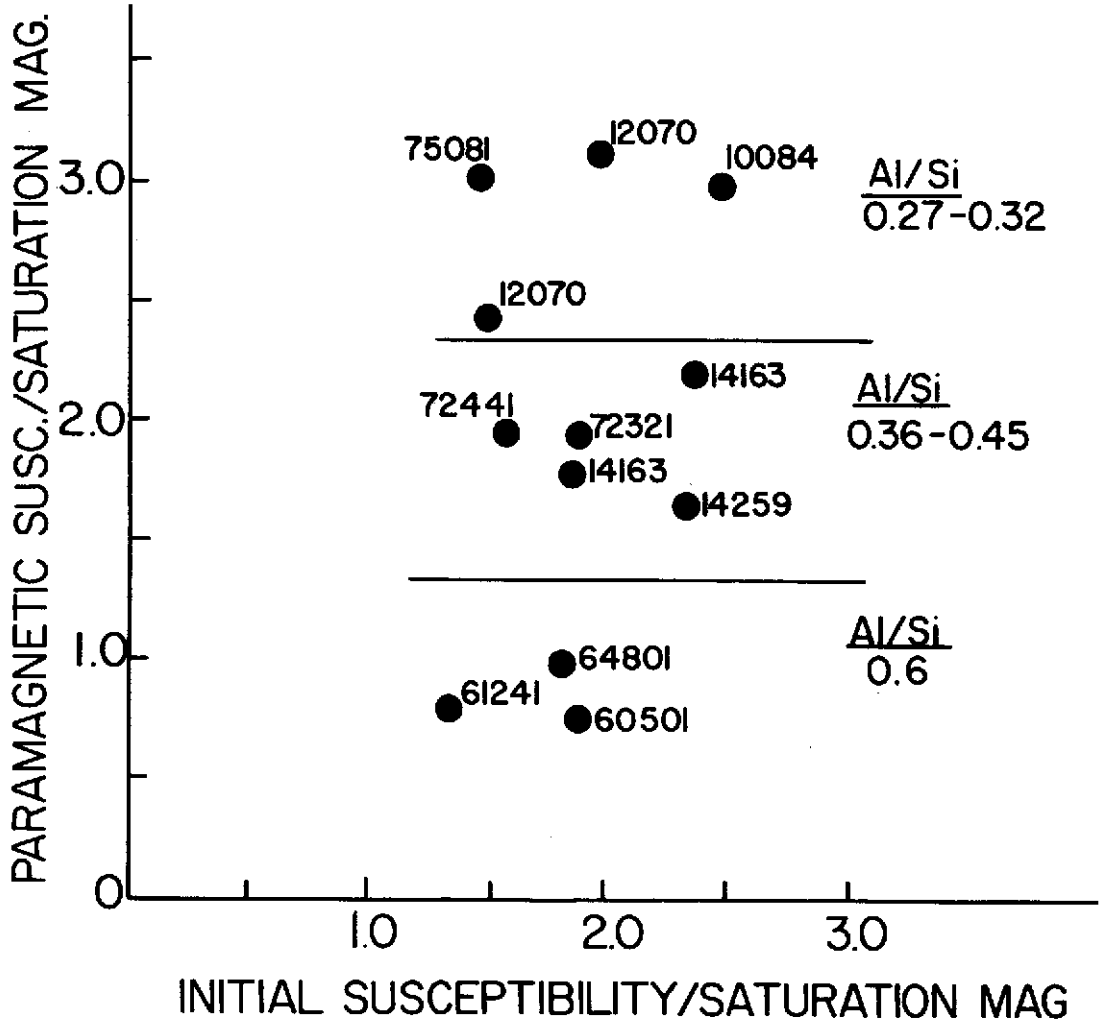

LUNAR REGOLITH MAGNETIC PROPERTIES FROM TELESCOPE SPECTRAL REFLECTIVITY CURVES AND ORBITAL GEOCHEMICAL EXPERIMENTS

P. J. Wasilewski, NASA, Goddard Space Flight Center, Greenbelt, MD 20771, and M. D. Fuller, University of California, Santa Barbara, CA 93106

Adams and McCord have shown that a match can be made between the laboratory spectral reflectivity curves for soils and telescope curves for the Apollo sites. Adler et al have utilized the solar induced X-ray fluorescence to derive the $Al/_{Si}$ ratio for broad regions of the lunar surface. Synthesis of magnetic property data, and major element chemistry and petrography, demonstrates conclusively that a classification of lunar samples in terms of their magnetic properties produces correlative chemical and spectral reflectivity curve shape classifications. The degree of mixing in a soil from any site is reflected in the contrast between the $Al/_{Si}$ ratio for the rocks and soil, and in the magnetic property data. Figure 1 presents a plot of $Al/_{Si}$ vs χ_p/I_s (ratio of paramagnetic suceptibility/saturation magnetization). Three soil groups are distinguished; the 16 highland, the 14 and 17 highland, and the 11, 12, 17 mare soils. Figure 2 presents a summary of relative spectral reflectivity curves taken from the MITPAL data book (copy furnished by Dr. McCord) and from Adams and McCord (1972). The line 1.0 would result for a ratio of any two individual curves which are identical. (a) Analyzed 16 soils, $MgO/_{FeO}$ shows considerable variation while TiO_2 and the $Al/_{Si}$ ratio are essentially constant. The $Al/_{Si}$ ratio for 16 rocks is 0.69 while for soils 0.68 indicating little mixing. The 1/3 etc., is a ratio of Descartes 1/Descartes 3 etc. The dotted area is the variation present for the Apollo 16 and Apollo 15 telescope curves as indicated. The Apollo 16 soils form a distinct magnetic group. (b) The Apollo 15 highland/mare contrast is clear, the resultant variation curve shape is highland. This explains in part why the $Al/_{Si}$ ratio for 15 rocks is 0.21 and for soil 0.42 (Rose et al, 1973). Compare the rocks 15418, 15058, 15555 for magnetic and chemical contrast between 15 highland and mare rock types. (c) Mare/mare contrast for 11/15 (12070 matches 12 telescope curves - 2.81% TiO_2). (d) Mare/mare soil contrast i.e., high TiO_2 10084 (7.82% TiO_2)/low TiO_2 12070 (2.81% TiO_2). (e) Highland (14259)/mare (12070) contrast. Inherent to each of the resultant ratio curves are magnetic property variations which will be described.

Based on the synthesis of magnetic property data, geochemical data, and the preliminary conclusions about the correlations with the telescope and laboratory spectral reflectivity curves, we are confident of being able to specify the magnetic properties of any lunar site for which a telescope spectral relectivity curve exists (i.e., mare or highland at present), or on a broader scale as indicated by the $Al/_{Si}$ ratio derived from the X-ray fluorescence experiments.

LUNAR REGOLITH MAGNETIC PROPERTIES

Wasilewski, P. J. and Fuller, M. D.

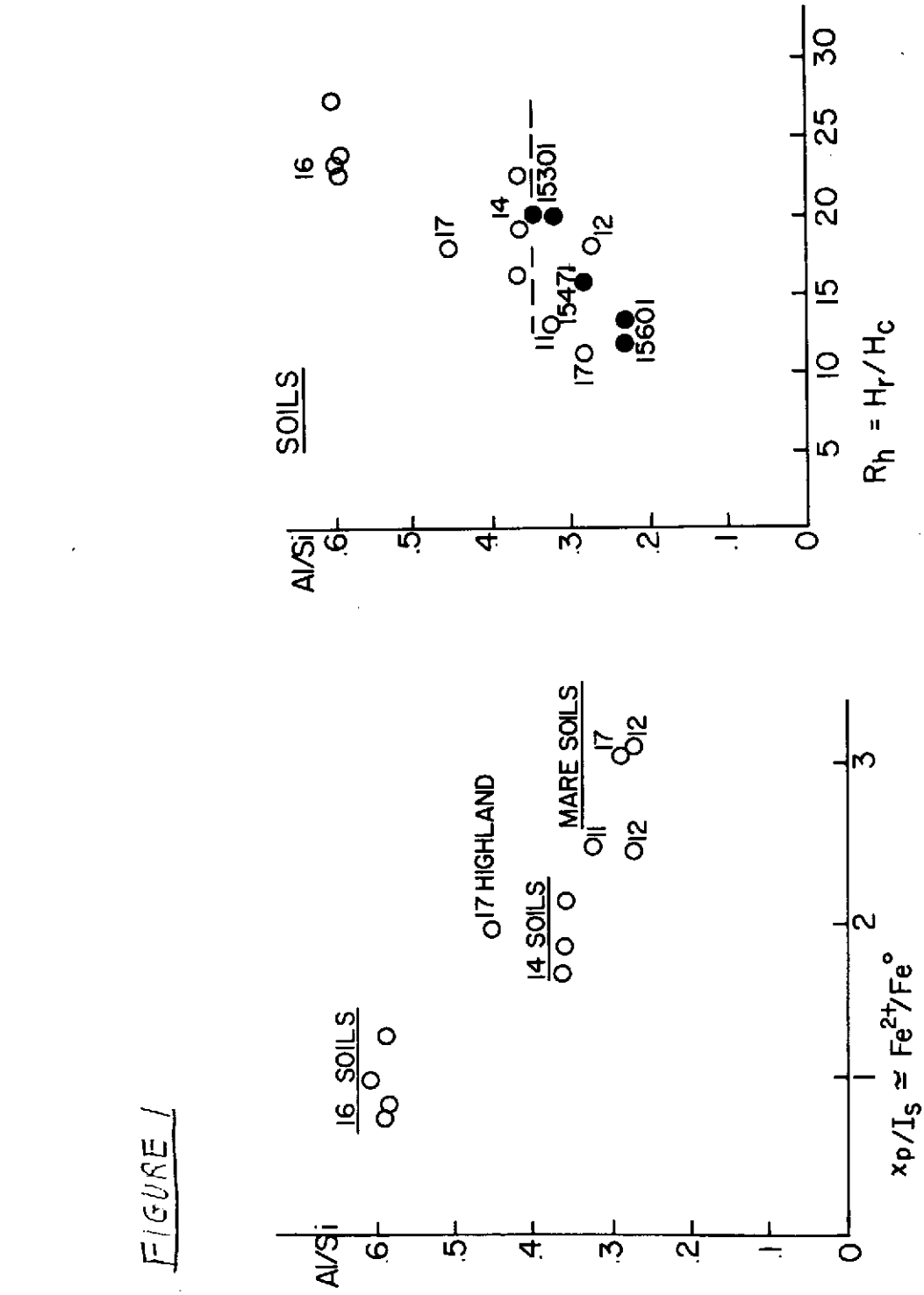

FIGURE 1

FIGURE 2

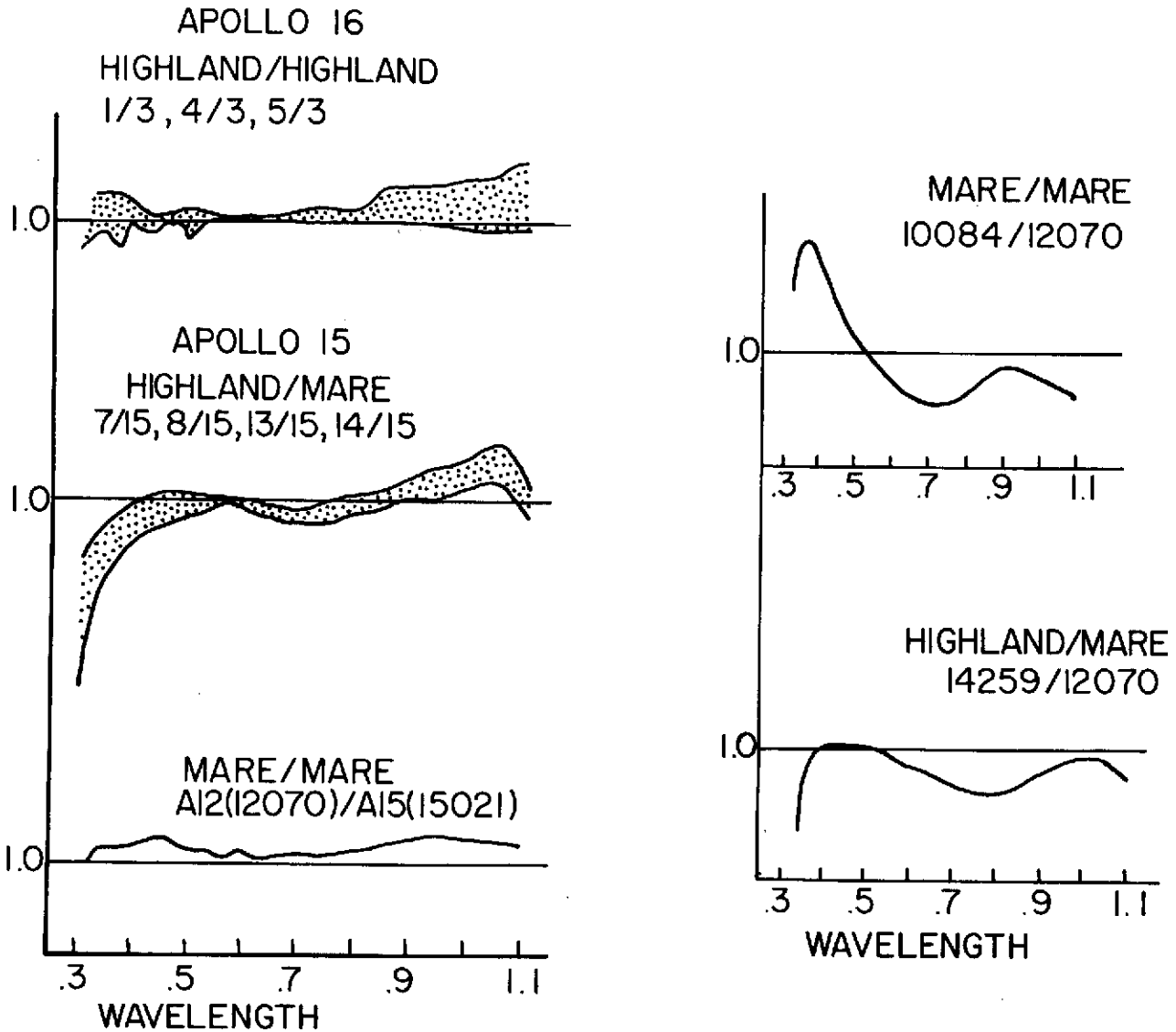
APOLLO 16
HIGHLAND/HIGHLAND
1/3, 4/3, 5/3
1.0
APOLLO 15
HIGHLAND/MARE
7/15, 8/15, 13/15, 14/15
1.0
MARE/MARE
A12(12070)/A15(15021)
1.0
.3
.5
.7
.9
1.1
WAVELENGTH
MARE/MARE
10084/12070
1.0
.3
.5
.7
.9
1.1
HIGHLAND/MARE
14259/12070
1.0
.3
.5
.7
.9
1.1
WAVELENGTH

THE LUNAR RADIATION ENVIRONMENT AND THE IMPLICATIONS FOR FUTURE LUNAR AND PLANETARY EXPLORATION, I. Adler, University of Maryland, College Park, MD; J.I. Trombka, Lo I Yin, E. Eller, and R. Schmadebeck, Goddard Space Flight Center, Greenbelt, MD.

The lunar surface is constantly under bombardment by a variety of particles and photons covering an enormous energy range. Some of these immediately produce characteristic secondary radiation from the lunar surface, and some, particularly the energetic particles also leave lasting records in the form of nuclear tracks and radioactive species. A number of interactions, in particular X-ray and gamma have been used as the basis for developing remote sensing techniques for producing geochemical maps of the lunar surface (1). These experimental techniques, flown on Apollo 15 and 16, have proved quite successful and provide the concepts for future exploration missions.

A partial view of the radiation at the lunar surface is shown in Fig 1. Also shown is the approximate depth from which useful chemical information can be obtained.

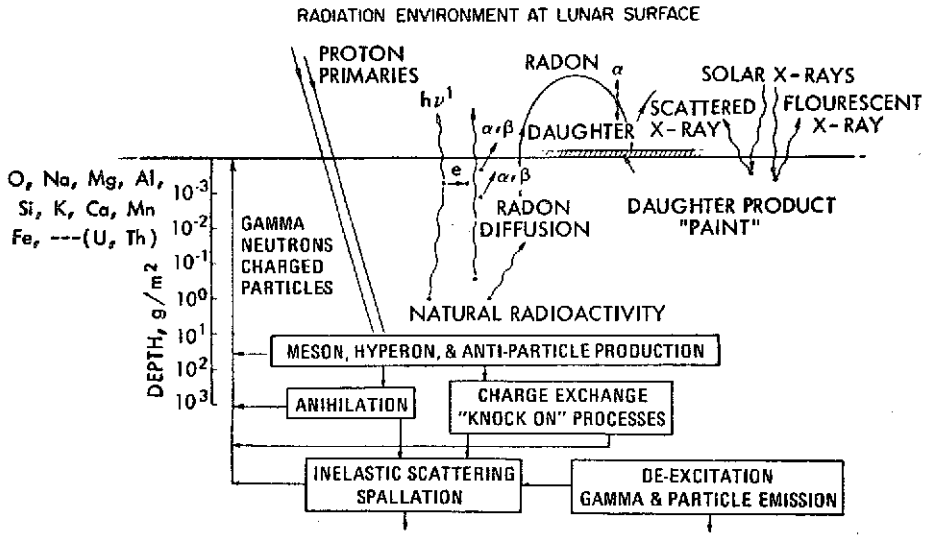

Fig. 1. The lunar surface radiation environment.

THE LUNAR RADIATION ENVIRONMENT

Adler, I. et al.

While the immediate concern in this paper involves the solar X-rays, cosmic ray interactions as well as the gamma flux through the surface from within the moon will also be briefly mentioned. The X-ray interactions have been estimated as involving depths of the order of microns where as, by contrast, the gamma rays sample the surface down to depths of approximately one third of a meter.

The secondary radiation produced by the X-rays results from photoelectron excitation (X-ray fluorescence), whereas the gamma rays are due mainly to prompt (n, γ) and (n, n', γ) reactions. Numerous calculations had shown that a typical "quiet" solar X-ray spectrum should be energetic enough to produce measurable amounts of characteristic X-rays from all the abundant elements of atomic number 14(Si) or smaller. This was precisely borne out during the Apollo 15 and 16 flights, where the sun proved to be generally "quiet" and remarkably stable. It was predicted and then observed that the energy distribution in the solar X-ray flux was effective only in exciting the light elements up to and including silicon. As had been expected in the gamma ray case, the total signal was made up to a large extent of continuum (85 percent), on which the characteristic lines were superimposed. By the use of appropriate analytical techniques described elsewhere (2), it was possible to make estimates of naturally-occurring radioactive species, as well as those elements excited by cosmic ray interactions.

In view of what is now known observationally about the X-ray and gamma ray fluxes, it is possible to design more effective measurements for future missions, as for example, a lunar-polar orbiter. Although the Apollo flights (15 and 16) occurred during a relatively quiet solar sun, substantial secondary fluxes were measured. A polar orbiter flown closer to solar maximum will enable us to capitalize in two possible ways: The increase in solar output of X-rays should lead to increased secondary fluxes, permitting us to fly collimated detectors, yielding much better spatial resolution, perhaps by a factor of two. Further, we know that a more active sun not only emits higher X-ray fluxes, but also a harder X-ray spectrum. This increases the likelihood of detecting the important, heavier elements such as Ca and K. To allow for this, a future flight will be designed to cover a larger energy range than the Apollo 15-16 instrument. Further extended flights will now and then probably encounter flares, which may hopefully produce excitation up to elements like iron. It is expected, however, that a more active sun is quite likely to be less stable, showing excursions in X-ray energy output both in flux and spectral hardness. The experience gained during the recent Apollo flights has taught us that a more effective way of

monitoring the sun is to use a secondary radiator, rather than looking at the sun directly. For example, the X-ray intensity ratio of Al/Si from a binary target of Al and Si should be an excellent indicator of the spectral character of the solar X-rays. We know that a hardening solar spectrum should decrease the observed Al/Si intensity ratio. Further advanced mathematical techniques have improved the spatial resolution of the X-ray experiment. Thus, by using these analytical techniques and the more active sun, we should be able to employ more effective collimation and the improved spatial resolution mentioned above.

It is obvious that the experience obtained in the recent Apollo flights about the radiation environment at the lunar surface are very important in the design of future exploration experiments. Our knowledge about the moon also gives us important data about the environment on inner planets, such as Mercury, should the time come to design geochemical experiments for its exploration.

REFERENCES

(1) Adler,I., Trombka,J.I., Lowman,P., Schmadebeck,R., Blodget, H., Eller,E., Yin,L., Lamothe,R., Osswald,G., Gerard,J., Gorenstein,P., Bjorkholm,P., Gursky,H., Harris,B., Arnold,J., Metzger,A., and Reedy,R. (1973), Apollo 15 and 16 results of the Integrated Geochemical Experiment, The Moon 7, 487-504.

(2) Reedy,R., Arnold,J., and Trombka,J.I., Expected -ray Emission Spectra from the Lunar Surface as a Function of Chemical Composition (1973), J. Geophys. Res., 5847.

LUNAR ELECTROMAGNETIC SCATTERING, B. L. Horning, and G. Schubert, Department of Planetary and Space Science, University of California, Los Angeles, California 90024

An analytic theory is presented for the steady-state and time dependent electric and magnetic fields induced inside the moon and its downstream cavity for plane wave interplanetary electromagnetic fluctuations incident at arbitrary angles to the cavity axis. The cavity is modelled as a nonconducting cylinder extending infinitely downstream with radius equal to that of the moon. The fields induced inside the conducting moon and in the far cavity are assumed confined to the moon and the cavity region by the supermagnetosonic solar wind.

To determine the induced electric and magnetic fields in the moon and downstream cavity, an electromagnetic boundary value problem is constructed. Since magnetosonic waves cannot propagate upstream, the solar wind is treated as an infinitely conducting medium. Accordingly, the normal component of the induced magnetic field is zero on the subsolar hemisphere. Since the cavity is nonconducting, both the normal and tangential magnetic field components are continuous across the antisolar hemispherical surface. From the continuity of charge equation, the radial component of the current density is set equal to the time derivative of the difference between the lunar and cavity electric field components normal to and at the antisolar surface. In the steady-state, the radial electric field of the moon on the antisolar hemisphere is zero. Continuity of the normal component of the magnetic field across the cavity wall and continuity of the tangential components of the electric field across the cavity and lunar surfaces complete the set of boundary conditions.

A plane wave incident at any angle to the cavity axis induces both spherical transverse electric (TE) and transverse magnetic (TM) modes in the conducting moon. These modes are coupled to the cylindrical TE and TM modes in the cavity. The TM response has usually been neglected in lunar electrical conductivity studies because of the low surface conductivity (1,2). The spherical TE field induces both cylindrical TE and TM modes in the cavity, however, the cylindrical TM fields are of order v^2/c^2 (where v is the propagation speed in the solar wind and c is the speed of light in vacuum) compared to the TE fields. Thus only the spherical and cylindrical TE modes need be considered to infer lunar electrical conductivity.

In the far cavity region, either the cylindrical TE or TM modes can be induced depending on the orientation of the incident interplanetary field. If the wave normal is parallel to the cavity axis, all linear polarizations of the incident field are equivalent since both the electric and magnetic fields are normal to the cavity axis. Only the cylindrical TE mode is induced

Horning, B. L. and Schubert, G.

in the far cavity region for the parallel propagating wave (3). For off-axis propagation, there are two fundamental orientations of the magnetic and electric fields, parallel and perpendicular to the cavity axis. When the wave normal is perpendicular to the cavity axis, the far cavity field is a pure cylindrical TE mode if the magnetic perturbation vector lies parallel to the cavity axis and a pure cylindrical TM mode when the magnetic vector is perpendicular to the axis. In the remainder of the abstract we consider the physics of the scattering problem in the two limiting cases of wave propagation, parallel and perpendicular to the cavity axis.

Propagation Parallel to the Cavity Axis

When the incident wave normal is parallel to the cavity axis the far cavity field propagates downstream with the same velocity as the interplanetary field. The far cavity field can be thought of as the result of an induced wave on the cavity boundary. The wave induces an axial magnetic field component which is 90 degrees out of phase with the interplanetary magnetic field (3). The cavity behaves as a cylindrical wave guide below cutoff for frequencies less than 50 Hz. For lower frequencies, the induced cavity field due to the presence of the moon attenuates with distance down the cavity.

Propagation Normal to the Cavity Axis

In contrast to the parallel propagating case, the case of normal incidence is not a wave guide problem but rather a problem of forcing an electromagnetic cavity response. The external wave propagates past the cavity at magnetosonic velocities, while inside the cavity, for frequencies greater than 0.1 Hz, the field is substantially reduced. At discrete values of frequency, however, the cavity resonates. Since we have assumed that the cavity is bounded by a medium of infinite conductivity, there are no losses in the cavity and the resonant cavity fields are thus infinite. The first resonance occurs at about 50 Hz if the interplanetary magnetic vector lies parallel to the cavity axis and at 66 Hz when the magnetic vector is perpendicular to the axis. These values are relatively insensitive to the phase velocity provided this velocity is not comparable to c.

Unlike the parallel propagating case, nodes in the electric and magnetic fields exist in the far cavity as a function of position, field orientation, and phase velocity. We distinguish two cases. First, when the interplanetary magnetic vector is perpendicular to the axis, the cavity electric field is along the axis. There are no normal or azimuthal electric field components. The first node in this electric field occurs at a frequency of approximately 0.01 Hz in the plane containing the cavity axis and the magnetic perturbation vector. There are no nodes in the magnetic fields for this case. Second, if the interplanetary magnetic vector lies parallel to the cavity axis, the cavi-

ty magnetic field is also parallel to the axis. The first node in this case occurs at a frequency of about 0.02 Hz in the plane containing the cavity axis and the solar wind electric field perturbation vector. For this orientation, there are no nodes in the electric field. Successive nodes in the magnetic field are approximately evenly spaced in frequency and the intervening maxima attenuate with increasing frequency. A similar behavior is true of the electric field nodes in the case where the solar wind magnetic field perturbation is perpendicular to the cavity axis.

At large frequencies, the cavity surface currents nearly shield the cavity interior from the solar wind magnetic field components parallel to the cavity surface. The cavity surface charge density attenuates slowly with increasing frequency, for sufficiently large frequency, eventually converging to the magnitude of the interplanetary electric field. As the phase velocity approaches the speed of light, the surface currents and charge density disappear and the cavity becomes completely transparent to the incoming radiation.

(1) Sonett, C. P., B. F. Smith, D. S. Colburn, G. Schubert, and K. Schwartz (1972) The induced magnetic field of the moon: conductivity profiles and inferred temperature, Proc. Third Lunar Sci. Conf., Geochim. Cosmochim. Acta, Suppl. 3, Vol. 3, pp. 2309-2336. MIT Press.

(2) Sill, W. R. (1972) Lunar conductivity models from the Apollo 12 magnetometer experiment, The Moon, 4, 3-17.

(3) Schwartz, K. and G. Schubert (1973) Lunar electromagnetic scattering 1. propagation parallel to the diamagnetic cavity axis, J. Geophys. Res., 78, 6496-6506.

FORMATION OF THE LUNAR ATMOSPHERE, R. R. Hodges, Jr., University of Texas at Dallas, Richardson, Texas, 75080

INTRODUCTION

The atmosphere of the moon is essentially a classical exosphere, in which atoms and molecules are gravitationally constrained to ballistic trajectories between encounters with the lunar surface. In the thermal distribution of velocities of particles going upward at lunar surface, those atoms going faster than the escape velocity are lost from the moon. The lower energy part of the distribution consists of particles which return to the lunar surface, with the average lateral extent of these trajectories being about twice the atmospheric scale height (i.e. $2 \times kT/mg$).

Since these ballistic particles only collide with the moon, the usual ideas of atmospheric dynamics are inapplicable. More specifically, the concept of hydrostatic equilibrium in an exosphere is that a gas tends to flow laterally so as to equalize $nT^{5/2}$ over the exobase (1) rather than to equilibrate pressure. In addition the lack of interaction of lunar gases results in separate and distinct global distributions for each species.

There are two basic types of global gas distributions on the moon. Gases which are not adsorbed on the cold nighttime part of the lunar surface have a nighttime concentration maximum, in accordance with the $T^{-5/2}$ law of exospheric equilibrium. Species which are adsorbed or condense at the cold temperatures of lunar night have both nighttime and subsolar minima of concentration, with an annular maximum at the terminator. The concentration of condensible gases is greatest near the sunrise terminator, where molecules which were adsorbed at night are released by photon and thermal effects. The maximum near the sunset terminator is due to the tendency of lateral transport to equalize $nT^{5/2}$.

The best available data on lunar gases is from the Apollo 17 lunar surface mass spectrometer. Of these, the only measurements which are obviously free of contaminant and instrumental uncertainties are those of ^{40}Ar and helium obtained during lunar nights. Fortuitously, argon behaves as a condensible gas while helium is unaffected by surface adsorption at night. Another important difference in these two gases is that argon is lost from the lunar atmosphere by acceleration of its photoions in the induced $\vec{v} \times \vec{B}$ field of the solar wind near the moon (2) while helium escapes thermally. In addition, ^{40}Ar arises from the radioactive decay of ^{40}K within the moon, while helium is produced by neutralization of impacting solar wind α-particles. The detailed study of the argon and helium data is important in learning the behavior of other, more poorly understood species of the lunar atmosphere.

ARGON

The fact that the atmosphere of the moon is quite tenuous is mainly indicative of efficient escape processes, but not necessarily of low rates of supply of gases. An important example is ^{40}Ar, which escapes from the moon at an average rate of about 5×10^{20} atoms/sec (3). This rate is only about an order of magnitude less than would occur if the rate of release of

FORMATION OF THE LUNAR ATMOSPHERE

Hodges, Jr., R. R.

^{40}Ar per unit mass of moon were the same as for earth. On earth all of the argon that has been released over geologic time is trapped in the atmosphere whereas on the moon its lifetime is only the order of 100 days. The result is that the present argon concentration on earth is about 10^{12} times as great as that on the moon.

What makes the lunar and terrestrial argon escape rates so grossly different is the lack of a lunar magnetic field to trap atmospheric photoions. Formed essentially in the solar wind, which is only slightly perturbed by the presence of the moon, these ions are accelerated by the $\vec{v} \times \vec{B}$ field induced in the solar wind, so that on the average roughly half of the photoions are driven away from the moon while the rest impinge on the moon and become implanted in surface rocks (2).

The average rate of effusion of ^{40}Ar from the moon during the first 9 lunations of 1973 (when the Apollo 17 mass spectrometer data was obtained) corresponds to about 0.5% of the total rate of production of argon within the moon, if the average abundance of potassium in the moon is 300 ppm (3). To put this in perspective, it would require the continual release of all of the argon being formed in the upper 3.5 km of the lunar crust to account for the average abundance of argon in the lunar atmosphere. The only reasonable explanation of the argon effusion rate is that it comes from great depths where the temperature is sufficient to drive enough gas from fractured materials.

However, there is a complication of this hypothesis, in that the rate of effusion of argon from the moon is apparently variable. This leads to speculation that argon percolates from a semi-molten core into one or more subsurface voids, which vent transiently to the atmosphere through deep fissures. If this is the correct explanation, then the mechanism of argon release must be related to some form of seismic activity, and perhaps it is the buildup of pressure of trapped argon which triggers its own release, and a seismic effect as well.

HELIUM

Helium is produced on the moon by neutralization of the solar wind α-particle influx. These ions have impact energies the order of 4000 eV, which should cause their implantation in surface rocks. In data from the Apollo 17 lunar surface mass spectrometer it is apparent that the abundance of lunar atmospheric helium responds rapidly to changes in the solar wind.

The fluctuations of helium on the moon during the lunar nights of the first 10 lunations of 1973 appear to be correlated with variations of the geomagnetic index Kp (4). More recent work shows that the coefficient of correlation of those parameters is 0.31. Assuming instantaneous response of helium supply and α-particle influx, the equivalent solar wind flux of helium during this period can be expressed as

$$\Phi\ [\mathrm{He}] = (5.6 \pm 1.9 + 0.44 \times \mathrm{Kp}) \times 10^{6}\ \mathrm{cm}^{-2}\mathrm{sec}^{-1}$$

This differs slightly from the flux reported in (4) because the current

result is based on an improved model atmosphere. The dependence of the flux on Kp is less than might be inferred from other studies of the solar wind suggesting that the release of trapped helium from the lunar soil involves two separate mechanisms: an impact process which responds instantly to changes in the solar wind; and a diffusion process which is essentially constant.

OTHER GASES

Evidence of other gases in the lunar atmosphere is less certain than that for helium and argon. It is necessary that the solar wind influx of hydrogen, carbon, neon and perhaps nitrogen be balanced by escape of these elements as atmospheric gases. The Apollo 17 ultraviolet spectrometer data of Fastie et al. (5) showed no evidence of atomic hydrogen on the moon, suggesting that the dominant gaseous form of hydrogen is H_2. Model calculations tend to give H_2 concentrations of about 4×10^3 cm^{-3} in daytime and about 10^4 cm^{-3} at night (6,7).

Carbon implanted in soil grains must react with impinging protons to form CH_4 and possibly other more complicated molecules. Methane does not appear to be a significant gas in the nighttime lunar atmosphere, and it does not exhibit a dramatic presunrise increase, as does argon, due to photo-desorption at the terminator. Nonetheless, the escape of carbon from the moon requires that a substantial amount of methane exists in the daytime lunar atmosphere. Methane is probably adsorbed readily at presunset surface temperatures ($\sim$ 150°K). A significant amount of methane should be deposited on soil grains and rocks near the poles, leading to polar atmospheric concentrations determined by a surface pressure equilibrium condition.

In addition to ^{40}Ar the moon also releases radon into its atmosphere (8). The mechamisms for release of both of these elements from the interior of the moon are apparently episodic in nature, and their release mechanisms may be related. It is conceivable that some trapped lunar gases may be released along with the radiogenic species. These are probably molecular gases which are completely adsorbed at night, but which may form a substantial daytime atmosphere. The lack of good daytime mass spectrometric data hampers a definitive examination of this problem.

REFERENCES

(1) Hodges, R. R. and F. S. Johnson, J. Geophys. Res., 73, 7303 (1968).
(2) Manka, R. H. and F. C. Michel, Proc. Second Lunar Sci. Conf., 2, 1717 (1971).
(3) Hodges, R. R. and J. H. Hoffman, Proc. Fifth Lunar Science Conf., in press, (1974).
(4) Hodges, R. R. and J. H. Hoffman, Geophys. Res. Letters, 1, 69 (1974).
(5) Fastie, W. G., P. D. Feldman, R. C. Henry, H. W. Moos, C. A. Barth, G. E. Thomas, and T. M. Donahue, Science, 182, 710 (1973).
(6) Hartle, R. E., and G. E. Thomas, J. Geophys. Res., 79, 1519 (1974).
(7) Hodges, R. R., J. H. Hoffman, and F. S. Johnson, Icarus, 21, 415 (1974).
(8) Gorenstein, P., L. Golub, and P. J. Bjorkholm, Proc. Fourth Lunar Sci. Conf., 3, 2803 (1973).

EVIDENCE OF REGOLITH CYCLING AND MIXING IN 72161 Abhijit Basu, D. J. DesMarais, J.M. Hayes*, and W. G. Meinschein, Department of Geology, Indiana University, Bloomington, Indiana 47401. *Also Department of Chemistry.

A refinement of approaches to the study of solar wind implanted elements in lunar fines involves extending analyses to different particle types in various size fractions thus combining techniques of petrography and analytical chemistry. Such extensions of methodology are necessary particularly for Taurus-Littrow samples which have a complex history (1) being mostly mixtures of regoliths of varying maturity. Recent work in our laboratory on lunar regolith 72161,11 (dark mantle, LRV 3) indicates not only that the sample is a mixture of mare and highland regoliths (cf. 2,3,4) but also that the characteristics of the transported component can be inferred.

The grain size distribution of <1 mm fines of 72161 is found to be defined by $M_Z = 3.88\ \phi$; $\sigma_I = 1.29\ \phi$; $SK_I = -0.23$; and $K_G = 1.38$ (parameters defined in (5)) which indicate that this is a mature regolith and that about 50% of it is expected to be agglutinates in the 90 μm to 149 μm fraction, provided that the sample is in a "steady-state" (6). However, our modal analyses data (Table 1) show that the agglutinate content in that size range is about 30%. A departure from the "steady-state" is indicated and we attribute this to the mixing of two or more particle populations. The data also indicate that (a) the maximum concentration of agglutinates occurs in the 2.5 ϕ to 3.5 ϕ range, (b) agglutinate contents correlate negatively with the dark vitric breccia contents for various size fractions, and (c) except for light vitric breccias, and, to some extent, for the agglutinates, there is no well defined size-dependent trend. These observations may also be explained by the mixing of different regoliths.

Analyses for total C indicate that 72161 is quite mature, with 204 μC/g (cf. 200 μg C/g by Moore (7)). The effects of prolonged exposure of the sample to solar wind remains manifest in the high C and H_2 contents, particularly in the finer grain sizes. The data (Table 2) show (Fig. 1,2) that in the bulk size fractions the concentrations of the H_2, CH_4, and total C increase continuously as the grain sizes decrease. On the other hand, the concentrations of H_2, CH_4, and total C show a linear increase with increasing grain size in the agglutinate fractions of sizes $>149\ \mu$m. The disparities in the distributions of H_2, CH_4, and total C in the bulk and agglutinate size fractions may be attributed to cycling and mixing. The agglutinates, formed from fine grained particles with high surface concentrations of C and H_2, show an upswing in concentrations of both in the grain sizes $> 149\ \mu$m. This upswing may be due to mixing of a dominant local population of coarser agglutinates, with higher C and H_2, and an imported population of finer agglutinates with relatively low C and H_2. The absence of increases in C and H_2 concentrations in the $>149\ \mu$m size fractions of the bulk sample, along with the atypically low percentage of agglutinates, suggests that the effects of local agglutinates have been obliterated by the admixture of coarse grained non-agglutinatic material with low C and H_2. Therefore, the added component of this complex regolith apparently contains a coarse-grained non-agglutinatic fraction and a formerly coarse grained agglutinate fraction whose grain size

REGOLITH CYCLING AND MIXING ...

Basu, A. et al.

Table 1. Modal analyses data for 72161,11 in different size classes (in number percent)

	0ϕ-2ϕ	2ϕ-2.5ϕ	2.5ϕ-3ϕ	3ϕ-3.5ϕ	3.5ϕ-4ϕ	4ϕ-4.5ϕ
Plagioclase	2.7	1.6	1.0	3.8	3.1	5.4
Pyroxenes, etc.	2.7	1.6	1.0	2.4	4.2	2.8
Rocks	5.4	3.1	3.1	2.4	3.1	1.3
Breccia						
Vitric, Dark	40.5	50.0	39.8	34.5	34.8	44.9
Vitric, Light	2.7	10.9	10.2	15.4	17.4	20.3
Recrystallized	2.7	1.6	2.5	2.0	4.2	1.9
Glass						
Spherules	8.1	4.7	4.1	1.0	3.5	2.8
Irregular	5.4	7.8	8.2	7.5	7.3	9.2
Agglutinates	29.7	18.8	30.1	31.1	22.3	11.4

Table 2. Distribution of C, CH_4, and H_2 in the size fractions of 72161,11; Intercepts and Correlation Coefficients of best line of fit.

M_Z = 3.88 ϕ $_I$ = 1.29 ϕ SK_I = -0.23 K_G = 1.38

Size fraction	H_2		CH_4		Total C	
m	Bulk	Aggl	Bulk	Aggl	Bulk	Aggl
420 - 1000	49	93	0.5	2.3	74	187
250 - 420	55	85	0.7	1.4	87	173
149 - 250	58	84	1.0	1.3	99	162
105 - 149	59	101	1.4	1.7	114	146
74 - 105	80	107	1.2	2.0	148	174
53 - 74	107	128	3.2	2.2	175	190
37 - 53	106	246a	4.2	4.1	225	242
30 - 37	99		4.8		236	
20 - 30	121		7.0		332	
20	193		9.0		465	
Average - Bulk Sample	144		3.8		204	
Intercept	52	67	0.58	0.37	78	98
Corr. Coeff.	0.97	0.98b	0.97	0.94b	0.99	0.99b

a - doubtful point - disregarded for regression analysis
b - for the 4 finest size fractions only

REGOLITH CYCLING AND MIXING

Basu, A. et al.

has subsequently been decreased perhaps by breakdown of these fragile particles during transport.

References: (1) Eberhardt, P. et al., 1974, Lunar Sci. V, 1, 197-199; (2) Baedecker, P. A. et al., 1974, Lunar Sci. V, 1, 28-30; (3) Philpotts, J.A. et al., 1974, Lunar Sci. V, 2, 599-601; (4) Rhodes, J.M. et al., 1974, Lunar Sci. V, 2, 630-632; (5) Folk, R.L. and Ward, W.C., 1957, J. Sed. Pet., 27, 3-26; (6) McKay, D.S. et al., 1974, Lunar Sci. V, 2, 480-482; (7) Moore, C.B. et al., 1974, Lunar Sci. V, 2, 520-522.

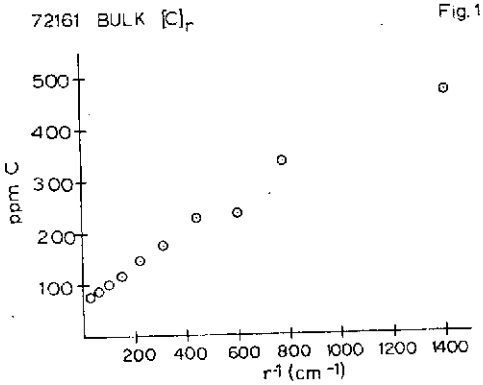

Figure 1 (a,b,c) Total C and CH_4 concentrations of sieved lunar fines (72161, 11) as bulk fractions and agglutinate separates.

Figure 2 (a,b) Total H_2 concentrations of sieved lunar fines (72161,11) as bulk fractions and agglutinate separates.

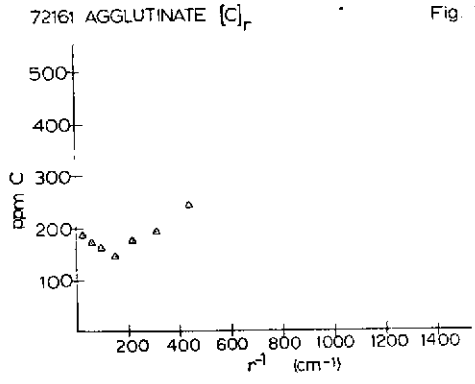

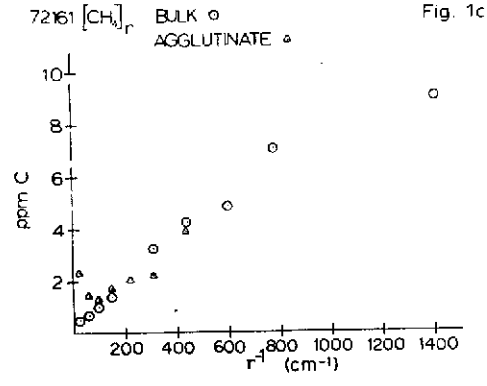

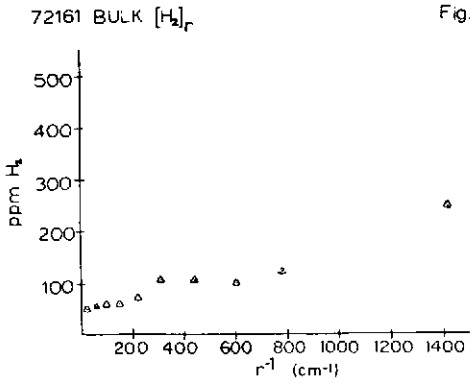

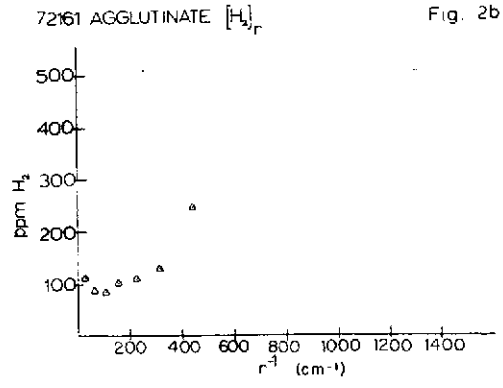

THE EVIDENCE FOR A SURFACE TRANSPORT MECHANISM ON THE MOON. T. Gold, Center for Radiophysics & Space Research, Cornell Univ., Ithaca, N.Y. 14850.

Evidence that the lunar soil has suffered some surface transport mechanism over long periods of time comes from many sources. Small scale and large scale topographic detail, cosmic ray and other surface exposure effects, layering of the soil, as well as regional chemical and gravity effects, must all be discussed in this context. Transportation by the explosive events of impacts, large and small, must of course have taken place, and the present discussion concerns features that cannot be accounted for by this process alone, but that appear to point towards some other, as yet unknown, mechanism having been at work.

On the smallest scale one frequently sees the soil surface to be very smooth, and the scattered rocks to be imbedded with the junction line sharp to a precision of 1 cm. The upper surfaces of such rocks are often quite free from dust. From the distribution of such rocks it is clear that they mostly reached their present positions as a result of being thrown there in a crater-forming event. The deformation of the soil that each rock must have caused as it landed has nowhere been seen. A comparatively fast transport mechanism must flatten the soil without throwing up material to build up a large fillet around each rock and to dust over the top.

On a larger scale we see the features at the junction lines between old mountains and adjacent level surfaces. Convex deposits, "shoulders", line a very large proportion of flat mare surface or flat surfaces in the interiors of craters or rills. The only origin for these that can be suggested lies in material transported down the neighboring slope, which, for an unknown reason, beds down in a convex deposit at the base, rather than the concave one, which is common on the Earth in these circumstances. All steep slopes on the Moon have a criss-cross pattern whose character is systematically related to the mean angle of the slope. These patterns are also seen on the shoulder material and are systematically on a finer scale there. Whatever the surface transportation mechanism may be, it appears to have a characteristic footprint in the form of these patterns.

Rocks are frequently seen concentrated along ridges and peaks. No satisfactory explanation has been found other than the selective downhill transportation of fines, causing the denudation of previously imbedded rocks.

In mountainous terrain local low spots, at whatever altitude they occur, have frequently a flat filling. One may consider that this was due to downhill transportation from neighboring slopes.

EVIDENCE FOR A SURF. TRANSP. MECH. ON THE MOON

Gold, T.

Meteoritic impacts must be distributing material all around the Moon. Impact velocities are clearly high enough for secondaries to have orbital velocities, as can be seen from the ray patterns of young craters. This must be true not only for the large craters for which rays can be seen, but also for craters down to a size of centimeters. The action of this would be to create a well-mixed surface over the top of the Moon, whatever the underlying chemical differences might have been. Such homogeneity is not seen, and one has to suppose that a downhill transportation mechanism acts sufficiently fast to keep re-exposing the underlying material of the mountains faster than they are being sprayed and "snowed over".

The cosmic ray exposure and other surface exposure effects of the soil are remarkably high and remarkably uniform. Very little of the soil, be it from the surface or from core tubes, seems to have escaped surface exposure. One could understand this small variance in the surface exposure of the grains if one supposed that the investigations had occurred chiefly in depositing rather than denuding areas and that the deposition mechanism involved every grain having moved over the surface before it came to its present resting place.

If large-scale surface transportation has taken place, then a layer of fill in any previously hydrostatically balanced basin would result in a positive gravity anomaly. The mascons can be understood in that case. If the surface transportation mechanism is facilitated by the electrodynamical phenomena in the wake of the Earth, then the difference in fill between low areas on the front and the back of the Moon can perhaps find an explanation.

ELECTROSTATIC TRANSPORTATION OF DUST. T. Gold and G. J. Williams, Center for Radiophysics & Space Research, Cornell University, Ithaca, N.Y. 14850.

A dust surface can, under certain circumstances, develop an electric charge distribution that causes individual particles to move. For the case of the Moon, an average electric field above the surface strong enough to dislodge or suspend dust grains cannot be expected. What can be expected, however, is a condition of unstable local charging circumstances, such that the scale of the irregularities corresponds to the scale of the topography or the electrical surface properties of the grains, a scale that is generally in the micron range. Electric fields on this scale can reach potential differences of a few hundred volts and thus electric fieldstrengths of the general order of a million volts per centimeter. It is fields of that strength that can readily move dust grains against gravity, or even against slight surface adhesion. This micron scale of electric fields can cause surface migration, and its statistical properties can be a downhill transportation, but it cannot throw grains to any great height, and the laboratory tests tend to show that the vertical scale of the phenomenon is generally restricted to a few millimeters.

There may be other electrostatic phenomena of importance to lunar evolution. Dr. Criswell has discussed, for example, electric fields associated with the terminator, and the transportation that may result from this. Evidence seems to exist also for a spray of particles at a greater height, and it is not yet clear whether this can be accounted for by meteoritic secondaries. However, there is substantial evidence that the surface transportation associated with a very small vertical height is an important process on the Moon, and there is evidence that it can occur in lunar circumstances.

Unstable charging, such that neighboring grains may be driven to very different potentials, occurs chiefly due to electron bombardment in the general range of bombarding energy where the secondary emission ratio first becomes larger than unity. This so-called "cross-over point" is basically unstable, and any individual point will either run away to a positive or a negative potential that is the most extreme it can reach. The two are separated from each other by the voltage corresponding to the electron bombardment energy. First cross-over points for many materials are in a general range of 200-600 volts, and electrons of this energy would therefore be most effective for causing spotty charging, and the potential differences between neighboring grains will then be of this general order.

ELECTROSTATIC TRANS. OF DUST

Gold, T. and Williams, G. J.

In practice, differences of microtopography and differences of surface chemistry will be the dominant factors that determine the sense in which any one grain will charge. Thus, a grain accessible to a direct beam of electrons will become a positive- or a negative-going one, depending on the solid angle accessible to its secondaries, on the solid angle for the infall of secondaries from other locations, and on the surface chemistry defining its secondary emission cross-over point. In the presence of any movement of the surface material, these conditions will constantly change, each further movement causing new unstable situations. It is under these circumstances that materials display a surface creep, which, in the laboratory, can be seen as the effects of a rapid succession of hopping movements of each surface grain. The statistical average of such movements is seen in the laboratory to be usually a downhill migration, though in detail, many more complex movements take place.

Laboratory tests show that under good vacuum conditions, and with bombarding voltages of electrons of the order of 300 volts, most insulating powders, including actual Moon dust, develop very active surface mobility when the current densities are a few microamps per cm^2. The quality of a vacuum, and therefore presumably gas adsorption on the surfaces of the grains, plays an important role and makes any extrapolation to lunar circumstances very difficult.

The presence of a profuse cloud of photoelectrons over the lunar surface in the lunar daytime has been thought to obliterate any spotty charging. In the presence of low energy electrons, certainly no point can develop a positive potential that would attract the great quantity of photoelectrons, no matter what the circumstances under simultaneous but weaker bombardment might be. However, the photoelectric effect acts as a very good rectifier. Any points in the local topography that can be reached by the hot electron plasma, but not reached by the UV photons that cause photoemission, can charge negatively only. Such points, very common in the intricacy of the fairy-castle surface structure, will reach negative potentials corresponding to the peak energies of the diffuse electron plasma. The strong, small scale electric fields will be between them and other positive-going grains that are exposed to the photons as well as the electrons. Electrostatic surface transportation is therefore not stopped even by intensive UV irradiation so long as a less collimated stream of electrons is present also.

Laboratory tests have shown many of the effects mentioned but leave many remarkable and puzzling features. They show that materials can be separated according to their surface chemical

composition and that mixtures of different materials behave quite differently from powders composed of either substance singly. Some of the most curious lunar erosion effects noted may have an explanation in these terms. Certainly if any electrostatic transportation has taken place on the Moon, its possible effects on chemical sorting must be considered.

Electrons in the interesting energy range occur in the stream behind the bowshock of the Earth and must hit the Moon preferentially on the side facing the Earth. If these electrons are responsible for a really large-scale transportation effect over geologic time, then the filling of the basins on the front side and the absence of such filling on the back can be understood.

MANIFESTATIONS AND POSSIBLE SOURCES OF LUNAR TRANSIENT PHENOMENA(LTP)

Winifred Sawtell Cameron, NASA Goddard Space Flight Center, Greenbelt, Md. 20771

Lunar transient phenomena (LTP) are observed in several different manifestations, such as: (1) brightenings - both sudden and slow, (2) reddish - both bright and dull, (3) bluish - both bright and dull, (4) fairly abrupt dimmings or darkenings, and (5) obscurations, which may be accompanied by any of the other four manifestations. The number of lunar features exhibiting such anomalies is less than 200 that have been reported at least once, but 80% of all observations are found in less than a dozen sites and 60% are found in about 1/2 dozen sites.

Extensive analyses with respect to several hypotheses show various correlations with various hypotheses, depending on how the data are divided. The most quantitative analysis to date shows that, for 759 observations for All Sites ($\sim$100 sites) with respect to the tidal effect hypothesis, there is a real dirth of phenomena in the first half of the anomalistic orbit (from perigee to apogee) and almost equal numbers for each 0.1 period from 0.6 to 1.1, in the last half (from apogee to perigee). There is not a concentration at perigee as is so frequently stated in the literature without statistical foundation. The correlation originally found by Middlehurst for 145 observations of All Sites has changed with the increase in number of observations. For other hypotheses such as magnetic tail, direct solar flare and sunrise effects, in 781 observations there were high correlations with sunrise and magnetic tail and a surprising number of coincidences of lunar and terrestrial magnetic storm events. When the data are compared with the number or percent expected on an even distribution of observations (thus no effects), the highest correlation for all data was with sunrise, but was also high for magnetic tail and had decreased considerably for tidal. Correlations will be illustrated. Behavior of the 1/2 dozen individual most active sites varied in their correlations, especially surprising was the quite different behavior between Aristarchus and Schroter's Valley. The distribution of the LTP sites is non-random and shows a strong bias for the edges of the maria, implying a genetic relation to them and to volcanism. Surprisingly, there is little or no correlation between LTP sites and the seismic zones obtained from the Apollo seismic experiments. None of the most frequently reported LTP sites are seismic sites - the two or three coincidences are of rarely reported LTP sites.

The LTP program I am supervising now for the Association of Lunar and Planetary Observers is designed to monitor the LTP sites, the seismic epicenter sites and non LTP-comparison sites. First year results from this, in which valuable negative observations are reported indicate the ratio of LTP to normal aspects is about one in 12 or 8%.

INTERACTION OF THE SOLAR WIND WITH MERCURY

K. W. Behannon, R. P. Lepping, N. F. Ness, and Y. C. Whang
NASA/Goddard Space Flight Center, Greenbelt, Maryland 20771

The first measurements in-situ of the nature of the magnetic and electric characteristics of the planet Mercury and interactions associated with the super Alfvênic, collisionless magnetized solar wind plasma flow have been conducted by instruments on the Mariner 10 spacecraft. Passing on the dark side of the planet on 29 March 1974, detailed measurements of the magnetic field, solar plasma electrons and energetic particles were made. Mercury is similar in physical size and surface characteristics to the Moon and we have detailed knowledge of the lunar magnetic and electrical properties and interaction characteristics from the Explorer 35, AISEP and Apollo subsatellite experiments. No bow shock is observed at the Moon and the solar wind wake perturbations of the magnetic field and plasma are small and depend upon surface and near surface magnetic/electrical characteristics as well as the plasma-field characteristics of the solar wind. The observed features of the solar wind-moon interaction are shown in model A of Fig. 1. This is the weakest type of interaction observed, and no bow shock is seen to develop. In all of the other models shown, a bow shock develops because of the deflection of super-Alfvênic flow around the planet. This deflection is due to (B) a sufficient atmosphere-ionosphere, (C) a sufficiently conducting planetary interior, or (D) a sufficient intrinsic planetary field, as in the case of the earth.

Very clear experimental evidence was obtained by the magnetic field and plasma experiments of the presence of a well developed bow shock wave. It appears that the obstacle to solar wind flow is "global" in size, i.e.,

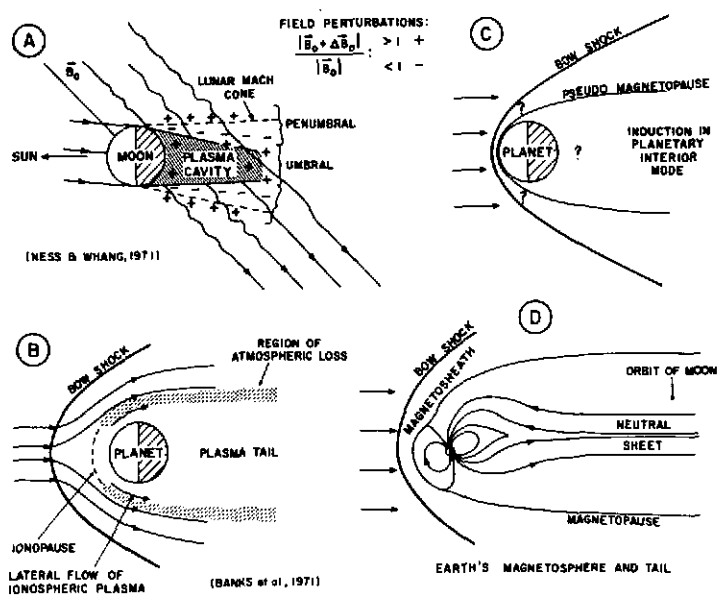

Figure 1

somewhat larger than the planet. As Mariner 10 approached closer to the planet, the magnetic field increased very smoothly to a maximum of 98 gammas at closest approach (730 km from the surface). The characteristics of this variation can be seen in Fig. 2 in the 6-sec. average field intensity $\overline{F}$. The effects of the inbound bow shock wave and "planetary field" boundary are also clearly seen. Vector directional variations during the encounter are shown by the solar ecliptic longitude angle ϕ and latitude angle θ, and RMS is a measure of the 6-sec. vector field fluctuation amplitude. Preliminary analyses suggest that the magnetic field on the surface of Mercury perhaps ranges from 100 to 2000 gammas. This is more than sufficient to deflect the solar wind and create the observed bow shock.

The origin of the observed enhanced magnetic field has not yet been uniquely established, but the complete body of data favors the conclusion that Mercury has an intrinsic magnetic field. The identifications of the

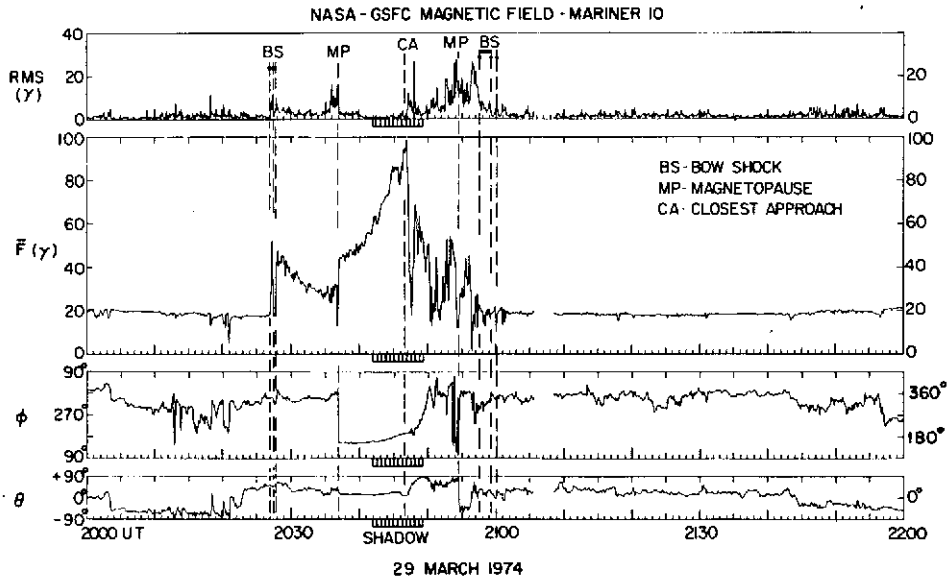

Figure 2

shock and planetary field boundary locations by both the magnetic field and plasma science experiments are in excellent agreement. The most plausible shock geometry resulting from the combined observations corresponds to a position relative to Mercury which is not consistent with direct electric contact between the solar wind and either a planetary ionosphere (if it exists) or the planetary surface. Such contact is required for the steady state or unipolar induction mode. Because of (1) this lack of direct contact, (2) the existence and topology of a magnetosphere-like region, and (3) the results of comparative solar wind interaction studies, it is concluded that this mode of interaction was not responsible for the magnetic field observed at Mercury. The transient induction mode cannot be ruled out

INTERACTION WITH MERCURY

Behannon, K. W. et al.

completely at present, but because of the very special set of circumstances required, it is a less plausible source of the observed field than to assume that Mercury has a modest intrinsic magnetic field. Such a field could be the result of a currently active internal dynamo or it may be a residual remanent magnetic field associated with a now estinct dynamo. The anomalously high average density of Mercury suggests the presence of a large iron core. The temperature may be high enough in the core, due to the presence of radioactive elements and the low thermal diffusivity of the mantle material, to support the fluid motions necessary for magnetic field generation even at Mercury's slow spin rate. It is also possible that Mercury rotated faster earlier in its history. Fig. 3 shows comparison of the observed field with a theoretical planetary field due to an offset, tilted dipole. Some of the lack of agreement between this model and the observations can be attributed to the distortion of the true field by the solar wind, by time variations in the field, and/or by the possibility that the field contains contributions from higher order multipoles that were observable at the close approach distance of the Mariner 10 flyby. The problems associated with fitting a model field to such data will be discussed.

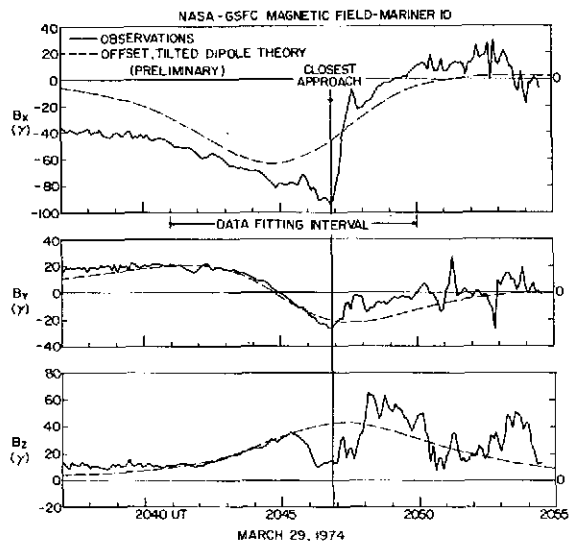

Figure 3

Assuming that the intrinsic dipole interpretation is correct, the large offset and modest size of the dipole moment suggest that under normal conditions Mercury should not have a trapped radiation belt. However, a magnetic tail should exist and should contain an embedded neutral sheet. Also because of the large dipole offset, the stagnation point distance should change considerably during the Mercurian year. Because of the changing value of the planetary field in the subsolar region it should be possible at times for the solar wind to compress the planetary field to the surface. The optical properties of the surface should thus reflect the effects of proton bombardment characteristically observed on the lunar surface.

NOBLE GASES AS SENSORS FOR REGOLITH EVOLUTION;

P. Signer, H. Baur, H. Ducati, U. Frick, H. Funk, Swiss Federal Institute of Technology, 8006 Zürich, Sonneggstr. 5, Switzerland

Some properties of the lunar regolith are the result of mechanical effects and of corpuscular and electromagnetic irradiation. The noble gas pattern in lunar samples represents a distinguished record of these processes. These noble gases are of solar (trapped gases), atmospheric (excess ^{40}Ar) or in-site (spallogenic or radiogenic gases) origin. Their present day distribution within the grains is also determined by mineral-specific sputtering and diffusion processes which in turn depend on thermal and irradiation history, on regolith turnover and shielding conditions. If these processes and their effects on the noble gas concentrations and distributions are understood, then one has an ideal sensor for regolith evolution. Our approach in this context consists in the mass spectrometric analysis of grain size fractions of mineral seprates. The results of our measurements of He, He and Ar in seprates from the soils 15421 and 15301 (1) pertinent in the context of the conference topic can be summarized as follows.

1. Solar Flare Noble Gases

We consider the following experimental observations which concern noble gases in feldspar from soil 15421 as due to solar flare irradiation leading to detectable amounts of solar flare light noble gases.

a) We assume a constant concentration of spallogenic argon in all grain sizes of the feldspar separate investigated. Then the 36-Ar/38-Ar ratios of the surface correlated argon are not independent of grain size and imply two isotopically different components occurring with grain size dependent mixing ratios. For the component predominating in small grains, a 36-Ar/38-Ar ratio of 5.45 $\pm$ 0.1 is extrapolated whereas the respective ratio in the component prevailing in large grains appears to be less than 5.0. In 100 μm grains, the component thought to be of solar flare origin amounts to about 20% of the total surface correlated argon. The concentration of non-equilibrated solar flare Ar, as evaluated in (1) and the surface residence time, deduced from a regolith turnover rate of (.5 - 1) x E7 y/cm (2,3), enable us to determine the solar flare 36-Ar flux. A value of about .5 x E8 particles/cm^2 y results which is in good agreement with a value estimated from solar flare iron flux, given in (4).

b) In feldspar He, Ne and Ar concentrations show a characteristic correlation with grain size, which can be understood, assuming most surface correlated gas distributed in an outer layer of about 10 μm thickness. This depth is consistent with the penetration depth of solar flare noble gases, although we cannot exclude solar wind particles diffused into considerable depth. This unique feature of feldspar may be explained as follows. The amounts of solar particles on the grain surface equilibrate depending on sputter rate and penetration depth of solar wind and solar flare particles. The low penetration of SW noble gases together with increasing sputter rate decrease the portion of SW against SF noble gases. For feldspar sputter rates which are about one order of magnitude larger than those measured for Fe, Mg-silicates or ilmenite have been found (e.g. 5).

c) In 15421 soil feldspar we obtained evidence for solar cosmic ray proton produced Ne. The evaluated spallogenic Ne ratios are clearly different from those inferred from "shielded" lunar rock and meteoritic feldspar. No such evidence

NOBLE GASES AS SENSORS

Signer, P. et al.

is detectable in olivine-pyroxene and green glass separates because of chemical composition and short solar exposure, respectively. In principle, it is possible to determine the exposure time for solar and galactic cosmic irradiation. However, more precise data on neon production rates, chemical composition and mineralogical homogeneity are needed.

2. Small Scale Regolith Evolution

The following observations have implications on the small scale evolution of the lunar regolith.

a) The variability of the 36-Ar/38-Ar ratios of the surface correlated argon mentioned above can only be understood if the integrated surface residence times are, on the average, grain-size dependent. Small grains are residing on the lunar surface frequently but for a comparatively short time only. In the 15421 soil, small feldspar grains appear to have been exposed to solar irradiation long enough to become equilibrated with solar wind gas over the total surface, whereas the exposure time was not sufficient to allow saturation with solar flare gases. Larger grains have on the average a longer integrated surface residence time and thus contain a larger fraction of solar flare gases.

b) Collection site dependent element abundance patterns of bulk soils are considered to reflect mostly mineral specific retentivities which is substantiated by measurements on ilmenite (6,7) olivine-pyroxene, green glass and feldspar (1,8).

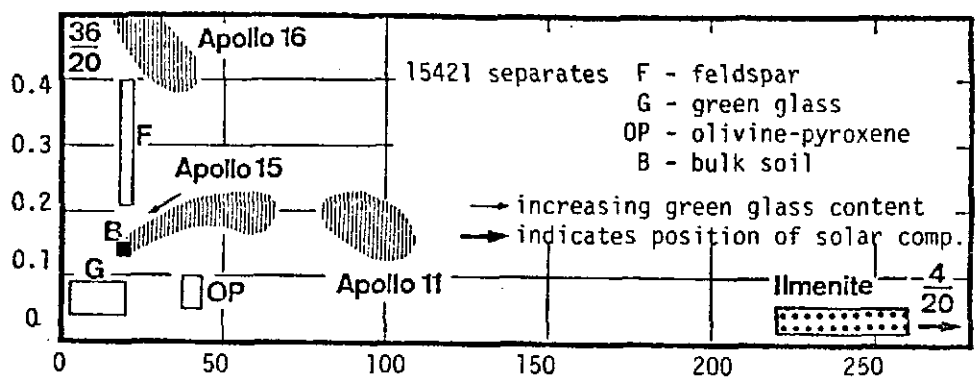

Elemental abundance signature of surface correlated noble gases in lunar soil separates and typical bulk soils, (Ilmenite, ref.6,7)

Of particular interest are the APOLLO 15 green glasses. Their cosmic ray exposure times are the same, - about 300 my. The concentrations of solar Ar in green glasses from soil 15421 (1) and clod 15426 (9) are, however, about a factor of ten lower than those from soil 15301 which compares to solar Ar concentrations found for other minerals and shows the same typical elemental pattern as the other green glass samples. From this we are led to speculate that
- elemental abundance pattern are established rather rapidly,
- green glasses have been exposed to solar irradiation for a short time which may be responsible for the lacking correlation between noble gas concentration and grain size. The well established correlation in bulk soil and mineral grain-size fractions is understood in terms of repeated solar exposure episodes. Thus an effective irradiation of the whole surface is secured.

c) 20-Ne/21-Ne and 22-Ne/21-Ne ratios of surface correlated Ne come out to high by a factor of 3. This is explained by grain-size dependent loss of spallogenic Ne and could have occurred indpendently of solar irradiation. But the dependence of this loss on the surface correlated gas distribution, as demonstrated by our model calculations, indicate that the surface layer of feldspar grains was depleted during solar irradiation in spallogenic Ne. This goes together with the above conclusions that solar exposure occurred indeed repeatedly and intermittently during the whole galactic cosmic ray exposure which in turn would have occurred repeatedly and intermittently.

3. The 40-Ar Excess as Sensor for the Lunar Atmosphere

The 40-Ar excess in lunar fines is attributed to retrapping of 40-Ar from the lunar atmosphere (10) and the variations of the 40-Ar/36-Ar ratios of the surface correlated argon is taken to reflect changes in the atmosphere density and/or modulations due to geographic latitude and slope of the collection site. In olivine-pyroxene, feldspar and green glass from soil 15421 we found for the surface correlated argon 40-Ar/36-Ar ratios of 3.5 ± 0.5, 7.4 ± 0.2 and about 10, respectively. These mineral specific ratios imply that the 40-Ar/36-Ar ratios in bulk soils are, at least partially, influenced by the mineralogic composition of the soils. Trapping efficiencies for low energy Ar are presumably similar in the silicates investigated and Ar retentivity determined by sputtering and diffusion appears to be lower in feldspar than in olivine-pyroxene. Thus, a low ratio would be expected in feldspar if all excess 40-Ar would have been retrapped. Retrapping as sole source for excess 40-Ar may also be questioned on the basis of the comparatively high 40-Ar fluxes required to cause the present-day 40-Ar/36-Ar ratios, the interdependance from the ancient lunar magnetic field (if retrapping occurred in ancient times) and the failure to detect the N-S shielding expected to be operable for recent retrapping. In summary, we maintain that surface correlated 40-Ar has at least one more source besides retrapping from the lunar atmosphere and is thus not exclusive sensor for the lunar atmosphere evolution. Our favored interpretation of the mineral specific surface correlation 40-Ar/36-Ar ratio rests on the transient potassium hypothesis (11,12).

This research has been supported by the Swiss National Science Foundation, Grant No. 2.589.71.

References:

(1) U.Frick, H.Baur, H. Ducati, H.Funk, D.Phinney & P.Signer, (1974) submitted to Geochim. Cosmochim. Acta.

(2) T.Kirsten, F. Steinbrunn & J.Zähringer, (1971) Geochim. Cosmochim. Acta, Suppl. 2, Vol. 2, 1651-1669.

(3) D.E.Gault, F.Hörz, D.E.Brownlee & J.B.Hartung, (1974) Lunar Science V, Part I, 260-262.

(4) P.B.Price, J.H.Chau, I.D. Hutcheon, D.McDougall, R.S.Rajan, E.K.Shirk & J.D.Sullivan, (1973) Geochim. Cosmochim. Acta, Suppl. 4, Vol.3, 2347-2361.

(5) J.P.Bibring, Y.Langevin, M.Maurette, R.Meunier, B.Jouffrey & C.Jouret, (1974), Earth Planet Sci. Lett., 22, 205-214.

(6) P.Eberhardt, J.Geiss, H.Graf, N.Grögler, U.Krähenbühl, H.Schwaller, J.Schwarzmüller & A.Stettler, (1970) Geochim. Cosmochim. Acta, Suppl. 1, Vol.2, 1037-1070.

(7) P.Eberhardt, J.Geiss, H.Graf, N.Grögler, M.D.Medina, M.Mörgeli,H.Schwaller, A.Stettler, U.Krähenbühl & H.R.v.Gunten, (1972) Geochim. Cosmochim.Acta, Suppl. 3, Vol. 2, 1821-1856.

(8) U.Frick, H.Baur, H.Funk, D.Phinney, Chr.Schäfer, L.Schultz & P.Signer, (1973) Geochim. Cosmochim. Acta, Suppl. 4, Vol. 2, 1987-2002.

(9) S.Lakatos, D.Heymann & A.Yaniv, (1973) The Moon, 7, 132-148.

(10) D.Heymann & A.Yaniv, (1970) Geochim. Cosmochim. Acta, Suppl. 1, Vol.2, 1261-1267.

(11) H.Baur, U.Frick, H.Funk, L.Schultz & P.Signer, (1972) Geochim. Cosmochim. Acta, Suppl. 3, Vol.2, 1947-1966.

(12) P.Signer, H.Baur, U.Frick, H.Funk, D.Phinney & L.Schultz, (1973) Meteoritics, Vol.8, No.4, 441-443.

ON THE MAGNETIZATION OF THE MOON BY THE SOLAR WIND;
L. J. Srnka, The Lunar Science Institute, Houston, Texas 77058.

The source of the ancient lunar magnetic field is one of the outstanding problems of lunar science. Studies of lunar samples suggest that fields of order 10^3 - 10^4 γ were present on the lunar surface from 4.6 - 3.1 b.y. ago[1]. A number of models for the ancient field have been presented, including deep and shallow internal convecting dynamos, fossil (whole-body) remanence, and solar wind effects.

Ancient lunar fields derived from solar wind sources can be divided into two types: (1) fields associated with a possible T Tauri phase of the primordial sun, during the first 10^7 - 10^8 years of solar system history, and (2) fields induced in the moon by the solar wind, after the T Tauri stage and up to the age of the youngest lunar samples.

If the sun exhibited a T Tauri stage in its evolution during the accretion of the moon, the enhanced solar wind flow could have heated and magnetized the lunar crust[2,3]. Both TE mode (internal eddy currents) and TM mode (unipolar dynamo) electrical induction may have been present. Although the peak value of the induced field in the TE response is not yet available from theory[4], the TM mode peak field at the surface could have approached 2 x 10^5 γ (2 gauss) if the lunar crust was sufficiently conducting[5]. However, the TE mode fields would lead to random magnetization of lunar material, with perhaps some preferred direction (transverse to the ancient solar wind motional electric field vector) for the TM mode. The general randomness of the response fields is due to the magnetic sector structure of the solar wind, the expected turbulence in the flow[3], and the rotation of the moon. It is conceivable that the solar field possessed an out-of-ecliptic (quadrupole) component along the lunar spin axis sufficient to give the whole moon a fossil magnetization[3], but this component would not give a preferred direction for electrically induced magnetization because of the lunar rotation.

After the T Tauri phase, the solar wind probably resembled the present tenuous flow. Because of the small dynamic plasma pressure, the peak TM mode surface field would be approximately 60 γ for a nominal quiet solar wind[6,7], too small to be the source field for the observed remanence in lunar samples. If the TE mode is to produce $\sim$ 2000 γ at the surface, large near-

ON THE MAGNETIZATION OF THE MOON

Srnka, L. J.

surface bodies of high electrical conductivity are required. This large amplification (a factor of 2-400 over the ambient field) can only occur if the electrical skin depth δ of the conductor at the highest frequencies in the plasma is much less than its thickness[8,9]. The most highly conducting bodies at the lunar surface would be lava flows and impact melts. Although the electrical conductivity of such bodies is unknown, it is suggested here that 1-10 $(\Omega\text{-m})^{-1}$ characteristic of molten terrestrial basalts[10] is representative. In this case,

$$\delta \approx \frac{160}{f^{\frac{1}{2}}} \text{ (meters)}$$

where f is the frequency (Hz) of the magnetic disturbance in the solar wind. Most of the power in the magnetic spectrum of the solar wind is associated with the alternating sector structure, with $f \times 10^{-5}$ Hz, and the power shows a frequency dependence $\sim f^{-1.6}$ at higher frequencies[11,12]. Plasma particle effects limit the power to $f \leq 1$ Hz in the present solar wind field at 1 AU, determined by the ion gyro frequency. Therefore, thicknesses $\sim 10^2 - 10^3$ m of molten basalt would be necessary to appreciably amplify the solar wind magnetic field at the lunar surface by TE mode induction. Recent evidence indicates that lunar lava flows have thicknesses of 5-10 m[13]. Very large craters may have had impact-melt pools with depths of hundreds of meters, but there is insufficient data available to allow further speculation.

In conclusion, it seems unlikely that TE or TM mode electrical induction can explain the observed remanence of lunar samples whose ages span 1.5 b.y. Unless the sun was very active up to $\sim$ 3 b.y. ago, with an enhanced turbulent plasma flow containing powerful magnetic fluctuations above $f \approx 100$ Hz, neither induction mode is a good candidate to produce 2000 γ surface fields in an initially cold moon, after the conjectural T Tauri solar episode.

References

1. Fuller, M.: 1974, Rev. Geophys. Space Phys., 12, 23.
2. Sonett, C. P., Colburn, D. S. and Schwartz, K.: 1968, Nature, 219, 924.
3. Sonett, C. P., Colburn, D. S. and Schwartz, K.: 1974, Proc. Fifth Lunar Science Conf., Geochimica et Cosmochimica

ON THE MAGNETIZATION OF THE MOON

Srnka, L. J.

Acta, Suppl. 5, in press.
4. Sonett, C. P.: 1974, private communication.
5. Srnka, L. J.: 1973, Ph.D. Thesis, University of Newcastle upon Tyne, England.
6. Hundhausen, A. J.: 1970, Rev. Geophys. Space Phys., 8, 729.
7. Sonett, C. P. and Colburn, D. S.: 1967, Nature, 216, 340.
8. Hollweg, J. V.: 1970, J. Geophys. Res., 75, 1209.
9. Schubert, G. and Schwartz, K.: 1969, The Moon, 1, 106.
10. Presnall, D. C., Simmons, C. L. and Porath, H.: 1972, J. Geophys. Res., 77, 5665.
11. Siscoe, G. L., Davis, L., Jr., Coleman, P. J., Smith, E. J. and Jones, D. E.: 1968, J. Geophys. Res., 73, 61.
12. Blake, D. H. and Belcher, J. W.: 1974, J. Geophys. Res., 79, 2891.
13. Howard, K. A., Head, J. W. and Swann, G. A.: 1972, Geochimica et Cosmochimica Acta, Suppl. 3, 1.

LUNAR REMNANT MAGNETIC FIELD MAPPING FROM ORBITAL OBSERVATIONS OF MIRRORED ELECTRONS. J. E. McCoy, NASA/Johnson Space Center, Houston, Texas 77058; K. A. Anderson, R. P. Line, H. C. Howe, and R. E. McGuire, University of California, Space Sciences Laboratory, Berkeley, California 94720.

As described previously (1), observation of energetic electron fluxes from lunar orbit using a detector sectored to distinguish direction of arrival with respect to the ambient magnetic field direction can be used to detect lunar surface magnetic field enhancements with a high degree of sensitivity and spatial resolution. The regions of intense lunar remnant magnetization discovered by the Apollo 15 and 16 PFS satellite magnetometers were observed to strongly scatter 14 Kev electrons back up the magnetic field lines to arrive at the satellite from directions blocked from direct access by the Moon. Such scattered return (mirrored) electron fluxes have also been observed from numerous other locations on the lunar surface, including several previously unreported.

The electrons, in effect, provide a probe along the magnetic field line from orbit to the lunar surface. This probe is sensitive to changes in field strength along its path. If no surface magnetization is present, the electrons are guided by the external magnetic field into the lunar surface where they are absorbed (except for a few percent which are coulomb backscattered). If surface remnant magnetism is present, the total field strength increases as the electrons enter the region of remnant magnetism, causing a fraction of the electrons to mirror or backscatter with an intensity (which may be observed from orbit returning along the field line from the surface) proportional to the strength and spatial extent of the surface field volume.

Since the energetic electrons needed to serve as field line tracers are always present in the lunar environment (2), this method is useable when the Moon is in the solar wind as well as when the Moon is in high latitude magnetotail. The primary requirement on stability of the ambient magnetic field is to provide directional reference to the location of intersecting the lunar surface during the period of each measurement (24 sec). Best results are obtained when electron fluxes are high enough ($>10/cm^2$sec ster Kev) to give good counting statistics and the external ambient field is oriented within 30°-40° of perpendicular to the lunar surface (to reduce errors involved in projecting the satellite observed field direction to determine the location of the surface point being observed).

Resolution of the technique is controlled by the gyro-radius of the electrons' spiral path along a field line, about 40 km for a 14 Kev electron in a typical 10 gamma external magnetic field. This, coupled with the orbital motion of about 1.6 km/sec, results in a probe averaged over an area roughly 80 km by 120 km for each 24 sec data cycle.

LUNAR REMNANT MAGNETIC FIELD MAPPING ...

McCoy, J. E. et al.

If the scale of the remnant field change is large compared to the gyro-radius, electrons of a given pitch angle (α) will be adiabatically mirrored back from any region where B exceeds the value

$$B_m = B/sin^2\ \alpha$$

where B and α are the magnetic field strength and pitch angle at the satellite orbit. Therefore, any large scale ($\geq$100 km) area of surface remnant field causing as little as 0.1 gamma increase in the total surface field (B_m) over that remaining at orbital altitude will mirror all incident electrons with pitch angles between 90°- 96°. This would result in observation of a return flux in Sector II (45°- 90°) of about 13% of the incident flux observed in Sector III (90°- 135°), more than twice the background in that sector due to coulomb backscatter from the unmagnetized lunar surface. Since extensive areas of the lunar surface on both sides of the Moon are observed to mirror less than 10% - 20% of the incident electrons in these sectors, this places a rather strong upper limit on the size of any net lunar dipole moment of about $10^{10}\gamma$-km^3 (i.e., radial component of any uniform lunar remnant magnetism is less than 2γ at the lunar surface between ±30° latitude).

If the spatial scale of the remnant magnetism is comparable or smaller than an electron gyro-radius, the electrons will undergo more complex scattering. This will still result in a significant return flux backscattered up the field line, if the region is of sufficient strength and volume to turn the electron's path upward before it hits the surface. For example, a subsurface dipole (15 km deep, moment of $2\times10^5\gamma$-km^3) was calculated (3) to backscatter about 50% - 60% of the incident flux into Sectors I and II in a 10γ external field. Such a remnant field would have a strength of 60γ at the lunar surface, falling off to 0.1γ at 100 km orbital altitude. Such scattering areas are distinguishable from an area of adiabatic mirroring by the more random pitch angle distribution of returning electrons. Sector II (45°- 90°) will show less than 100% returning flux, while Sector I (0°- 45°, which requires stronger scattering to mirror) shows a significant number of returning electrons. For the case of purely adiabatic mirroring, all electrons with pitch angles above the critical value $\alpha=sin^{-1}\sqrt{B/B_m}$ will mirror back to the satellite, while all electrons with smaller pitch angles impact the lunar surface. This would require the flux ratio between Sector II/ Sector III increase to unity before any mirrored flux would appear in Sector I.

As well as independent verification of the location of magnetic anomalies reported by the UCLA magnetometer group near the crater Van de Graaff with PFS-1 and near 149°E and 165°E (8°N) with PFS-2 data, this method has been used to locate previously unreported areas of remnant magnetism on both the

front and back sides of the Moon. Locations of several are listed in Table 1.

The probable utility of this electron scattering technique for generation of maps of lunar surface remnant magnetism is illustrated in Figure 1, which is a plot of electron backscattered intensity observed in Sector II (upper group) and in Sector I (lower group) for four orbital passes across the Van de Graaff region. Each trace is displaced 50% in vertical scale for legibility. Portions of data for which return flux is less than 25% are deleted for legibility. The ground track is displaced about 30 km per orbit by lunar rotation. Evidence of numerous non-adiabatic scattering centers is seen, perhaps surrounded by areas of adiabatic scattering visible in Sector II. The scattering centers run together between 140°- 175°E. Only a single isolated area of scattering is observed east of 150°W.

Longitude	Latitude
55W	16S
14W	7S
50W	10S
42W	10S
153W	0S
111E	10N
169E	6N

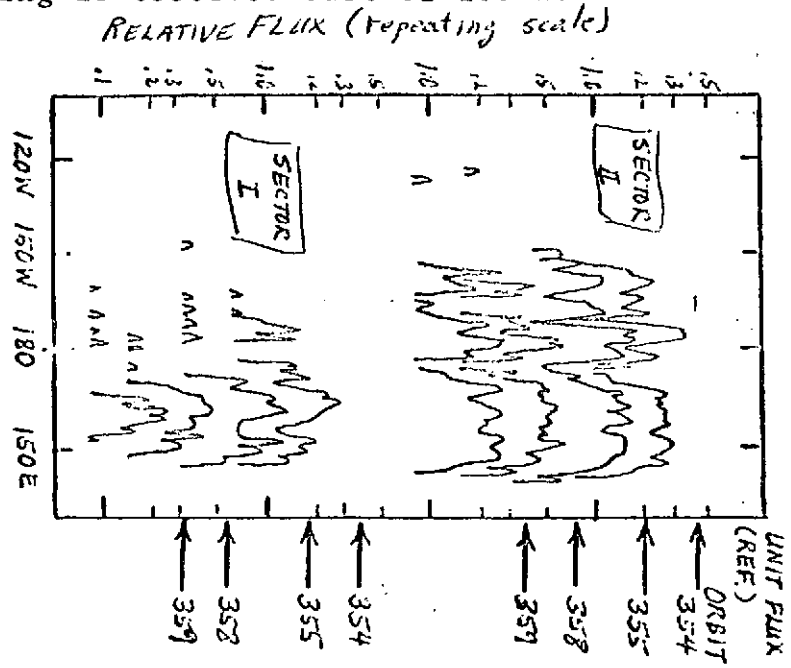

Acknowledgments

This work was partially supported by NASA Contract NAS9-10509. Magnetic field data were provided by the UCLA magnetometer group.

References

1. Anderson, K. A., H. C. Howe, R. P. Lin, R. E. McGuire, L. M. Chase, and J. E. McCoy, Observation of energetic electron mirroring from the lunar remnant magnetic field (abstract), Fifth Lunar Science Conf., Houston, Texas 1974.
2. Anderson, K. A., L. M. Chase, R. P. Lin, J. E. McCoy and R. E. McGuire, Solar wind and interplanetary electron measurements on the Apollo 15 subsatellite, *J. Geophys. Res.* 77, 4611, 1972.
3. Howe, Herbert C., R. P. Lin, R. E. McGuire, and K. A. Anderson, Energetic electron scattering from the lunar remnant magnetic field, *Geophys. Res. Letters* 1, 101, 1974.

ELECTROSTATIC MIGRATION, SURFACE EXPOSURE, AND LAYERING. G.J. Williams, Dept. of Astron., Cornell Univ., Ithaca, N.Y. 14850.

Surface exposure effects can be used to decide the extent to which material has been implaced by random churning as opposed to systematic deposition of each grain. In the former, a very great variety in degree of surface exposure will result. In the latter, each must have been exposed in order to reach its present site. Calculations therefore have been performed concerning the processes, and the result is that they tend to favor orderly processes (among which is surface or above-surface transport) rather than mere churning. The observed distributions in near-surface residence time of grains of lunar material (as judged from solar and galactic cosmic ray track densities, neutron exposure, and albedo) are considered. A three-dimensional model of meteoritic surface tilling was used to yield Monte Carlo statistics for exposure ages. The theoretical results clearly indicate the necessity of additional processes having been at work -- grain-by-grain horizontal transport along or above the surface and/or exposure of the material in space before accretion onto the Moon. (This is so because cratering and blanketing by meteorites, reaching to any average depth one wishes, necessarily entails admixture of unexposed grains from beneath. A rigid cut-off in maximum cratering depth would be required, with thorough processing of all the material down to that depth, which is statistically inadmissible.) The current calculation was motivated by the indications of the earlier one-dimensional mixing study by Gold and Williams (1974). Impact ejecta blankets were taken here to have thickness equal to an eighth the crater depth, and the relative frequencies of cratering to various depths deduced by Shoemaker et al. (1971) were employed. Requisite rates of transport and/or accretion are discussed.

The model also was used to determine: (i) the amount of homogenization which results when one has meteorite reworking to various depths and (ii) the typical vertical distance over which properties of the material can change by a certain amount. The ejecta blanket is taken to preserve some of the layering which was present at the impact site. Comparison to layering in lunar core samples again emphasizes the inadequacy of meteoritic redistribution.

References (1)Gold T. and Williams G.J. (1974) On the exposure history of the lunar regolith. Proc. Fifth Lunar

ELECTROS, MGRTN., SRFC. EXPSR., AND LAYERING

Williams, G. J.

Sci. Conf., Geochim. Cosmochim. Acta, Suppl. 5, in press.
(2)Shoemaker E.M., Hait M.H., Swann G.A., Schleicher D.L., Schaber G.G., Sutton R.L., Dahlem D.H., Goddard E.N., and Waters A.C. (1970) Origin of the lunar regolith at Tranquillity Base. Proc. Apollo 11 Lunar Sci. Conf., Geochim. Cosmochim. Acta, Suppl. 1, Vol. 3, pp. 2399-2412. Pergamon.

SPALLOGENIC AND "COSMOGENIC" XENON-YIELDS FROM BARIUM IN THIN- AND THICK-TARGET-EXPERIMENTS; THE NATURE OF THE Xe-131 ANOMALY

W.A. Kaiser, K.P. Rösner, and W. Herr

Institut für Kernchemie der Universität zu Köln, 5 Köln 1, Zülpicherstr. 47, West Germany

Thin Target Xe-σ(spall.) from Barium were determined in 10 steps for proton energies ranging from 50 - 600 MeV by means of rare gas mass spectroscopy and independently by γ-counting (Fig. 1).Rather surprising results were obtained. Xe-124, Xe-126, and Xe-127 increase monotonically with energy covering up to 4 orders of magnitude in their σ(spall.). Xe-128, Xe-129, and Xe-131 show maxima in their excitation functions at low energies (100 - 300 MeV) whereas Xe-130, Xe-132, and Xe-134 display minima in this energy region. Thus, the purely spall. Xe-131/Xe-126-ratio as a function of energy changes abnormally from 1.139 +- .037 to 247.9 +- 3.8. The presence of spall. Xe-136 was established. Estimation of the spall. Xe-production rates by using the galactic cosmic ray (GCR) spectra given by REEDY and ARNOLD [1] for different depths in the lunar surface (2π-geometry) led to strong variations of the Xe-ratios with depth (Fig. 2 and 3) sufficient to explain most of the variations of the "cosmogenic" Xe-ratios found in extraterrestrial matter whereby especially the relativly wide range of the spall. Xe-131/Xe-126-ratio (2.3 at 0 g/cm^2 - ~7 at 500 g/cm^2) is remarkable.

A "Lunar Surface" simulating Thick Target was exposed to 1.9 +- .3 x 10^{16} protons of 600 MeV at the synchro cyclotron at CERN (Genève) nuclear research facility. The experimental arrangment was of the dimensions 50 x 50 x 140 cm. The material used was of the composition of the soil at the APOLLO 11 landing site (MORRISON et al.)[2] and had a ρ = 1.5 g/cm^3. Some of the nuclear reactions occuring on the moon and caused by the GCR were studied. Especial consideration was given to the spatial distribution of spallogenic and n-capture produced Xe-isotopes on Ba-targets. Associated but independent experiments (MICHEL et al.[3], WEIGEL et al.[4], and THIEL et al.[5]) simultaneously executed were used for obtaining the spatial and energetic distribution of the protons and the neutrons (Fig. 4). The spatial distribution of the produced Xe-isotopes was determined by 45 high vacuum molten $BaCl_2$-probes kept under vacuum in quartz containers with breakable seals. The purely spall. Xe-124/Xe-126-ratio had for pencil geometry its maximum value of .723 +- .002 at a depth of 0 g/cm^2 and its minimum value of .343 +- .014 at a depth of 180 g/cm^2 in beam center (Fig. 5). This confirms the result of the Thin Target study that this particular ratio decreases with decreasing p-energy. The Xe-M/Xe-126-ratios for M = 128, 129, 130

SPALLOGENIC AND "COSMOGENIC" XENON-[illegible]

Kaiser, W. A. et al.

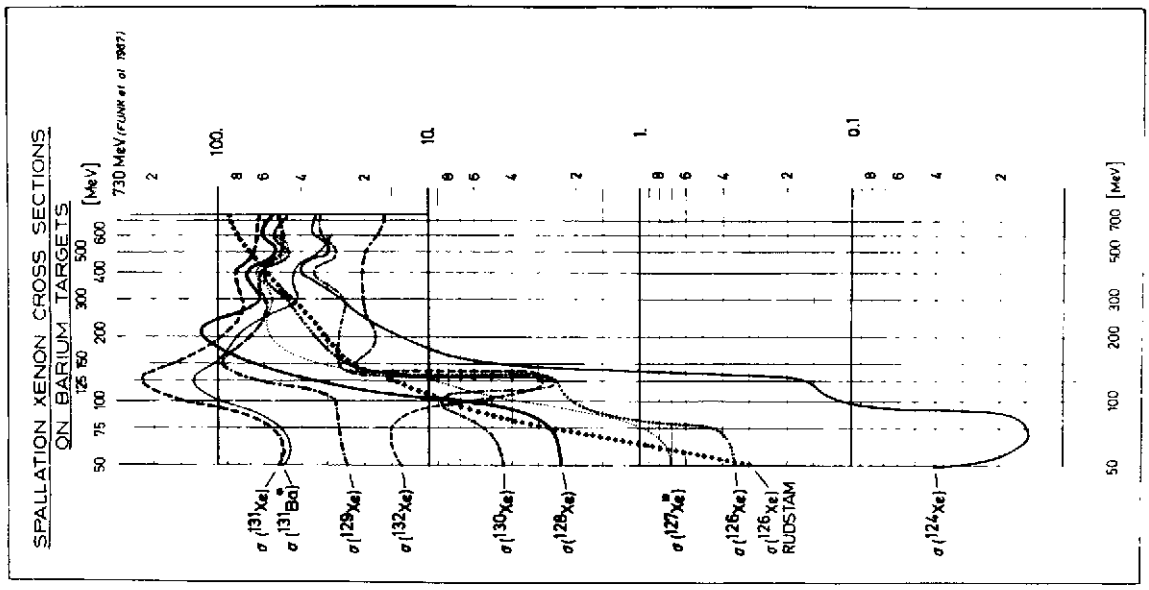

Fig. 1

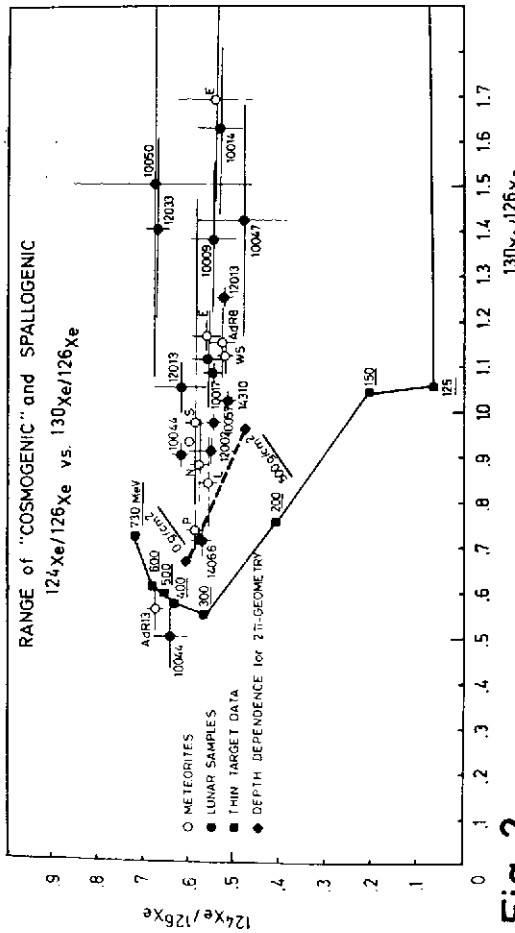

Fig. 2

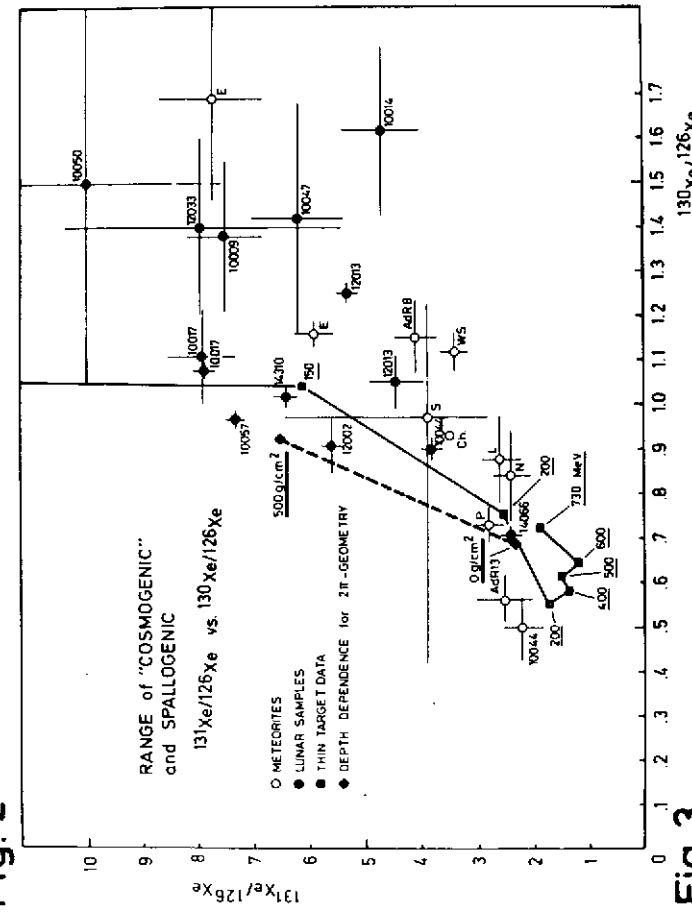

Fig. 3

SPALLOGENIC AND "COSMOGENIC" XENON-YIELDS...

Kaiser, W. A. et al.

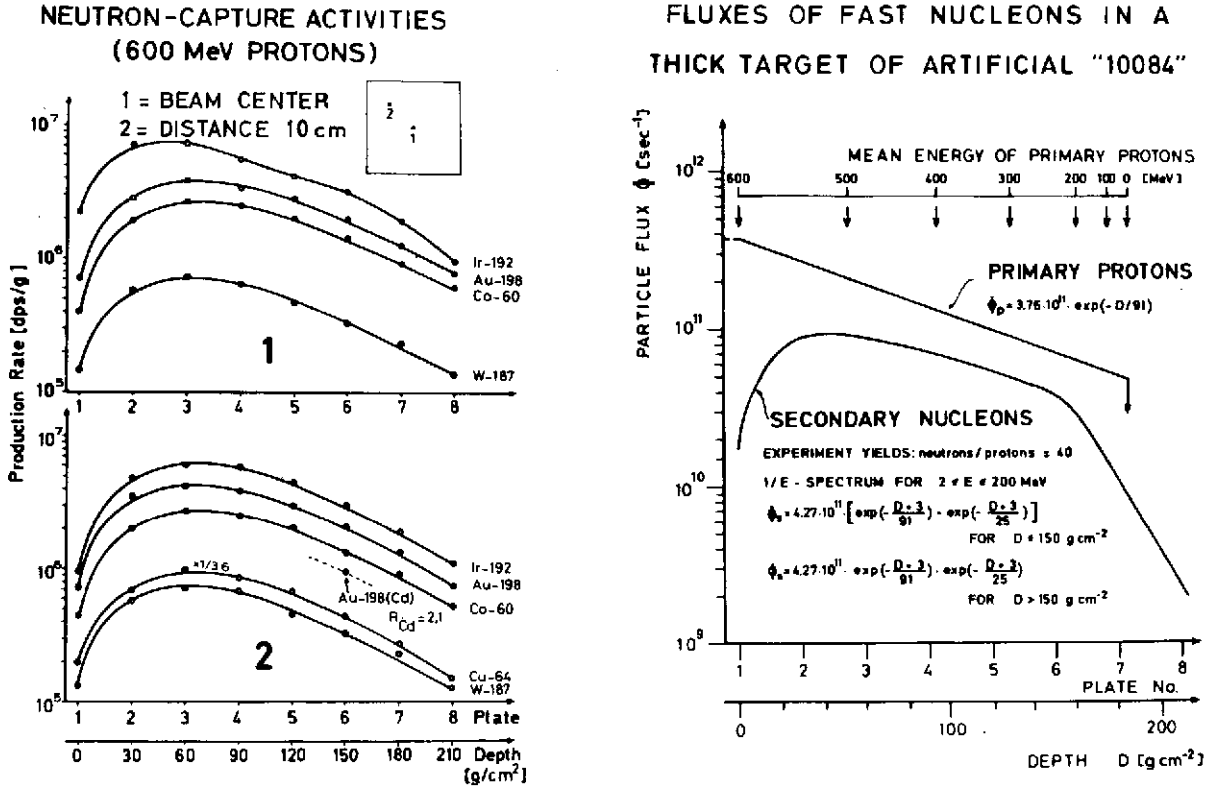

Fig. 4 (MICHEL et al.) [3]

131, 132, and 134 show essentially similar distribution patterns. They have their maximum- and minimum-values in beam center - anti-correlated to the Xe-124/Xe-126-ratio - whereby the maximum values are all at a depth of 180 g/cm^2. Thus, e.g. the spall. Xe-128/Xe-126-ratio ranges from 1.103 +- .004 at 0 g/cm^2 to 2.912 +- .037 at 180 g/cm^2; the spall. Xe-129/Xe-126-ratio ranges from 1.121 +- .015 at 0 g/cm^2 to 5.197 +- .044 at 180 g/cm^2. The respective range of values measured in extraterrestrial matter is for Xe-128/Xe-126 1.2 - 2.4 and for Xe-129/Xe-126 1.0 - 4.5. The most surprising and unexpected result of this investigation was the spatial distribution of the Xe-131/Xe-126-ratio (Fig. 6). Although it ranges from 1.147 +- .004 at 0 g/cm^2 to 17.26 +- .15 at 180 g/cm^2 and so exceeding the respective range found in extraterrestrial material (2.4 - ~10) it follows exactly - only more pronounced - the pattern of the Xe-M/Xe-126-ratios for M = 128, 129, 130, 132, and 134; isotopes not produced by n-capture on Barium. The Xe-131 "anomaly" seen in this Thick Target experiment is therefore a truely low energy spallation depth effect. Xe-131 due to capture of thermal and epithermal neutrons on Ba-130 did not contribute essentially. The conclusion of these investigations

SPALLOGENIC AND "COSMOGENIC" XENON-YIELDS...

Kaiser, W. A. et al.

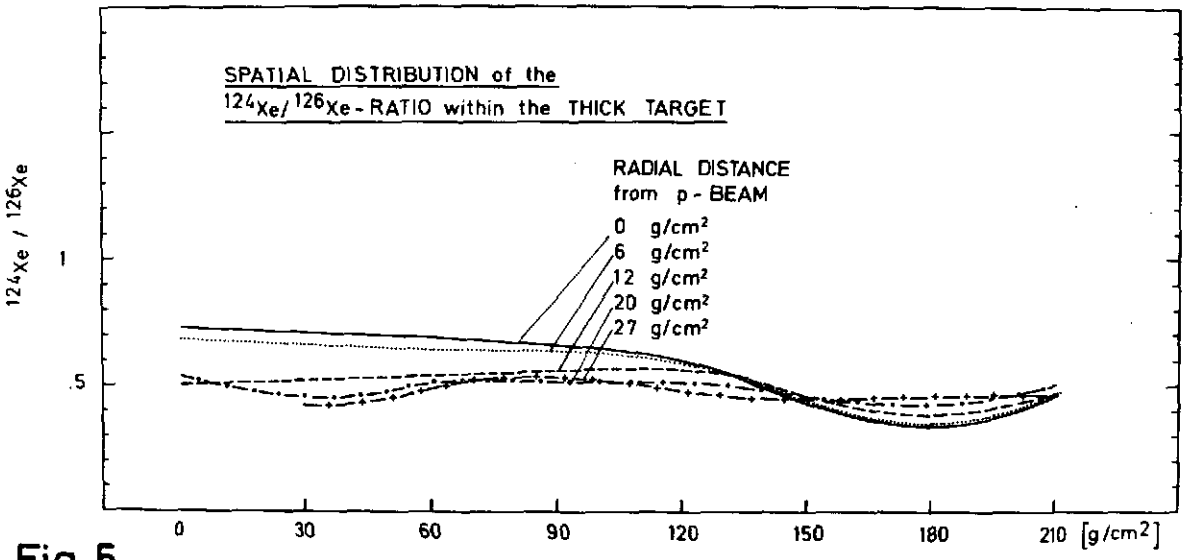

Fig.5

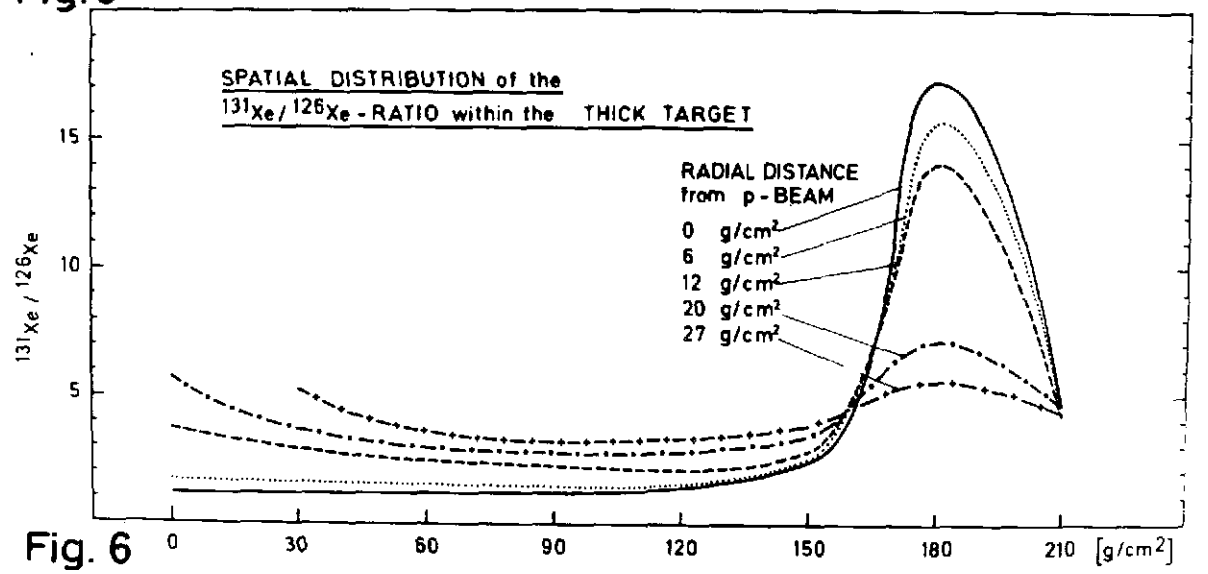

Fig. 6

is that the "cosmogenic" Xe-131 anomaly is caused not only by n-capture on Ba-130 but also to an important part by low energy spallation reactions on Barium.

Lit.:
[1] REEDY R.C. and ARNOLD J.R. (1972), JGR, 77, pp. 537
[2] MORRISON et al. (1971), Proc. Apollo 11 Lunar Science Conf., Geochim. Cosmochim. Acta, Suppl. 1, Vol. 2, pp.1383
[3] MICHEL et al. (1974), in preparation
[4] WEIGEL et al. (1974), in preparation
[5] THIEL et al. (1974), in preparation

LUNAR MAGNETIZATION AND SURFACE CHARGE VARIATIONS : Román Alvarez, Instituto de Geoffsica, UNAM, México 20, D. F.

Various hypotheses have been advanced to account for the observed lunar magnetization; however, little is definitely known (1). In the present work a possible mechanism for magnetization of the regolith and uppermost layers of the moon is proposed. Such a mechanism would operate independently of other magnetic sources such as fossil (2) or internal (3) fields in case of their existence. It is considered, thus, as one of several possible contributions to rock magnetization on the moon.

Reasoner and Burke (4) experimentally determined a surface potential of at least +200 volts for the sunlit hemisphere of the moon when in the magnetotail; lower potential values being acquired ($\sim$ +100 volts) in the solar wind. Anderegg et al. (5) pointed out that lunar surface charge and potential are dependent on solar wind flux, photoemissive properties of the lunar material , energy distribution of magnetospheric electrons (i.e., when the moon is in the magnetosphere) and secondary electron yield from the lunar surface. Manka's (6) theoretical discussion establishes a potential of - 40 volts for the dark side of the moon and various possible positive potentials for the sunlit side. These remarks suggest the existence of a net potential difference between the dark and sunlit hemispheres of the moon. Its absolute value is difficult to establish with presently available data; however, one can assume that it will vary depending on whether the moon is in the magnetosphere or in the solar wind.

Assume Φ_1 and Φ_2 are the lunar surface potentials on the sunlit and dark hemispheres. Consider a unit area at the equator having a constant surface charge density Σ_1 (i.e., corresponding to potential Φ_1) while on the sunlit hemisphere, and Σ_2 while on the dark hemisphere. When approaching the terminator the surface charge density Σ will vary from Σ_1 to eventually reach the value Σ_2 . Let $\Sigma(x)$ represent the way in which the charge distribution varies in the unit area between end values Σ_1 and Σ_2 ; x (positive or negative) is the distance with respect to the terminator.

$\Sigma(x)$ is thus a charge distribution fixed with respect to the terminator (i.e, every surface element will have the same Σ_0 when at the same distance x_0 from the terminator). Figure 1 shows schematically the charge belt, around the terminator , in which Σ varies from Σ_1 to Σ_2 . An observer fixed on the lunar surface will see no time variation of the surface charge density (i. e., $\partial\Sigma/\partial t = 0$) except in the terminator's vicinity, in which the unit area will gain or lose charge in order to adjust its potential to Φ_1 or Φ_2 . During this transition $\partial\Sigma/\partial t \neq 0$ defines a net surface current density in the unit area and, consequently, an associated magnetic field B.

The linear speed of an element of area decreases when approaching the poles of rotation; consequently the distance in which the transition takes place

MAGNETIZATION AND CHARGE

Alvarez, R.

decreases at higher latitudes. Solar radiation intensity also decreases at higher latitudes. The overall effect of these two phenomena implies decreasing amounts of charge transfer in decreasing arc lengths at higher latitudes (Figure 1). Magnetization effects at higher latitudes, from this source, could be expected to be minimal.

An area element crossing the West terminator will gain negative charge (i.e., to reach Σ_2); when crossing the East terminator it will lose negative charge. An observer on the lunar surface would see a (positive) current distribution as the one depicted in Figure 2. The resultant magnetic field of such a current distribution would be maximum at the equator and minimum at the poles. The polarity of the magnetic field would be opposite at the East and West terminators. Such a field acting during geologic times would tend to magnetize materials on the lunar surface either in the north or the south directions. - Runcorn and Urey (7) list a weak field applied for a long time as one of the few possible ways in which lunar rocks could be magnetized. The field suggested here would consist of a series of periodic, magnetic spikes.

Notice that an observer outside the moon, at rest with respect to the terminator , will not see the current or its magnetic field; he will only see a charge distribution which varies in space in the direction normal to the terminator on the surface, but constant in time. However, if the observer is in relative motion with respect to the terminator (e.g., the solar wind) he will also see a current and a magnetic field in the vicinity of the terminator whose values will depend on the relative observer-terminator velocity. Positive solar wind charges traveling in trajectories tangential to the lunar surface at the terminator-equator intersection would experience outward Lorentz forces at the East and West terminator.

The effectiveness of the mechanism proposed as a source of superficial magnetization is strongly dependent on the potential difference between dark and sunlit hemispheres. If it is eventually proven to be effective on the moon, similar considerations could be made for other planetary objects devoid of, or with tenuous, atmospheres.

REFERENCES

(1) Fuller, M., Lunar Magnetism, Revs. Geoph. Space Phys., 12, 23, 1974

(2) Strangway, D.W., H.N. Sharpe, W.A. Gose, and G.W. Pearce, Magnetism and the early history of the moon, in Lunar Science IV, p. 697 edited by J.W. Chamberlain and C. Watkins, Lunar Science Institute, Houston, 1973.

MAGNETIZATION AND CHARGE

Alvarez, R.

(3) Murthy , V.R. and S.K. Banerjee, Lunar evolution: How well do we know it now? , Moon, 7 , 149, 1973.

(4) Reasoner, D. L. and W. J. Burke, Direct observation of the lunar photoelectron layer, in Proc. Third Lunar Sci. Conf., vol. 3, p. 2639 , edited by D. R. Criswell, MIT Press, 1972.

(5) Anderegg, M., B. Feuerbacher, B. Fitton, L.D. Laude, and R. F. Willis, Secondary electron characteristics of lunar surface fines, in Proc. Third Lunar Sci. Conf., vol. 3, p. 2665, edited by D. R. Criswell, MIT Press, 1972.

(6) Manka, R.H. and F.C. Michel, Lunar ion energy spectra and surface potential, in Lunar Science IV, p. 496, edited by J.W. Chamberlain and C. Watkins, Lunar Science Institute, Houston, 1973.

(7) Runcorn, S.K. and H.C. Urey, A new theory of lunar magnetism, Science, 180, 636, 1973.

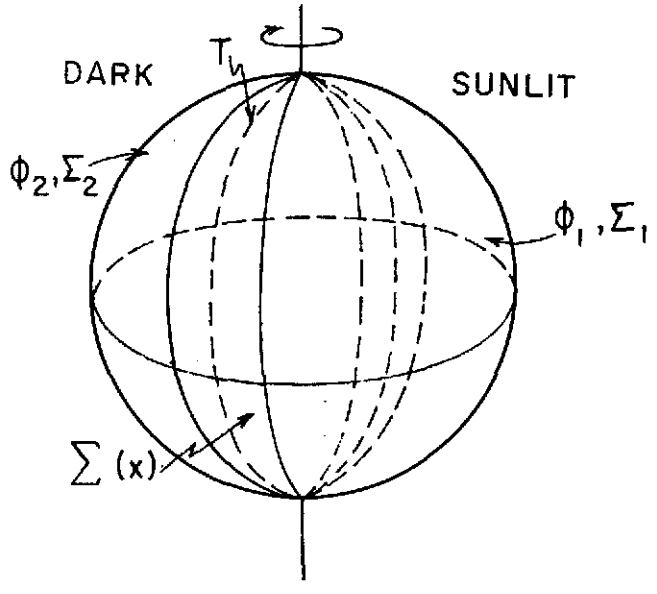

Fig. 1. Belts of variable surface charge around the lunar terminator T.

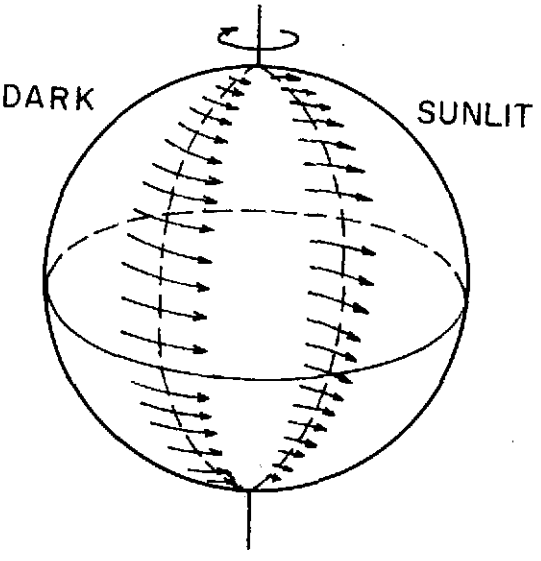

Fig. 2. Surface current distribution as seen by an observer on the lunar surface in the vicinity of the terminator.

LUNAR MAGNETIC FIELD: ORIGIN, EVOLUTION, AND PRESENT CHARACTERISTICS ACCORDING TO A DUAL PRIMEVAL PLANET HYPOTHESIS, J. H. Tatsch, Tatsch Assoc., 120 Thunder Rd., Sudbury, MA 01776.

The origin of the Moon's magnetism is unknown and points to a mysterious epoch in lunar history. The present Moon is not hot and molten inside but relatively cool; its surface appears to have been modified more by impact than by volcanic activity during the past 3 b. y. Most evidence suggests that the present Moon does not have an internal dynamo. The variation in lunar magnetic readings, from less than 10 gammas to values at least an order of magnitude greater, suggests that the lunar field is motivated by highly magnetized local sources rather than by an overall lunar dipole field analogous to that of the Earth.

There is strong evidence that much of the lunar surface, perhaps even a crustal shell around most of the Moon, was uniformly magnetized at some time during the past 4.6 b. y. Subsequent processes, such as tectonic activity, fracturing, shock, and other conditions may have altered this once uniformly magnetized field. The material near the surface was probably magnetized at the time of the Moon's crustal solidification, perhaps over 3.6 b. y. ago. The present magnetism of the rocks, as seen in samples from the Apollo flights, could have resulted either from an external magnetizing field stronger than 1000 gammas or from a smaller internal dynamo-type lunar field that existed within the promordial Moon.

The Earth's magnetic field could have magnetized the lunar material if (a) the Earth's field was much stronger in primordial times than it is now; or (b) the Moon's orbit was once much closer to the Earth; or (c) a combination of (a) and (b). If the Earth's field was never stronger than it is today, then the Moon would have had to approach dangerously close to the Earth in order to have been subjected to a magnetic field of 1000 gammas.

For the Moon's magnetic field to have been produced by an intrinsic lunar dynamo, the Moon would have had to possess both a hot core and a fairly high rate of spin at the time the lunar surface material cooled through the Curie temperature, at which time the magnetism would have been frozen into the material. This requires some mechanism, presently undefined, for lowering the primordial temperature of the lunar interior and for slowing the spin rate of the Moon. One mechanism for accomplishing this dual function in the Moon is provided by the Earth-Moon evolutionary sequences that are predictable from the application of a dual primeval planet hypothesis to the primordial solar system.

LUNAR MAGNETIC FIELD

Tatsch, J. H.

In this hypothesis, the Earth's tectonosphere and the Moon evolve as separate entities of the same closed system. Briefly, when a dual primeval planet hypothesis is applied to an analysis of the early solar system, one of the consequences is a primordial Earth and a co-orbital companion, Earth Prime (1). Each of these modified Bullen-type bodies had a radius of about 5400 km and was fractured into octants early in the history of the solar system. The 5400-km primordial Earth became the "subtectonosphere" of the present Earth. The Earth's tectonosphere (upper 1000 km in this model) is an accretion onto the primordial Earth of the remnant substance of five of the octants of Earth Prime, which had separated into octantal parts early in the history of the solar system. The Moon is derived, through one of several alternative evolutionary sequences, from the remnant substance of one of the octants of Earth Prime (1: p 25-41). The other two octants of Earth Prime assumed hyperbolic orbits and were lost from the local system.

Depending upon the degree of secondary collisions and fragmentations that are assumed, two basic types of Moon model may be derived from the primordial Earth-Moon system that is predicted by the dual primeval planet hypothesis: (a) the "octantal-fragment" Moon model; and (b) the "twice-accreted" Moon model.

In the octantal-fragment Moon model of the dual primeval planet hypothesis, as soon as the "lunar octant" separated from the quasi-stable environment of the fragmentizing Earth Prime, that octant was subjected to an extremely rapidly changing environment. This is particularly important in connection with the erstwhile interior molten material (i. e., that which comprised the apex of the lunar octant of Earth Prime), which was subjected, almost instantaneously, to a rapidly-cooling, highly-reducing environment when Earth Prime separated into octants.

In addition of the expected flow and subsequent solidification of part of the lunar octant of Earth Prime, this octant would receive severe buffeting from subsequent collisions with other parts of Earth Prime as they orbited the primordial Earth. This buffeting would tend to remove the four "horns" from the lunar octant. Some of the heavier molten material of Earth Prime would be "lost" from the Moon prior to its solidification (1: p 98-106).

In the octantal-fragment Moon model, this produces the present Moon after additional buffeting, further readjustments of the liquid and plastic parts of the lunar octant, and such

LUNAR MAGNETIC FIELD

Tatsch, J. H.

gravitational sliding, fracturing, accreting, and smoothing as might be expected in such a system in that environment. An idea of the relatively small amount of such buffeting, flowing, sliding, fracturing, accreting, and other smoothing required is suggested by the fact that the center of gravity of a homogeneous spherical octant is only 13% removed from that of a sphere of the same volume. For a differentiated body, such as was Earth Prime, it would have been even less than 13%.

When Earth Prime separated into octants, each of the separating parts acquired, according to this model, the remanent magnetism derivable from the "dynamo" that existed within Earth Prime during primordial times.

In the octantal-fragment model, the present magnetism of the lunar material comprises the remnants of the magnetism that was "frozen into" the lunar octant of Earth Prime as it cooled through the Curie temperature following separation of Earth Prime into octants. This remanent magnetism has been modified into the Moon's present magnetism, according to this hypothesis, by the action of tectonic fracturing, by the shock of impacts that have occurred in the lunar material, and by other actions of the lunar environment since primordial times.

In the twice-accreted Moon model of the dual primeval planet hypothesis, the Moon evolved from the equivalent of the remnant substance of one of the primordial octants of Earth Prime. This evolution occurred in two fundamental steps: (a) a greater degree of fragmentation through repetitive collisions of the octants of Earth Prime; and (b) a re-accretion of some of this material to form the present Moon. The basic difference between the octantal-fragment Moon model and the twice-accreted Moon model is essentially a matter of the degree of primordial repetitive collisions and fragmentations that occurred with respect to those portions of Earth Prime that later became the present Moon (2). The origin, evolution, and present characteristics of the Moon's magnetism are derivable from either of these two basic models for the formation of the Moon according to the dual primeval planet hypothesis.

1. Tatsch, J. H. (1972) The Earth's Tectonosphere: Its Past Development and Present Behavior. Tatsch Assoc., Sudbury, 889 p.

2. Tatsch, J. H. (1974) The Moon: Its Past Development and Present Behavior. Tatsch Assoc., Sudbury, 338 p.

SPECTROSCOPIC MEASUREMENTS USING SYNCHROTRON RADIATION AS A LIGHT SOURCE. James W. Taylor, Department of Chemistry, 1101 University Avenue, Madison, WI 53706

The electromagnetic radiation resulting from the high velocity centripetal acceleration of electrons is an intense continuum beginning in the x-ray region and extending through the infrared. Numerous research groups throughout the world are employing this radiation as a light source for spectroscopic studies involving absorption, reflectance, transmission, ionization, electron spectroscopy, fluorescence, and intensity calibration.[1-4] The more recent efforts appear to be concentrating at sites where storage rings produce the synchrotron radiation,[5] in contrast to synchrotrons, and major facilities are in operation or under construction in England, France, Germany, Japan, the USSR, and the United States.

The following characteristics explain the spectroscopic interest in this type of light source. [1] The spectrum is a true continuum and devoid of line structure. [2] The intensity of the photon flux, particularly from the x-ray to 1000 Å, can be greater than any other available source and can approximate the peak intensity of many intense line sources. [3] The light is polarized with the electric vector oriented in the plane of the electron orbit. [4] The light arrives at an experimental port in short time pulses, on the order of nanoseconds, with a highly precise pulse repetition frequency in the megahertz range. [5] The light is produced from a vacuum environment in the 10^{-10} to 10^{-11} torr range.

At Wisconsin, the Physical Sciences Laboratory operates a 240 MeV electron storage ring.[6-8] This ring produces a spectrum with a maximum intensity at 190 Å (65.3 eV) and a useful range, depending on the experiment and experimental port, of 25-2000 Å (496-6.2 eV). Shorter wavelengths are produced at higher energies with DORIS, the German storage ring at Hamburg, and SPEAR, a high energy storage ring located at Stanford, producing useful radiation at wavelengths as short as 0.3 Å.[9]

In our gas phase work we have used the Wisconsin ring in conjunction with a vacuum ultraviolet monochromator to study molecular fragmentation by photoionization mass spectrometry, to obtain precise ionization potentials, to measure ionization cross sections, to make absolute intensity measurements in the VUV, and to measure the ejected electron kinetic energies as a function of orbital, photon energy, and angle of ejection.[10-15] For these latter studies the polarization of the light provides an additional aid in probing molecular bonding and in decon-

SPECTROSCOPIC MEASUREMENTS

Taylor, J. W.

voluting overlaping photoelectron bonds.

Synchrotron radiation has also been employed to gain understanding of problems in solid state chemistry and physics. In this work the optical properties of solids are measured as a function of wavelength, temperature, and light polarization. Here the photoelectron production as a function of angle and temperature provide a sensitive probe for surface composition as well as bonding.[1-4]

The solid phase work, to date, has not embraced the multicomponent mixtures expected for lunar samples, but there is reason to expect that the use of synchrotron radiation may be of aid in understanding the optical properties, probing the surface layers, in calibrating light measuring devices, and in determining photoelectron ejection efficiencies over a wide spectral range.

References

1. G. V. Marr, I. H. Munro, and J. C. C. Sharp, "Synchrotron Radiation: A Bibliography," DNPL/R24 Daresbury Nuclear Physics Laboratory, Daresbury, Nr. Warrington, Lancashire, 1973.

2. R. E. Watson, and M. L. Perlman (Eds.), "Research Applications of Synchrotron Radiation, BNL 50381, Brookhaven National Laboratory, Upton, New York, 1972.

3. E. Rowe (Ed.), "Notes on the Annual Synchrotron Users Conference," Physical Sciences Laboratory, Stoughton, WI, 1968 to 1973.

4. G. V. Marr and I. H. Munro, (Eds.), "International Symposium for Synchrotron Radiation Users," DNPL/R26 Daresbury Nuclear Physics Laboratory, Daresbury, Nr. Warrington, Lancashire, 1973.

5. M. L. Perlman, E. M. Rowe, and R. E. Watson, *Physics Today* (July), p. 30 (1974).

6. C. H. Pruett, R. A. Otte, E. M. Rowe, and J. D. Steben, *Bull. Amer. Phys. Soc. Series II (No. 1)* 14, 17, 1969.

7. E. M. Rowe, R. A. Otte, C. H. Pruett, and J. D. Steben, *IEEE Trans. Nucl. Sci. (No. 3 Part I)* NS-16, 1969.

8. W. Trzeciak, *IEEE Trans. Nucl. Sci. (No. 3)* NS-18, 213 (1971).

9. J. W. Taylor in "Chemical Spectroscopy and Photochemistry in the Vacuum-Ultraviolet," C. Sandorfy, P. J. Ausloos, and M. B. Robin, (Eds.), D. Reidel, Dordrecht-Holland/ Boston, 1974, pp. 543-557.

10. W. L. Steblings and J. W. Taylor, *Int. J. Mass Spectrom. Ion Phys.* 9, 471 (1972).

11. B. M. Johnson and J. W. Taylor, *ibid.*, 10, 1 (1972).

12. J. A. Kinsinger and J. W. Taylor, *ibid.*, 10, 445 (1973).

13. J. A. Kinsinger and J. W. Taylor, *ibid.*, 11, 461 (1973).

14. G. R. Parr and J. W. Taylor, *Rev. Sci. Instrum.*, 44, 1578 (1973).

15. G. R. Parr and J. W. Taylor, *Int. J. Mass Spectrom. Ion Phys.*, 14, 333 (1974).

SOLAR-WIND INTERACTIONS AND LUNAR ATMOSPHERE, N. R. Mukherjee, Biotechnology and Space Sciences Subdivision, McDonnell Douglas Astronautics Company, Huntington Beach, California 92647

The solar wind interacts directly with the surface material of a planetary body like moon with tenuous atmosphere. The interaction products are probably the main source of most neutral species in the atmosphere [1]. The other sources are planetary degassing, effects of meteoritic impacts, and cosmic rays. In this paper we discuss the comparative importance of these sources for the lunar atmosphere on the basis of theoretical and experimental investigations. A special emphasis is given to the sources of H_2O.

The meteoritic impacts are occasional events, and the cosmic ray flux is three to four orders of magnitude smaller than solar wind flux. The present day contributions to the lunar atmosphere from these two sources are small compared to the contributions from the solar wind and degassing. To evaluate the latter contributions, it is important to know the lunar atmospheric density which is very tenuous with a surface pressure of $\sim 10^{-14}$ atm. This atmosphere contains certain atomic and molecular species as well as their ions. Several techniques have been applied for the determination of the atmospheric density and composition [1, 2, 3] and the results are generally consistent with one another. Here we shall discuss the technique of [1]. The solar wind interacts with the atmosphere, and this interaction is considered to cause perturbations in the solar wind near the lunar limb. These perturbations are due to "single-fluid" and "two-fluid" couplings between atmospheric ions and the solar wind. The perturbation measurements by Explorer 35 spacecraft were utilized to determine the upper limits of number densities of more than a dozen atmospheric neutral species. The dominant species was found to be He with the average number density of 9.4×10^4 cm^{-3} in the day side, followed by H_2, Ne and Ar with densities 9.3×10^4, 6.9×10^4 and 1.9×10^4 cm^{-3} respectively. The total number density value of all species obtained by this technique is consistent with the value obtained by others. For exploration of planets with tenuous atmosphere, one can measure the perturbation in the solar wind near the planet's terminator and use the perturbation data to calculate it's atmospheric density [4]. This technique is particularly useful in those cases where the remote sensing of optical characteristics of atmospheric species may not be possible or the measurement accuracy questionable.

The species in the lunar atmosphere are expected to be H_2, He, Ne, Ar, O_2, N_2, H_2O, NO, CO, CO_2, CH_4, OH, H, O and N. The atomic species and OH radical in the atmosphere are primarily produced from the molecules by photodissociation and solar wind interactions. Most molecular species and noble gases are supplied by solar-wind interactions with lunar surface and some of the species are supplied to a certain extent by degassing and radioactivity. The contribution from the lunar degassing is possible, because besides the probable continuous degassing through the soil, emanations from the hot spots, transient events and active spots are also possible sources. Many observers

SOLAR-WIND INTERACTIONS AND LUNAR ATMOSPHERE

Mukherjee, N. R.

have detected these spots and events, have found some active spots to be repeatedly active, and have detected gas emissions from some of the active spots. First, we discuss the solar wind contribution to the atmosphere. The relative abundances of protons, alpha particles and atomic oxygen ions in the solar wind are about 5000, 150 and 1.00, the proton flux on the lunar surface being about 3×10^8 cm^{-2} sec^{-1}. These species with average energy of about 1 keV penetrate the lunar surface material to a depth of about 0.05 to 0.1μm. While penetrating they ionize the elements of the top 50 to 100 layers of the surface material and ultimately become neutral H, He and O. These active atomic species, while diffusing in the material, form molecular and radical species such as H_2, O_2, OH and H_2O, because the reactive atomic species generally diffuse with slow rates in radiation damaged material and because the lunar surface materials are saturated with neutralized solar wind species. These latter species, while diffusing in the material, encounter the oncoming solar-wind particles and their degradation products, energetic neutrals. These encounters result in a complex set of reactions of the diffusing species such as ionization, dissociative ionization, dissociation and exchange reactions. Each of the fragmented species subsequently undergoes another set of reactions during its residence time in a location and its diffusion through the material. The solar wind particles may also react with the elements of silicate lattice, for example, protons or energetic hydrogen atoms producing OH^+ and OH. After their formation they undergo similar reactions as described above. A detailed analysis of these processes (diffusion, encounters with solar wind particles, and reactions) show that most of the solar wind protons, in the presence of the solar-wind particulate radiations, appear in the atmosphere as H_2 instead of H, OH and H_2O. In the absence of the radiation a fraction of the hydrogen atoms derived from the solar wind would appear as H, OH and H_2O provided the temperature of the material is about the same as that in the presence of radiation. The particulate radiation on the moon is three to four orders of magnitude smaller on the night side than on the day side. The average temperature on the night side is about 100°K as compared to about 350°K on the day side (the average of noon and near terminator temperatures of 400° and 300°K). The H_2O molecules formed from H and O atoms would remain practically frozen in the locations where they are formed, because the diffusion coefficient of the polar molecule, H_2O, through the lunar material at 100°K is estimated to be less than $\sim 10^{-30}$ cm^2 sec^{-1} as compared to $\sim 10^{-21}$ cm^2 sec^{-1} at 400°K. Upon exposure, the solar wind radiation destroys essentially all H_2O molecules before they escape from the lunar surface material to the atmosphere. Based on the above analysis and the information in a previously published paper [5] we conclude that if H_2O is present in the lunar atmosphere its main source is lunar degassing. Our analysis shows that probability of solar wind destruction of H_2O during degassing through the void space between lunar soil grains and through the pores in the grain is a very small; therefore, most H_2O molecule will survive to escape from the lunar interior to the atmosphere.

Petrographic and chemical analysis of lunar samples did not reveal the

presence of hydrated minerals. If formed, hydrated minerals would have been stable even in the lunar environment. Trapped H_2O was also not detected but various gases including hydrogen were found in the lunar samples. Our experiments on the high-vacuum and low vacuum N_2-stored lunar samples showed that, upon their exposure to O_2, H_2O, and their mixtures, many of the bonded particles separated, and that prolong exposure to nearly saturated H_2O vapor sensitized the lunar grain which released trapped gases during subsequent recycling steps of adsorption studies. These and other studies of lunar samples indicate that the lunar surface grains did not contain H_2O or OH for any substantial length of time. It is reasonable to conclude from the theoretical analysis outlined above and the lunar sample study results of ours and others that OH and H_2O which may form from the solar wind species are essentially destroyed by the solar wind particulate radiations before they could escape the material grains to the lunar atmosphere. Hydrogen derived from the solar wind protons escape the material grains to the atmosphere in the form of H_2. If H_2O is present in the lunar atmosphere, its source is in the lunar interior. Details of the processes and calculations substantiating the above conclusions will be presented in the paper.

REFERENCES

1. Siscoe, G. L., and Mukherjee, N. R. (1972) Upper limits of lunar atmosphere as determined from solar-wind measurements, J. Geophys. Res., 77, 6042.

2. Freeman, J. W., Jr., Fenner, M. A., Hill, H. K., Lindeman, R. A., Medrano, R. and Meister, J. (1972) Suprathermal ions near the moon, Icarus, 16, 328.

3. Johnson, F. S. (1972) Lunar atmosphere (abstract), Lunar Sci. Conf. 3rd, 389, NASA Manned Spaceflight Center, Houston, Texas 1972.

4. Siscoe, G. L., and Mukherjee, N. R. (1973) Solar wind - Mercury atmosphere interaction: Determination of the planet's atmospheric density, J. Geophys. Res., 78, 3961.

5. Mukherjee, N. R., and Siscoe, G. L. (1973) Possible sources of water on the moon, J. Geophys. Res., 78, 1741.

ANCIENT SOLAR WIND AND SOLAR FLARE ACTIVITY, S. K. Bhattacharya, K. Gopalan, J.N. Goswami, D. Lal and M.N. Rao, Physical Research Laboratory, Navrangpura, Ahmedabad-380009, India.

Silicate grains, having high track densities due to solar flare bombardment as well as high rare-gas contents due to solar wind implantation, occur in varying proportions in lunar soils and in the dark portions of the gas-rich meteorites[1-4]. A comparative study of the correlation between the gas contents and the track-rich components in lunar soils and the gas-rich meteorites is carried out here to understand the behaviour of the solar wind and solar flare activity in the past.

A convenient parameter describing the solar flare bombardment is N_H/N, which denotes the fraction of grains that have received flare irradiation, resulting in high track densities $\geq 10^8/cm^2$, and/or steep track density gradient. Ar^{36} is used to represent the trapped solar wind gases. Large amount of data for the lunar soils and gas-rich meteorites from this laboratory and published literature, are used for plotting Ar^{36} vs N_H/N (Fig. 1). This interrelationship between Ar^{36} and N_H/N shows a saturation effect for Ar^{36}: $\sim 3 \times 10^{-4}$ cc STP Ar^{36}/gm for N_H/N values exceeding 0.5. For gas-rich meteorites, for $N_H/N < 0.4$, the available data points fall on a smooth curve without showing evidence for gas-saturation; the gas contents are lower by 2-3 orders of magnitude compared to the lunar saturation value.

In order to understand the above observations we have made determinations of the grain-size distributions in gas-rich meteorites. These data for meteorites and the published extensive data for lunar soils are used to deduce specific gas contents of Ar^{36} in meteoritic and lunar samples: cc/cm^2 surface area.

A significant reason for the low gas contents in the dark portions of gas-rich meteorites, compared to the lunar soils, is due to the fact that the N_H/N is ~ 1 for many lunar soils whereas for the meteorites the values range from 0.02 to 0.3. This means that in these lunar soils all the grains are exposed to solar radiation at some time or other. But the gas-rich meteorites contain an appreciable amount of grains that were never exposed to solar wind and solar flares in the past. This fact gives rise to the dilution of gas-rich grains by non-irradiated ones. The relative proportion of the irradiated to the non-irradiated grains determines the gas contents in gas-rich meteorites.

ANCIENT SOLAR WIND

Bhattacharya, S. K. et al.

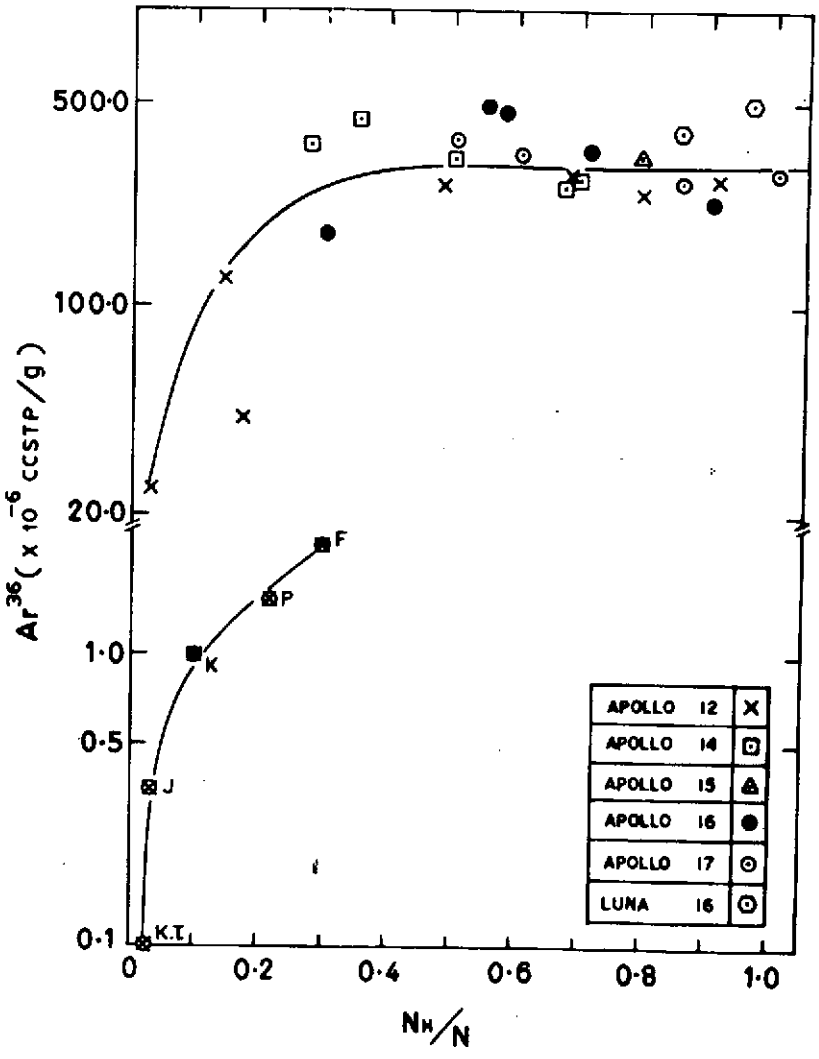

Fig. 1 Correlation between observed N_H/N values and the Ar^{36} contents of several bulk lunar soil samples and dark portions of the gas-rich meteorites.

After accounting for the dilution effect due to mixing with unirradiated grains and taking into account expected differences due to different grain size distributions in meteorites and lunar samples, we find that the

amount of solar wind gas in the lunar samples, relative to flare tracks, is too high compared to meteorite samples. One of the possible explanations which reasonably accounts for this difference lies in the hypothesis that the solar flare activity was much higher in the early history of the solar system than at present.

References

1. Suess, H. E., Wanke, H. and Wlotzka, F., (1964), Geochim. Cosmochim Acta, 28, 595-607.

2. Eberhardt, P., Geiss, J. and Groegler, N., (1965), J. Geophys. Res., 70, 4375-4378.

3. Lal, D., Rajan, R.S., (1969), Nature, 223, 269-271.

4. Pellas, P., Poupeau, G., Lorin, J.C., Reeves, H. and Adouze, J., (1969), Nature, 223, 272-274.

THERMAL ENVIRONMENT AND HISTORY OF SOME APOLLO 17 SOILS. F.S.W. Hwang and S.A. Durrani, Physics Dept., Birmingham University, Birmingham B15 2TT, England.

Two soil samples returned from the Apollo 17 mission were studied by thermoluminescence (TL) technique. Both samples had already been sieved in the Lunar Sample Preparation Laboratory of NASA, and grains of less than 38 microns were further separated by us for this investigation. Sample 76241 was collected from about 1 meter under the north overhang of boulder 4 at station 6. The other sample 76261 was collected on the open ground just outside the shadow. The natural glows of these two samples strongly reflect their thermal environment. The former, which was shadowed permanently from the sunlight by the boulder and hence received no direct solar heating, had a better storage condition for its natural TL. The latter, however, which was exposed directly to sunlight throughout the 14 days sunrise period when the temperature reaches 375°K, showed natural TL only at the high temperature region. The boulder track, described by the astronauts as still fresh, indicates that the boulder probably has not been there for a great length of time. This implies that the build-up of the low temperature natural TL in sample 76241 started only after the arrival of the boulder because the sub-zero temperature in the shade provided a better storage condition for a dynamic equilibrium. By assuming that the two samples are identical in mineral composition and TL characteristic, and also using the Randall and Wilkins model, an attempt has been made to estimate when the boulder arrived, the last heating-up of the soil, and the temperature in the shade during lunar daytime.

Successive doses, ranging from a few kilorads to a few megarads, were added to these natural samples. The response to γ-rays (^{60}Co) irradiation of these samples is linear to about $1\frac{1}{2}$ megarad, then the total glow area between room temperature and 520°C is saturated with higher doses. This behaviour is generally found in other samples from the previous missions. The integrated area of glows of various temperature ranges were plotted against the dose added. The "Half-Dose" was determined for the high temperature glow of each specimen and from this the storage temperature of the sample on the moon was estimated. The low temperature glow of sample 76241 was also used for the estimation of its storage temperature in the shade. The result can be compared with that obtained from above and provides an inter-check of the two models employed.

The trapping parameters, trap depth and frequency factor were determined using the initial rise technique. The results agree with the electron trapping model and are also consistent with the previous results.

THERMAL ENVIRONMENT AND HISTORY OF SOME APOLLO 17 SOILS

Hwang, F. S. W. and Durrani, S. A.

Sample 76241 is one of the two samples which have been kept at freezing temperature since their arrival. However, the samples were left at room temperature for about a fortnight after the splash down before actually going into the deep freezer. Therefore, an experiment was performed to see if any natural TL had faded during that period. A specimen was divided into two portions after its glow at low temperature region was reinstalled (matching the shape of its natural glow) by adding an artificial dose of 40 kilorads β (^{90}Sr), one portion was left at room temperature and the other at 60°C for 14 days (also equivalent to the length of a lunar day) before their TL were read out. The results showed that the natural TL induced by radiations in space was not affected by that storage condition. The counterpart of this sample has been kept at room temperature ever since its arrival. The natural glows of these two parts are also compared. Sample 72321 is the other deep-freeze sample which was collected from about 20cm inside the shadow under an overhang of boulder 2 at station 2. However, the natural glow obtained from this sample implies that it has suffered severe thermal annealing in the past.

THERMAL ENVIRONMENT AND HISTORY OF SOME APOLLO 17 SOILS

Hwang, F. S. W. and Durrani, S. A.

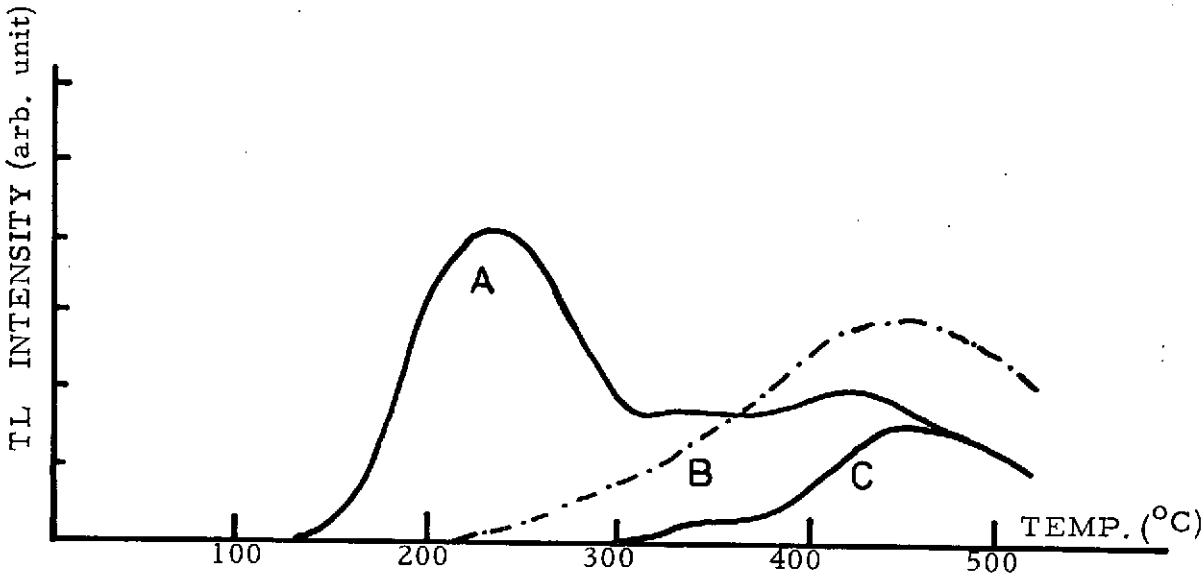

Fig. 1; Natural TL glow from samples A) 76241, B) 72321 and C) 76261.

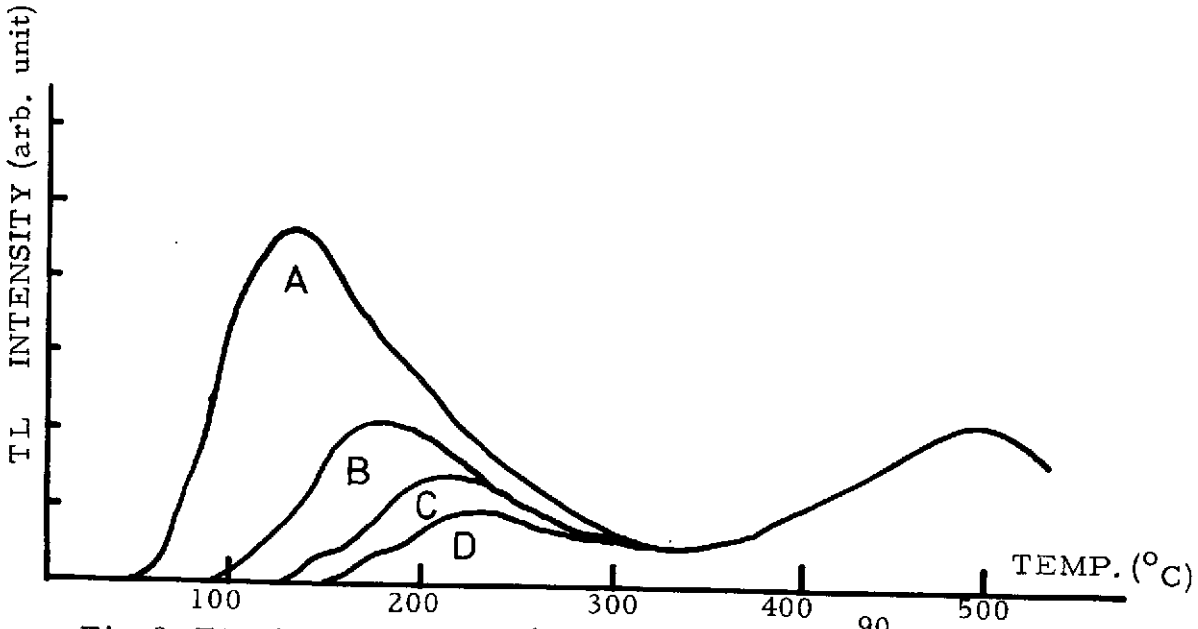

Fig. 2; TL glow of sample 76241:A) 40 Krads β (^{90}Sr), B) 40 Krads β +14 days at room temperature, C) 40 Krads β + 14 days at 60°C and D) natural glow.

THE INTERACTION OF THE SOLAR WIND WITH THE MOON: OBSERVATIONS. C.T. Russell, Institute of Geophysics and Planetary Physics, University of California, Los Angeles, Calif. 90024.

The interaction of the solar wind with the moon is distinct from the interaction with the other celestial bodies for which we have in-situ data. The moon has neither a dense atmosphere to absorb the solar wind; nor a highly conducting ionosphere, or surface, through which the solar wind could set up unipolar induction currents to deflect the solar wind; nor does it have a strong intrinsic planetary magnetic field. Thus, the solar wind directly impacts the lunar surface over the daylit hemisphere. This fact enabled the solar wind to be probed quite successfully during the Apollo program with instruments on the surface. In fact, analyses of lunar soil samples have provided measures of solar wind properties for the past 10^9 years.

Downstream of the moon there is a wake or cavity in the solar wind in which close to the moon there is no flowing solar wind plasma. The magnetic field strength in this region is slightly greater than in the undisturbed solar wind, but it is not as enhanced as would be expected if this region were a void. The flowing solar wind is expected to expand into this cavity and some evidence of this expansion is seen as depressions in the magnetic field bounding the wake region. However, this signature is often very weak and appears to be strong only when there are large disturbances upstream from the limbs.

Compressional disturbances in the field and plasma, called external maxima, penumbral increases and limb shocks by Explorer 35 experimenters, are even more evident in low altitude Apollo subsatellite data above the lunar limbs. Strong limb compressions $\Delta B/B \geq 0.5$, are observed 23% of the time. They occur under all solar wind plasma conditions, and upstream magnetic field orientations. However, they never occur over some regions of the moon, while they almost always occur over others. The most probable cause of these features is deflection of the solar wind near the terminators by the lunar magnetic field.

The magnetic dipole moment of the moon as measured by the Apollo 15 and 16 subsatellite magnetometers is less than 10^{19} Gauss-cm^3 and is far too weak to cause such a deflection. However, these same satellites reveal a complex pattern of surface fields which could cause local deflections of grazing-incidence solar wind. There are but two regions of overlap of occurrence statistics on lunar limb compressions and the surface field. In the first, there is no measurable lunar field and no limb compressions; in the other, there is a variable field and a variable occurrence rate with an almost one to one correspondence.

SOLAR WIND INTERACTION

Russell, C.T.

While limb compression occurrence statistics, the Berkeley particle scattering technique, and direct high altitude ($\sim$100 km) measurements reveal that large scale lunar fields with coherence lengths of the order of 100 km cover only a fraction of the lunar surface, low altitude (<60 km) data and surface measurements reveal the lunar surface to be magnetized everywhere. Perhaps due to these small scale fields, the lunar limb regions are almost continually disturbed, even when limb compressions are absent.

The scattering of fluctuations in the interplanetary magnetic field by the moon has been used to probe the interior conductivity of the moon by inversion of the lunar transfer function. This approach, however, depends on using the proper boundary conditions in the inversion technique. While the dayside interaction is well understood, knowledge of the properties of the wake is lacking. If lunar conductivity studies are to progress, we must understand the plasma in this region better. Thus the lunar polar orbiter should be instrumented with modern plasma instrumentation, in addition to a magnetometer and x-ray and γ-ray spectrometers.

METHANE AND AMMONIA IN THE LUNAR ATMOSPHERE, J. H. Hoffman and R. R. Hodges, Jr., University of Texas at Dallas, P. O. Box 688, Richardson, Texas.

The Apollo 17 mass spectrometer experiment has confirmed the existence in the lunar atmosphere of several of the noble gases, viz. helium and argon, as has been reported previously.

The observed helium concentrations and distribution agree closely with model predicitions for a non-condensable gas based on a solar wind source, thermal escape and a Monte Carlo random walk calculated longitudinal distribution. Heavier gases are lost by photoionization and subsequent sweeping away by the solar wind electric field. Argon, is adsorbed on the lunar surface late at night when the surface temperature is lowest. It shows the expected pre-dawn enhancement exhibited by condensable gases released into the atmosphere at the sunrise terminator.

Evidence exists for the pre-dawn enhancement, similar to that for argon, of mass peaks at 15, 16 and 17 amu in spectra from late in the lunar night. The enhancement of these peaks is likely due to a pre-dawn increase in methane (15 and 16 amu) and ammonia (17 amu), both condensable gases which are boiling off from the warm approaching terminator. The enhancement begins 5 to 10° before the terminator crosses the Apollo 17 site and continues until local sunrise, which occurs some 4° after the terminator has passed the site. These condensable gases should have their maximum concentrations at sunrise. The values obtained are somewhat less than those for ^{40}Ar (10^4 cm^{-3} range) and more consistent with ^{36}Ar (3×10^3 cm^{-3}) which has a solar wind origin.

MICROMETEORITES AND SOLAR FLARE PARTICLES IN AND OUT OF THE ECLIPTIC. I.D. Hutcheon, Physics Dept. Univ. of Calif., Berkeley, Ca. 94720.

The utilization of lunar rocks as micrometeoroid detectors has provided a wealth of information on the mass frequency distribution and physical properties of interplanetary dust particles. Due primarily to a lack of appropriate samples, three areas of great interest have yet to be carefully investigated: (1) the angular distribution of the flux of micrometeoroids; (2) the physical properties of non-zodiacal (possibly interstellar) dust grains; and (3) the angular distribution of the flux of solar flare particles. Vugs chipped from the Apollo 17 vesicular basalts whose lunar surface orientations are well documented (71055 and 74255) have provided the first opportunity to investigate these problems. Although studies are still in progress, we report a preliminary measurement of the angular anisotropy of the micrometeoroid flux and demonstrate that the mass frequency distributions and characteristic shapes of zodiacal and non-zodiacal particles are very similar. We also report a tentative measurement of a shallow solar flare track gradient in a South facing vug that requires further analysis, but may indicate a real difference in the energy spectrum of solar particles in and out of the ecliptic plane.

Evidence from studies of the intensity of the zodical light and from satellite measurements of interplanetary particles[1] suggests that dust grains in the solar system should be strongly concentrated near the plane of the ecliptic. To search for an anisotropy in the micrometeoroid flux we have observed microcraters on crystal faces located deep within oriented vugs from 71055 and 74255. The narrow opening of a vug allows the crystal to intercept only particles streaming in within a limited solid angle. In particular, we have selected vugs from 71055,12 which were pointed approximately lunar South and should intercept only non-ecliptic particles and vugs from 74255,49 which were pointed lunar East or West and should intercept only particles confined to the ecliptic plane.

The size frequency distributions of microcraters have been measured on crystal faces within vugs of orthogonal orientation over the diameter interval 0.05 μm to 1.0 μm. All microcraters counted have the morphology of craters produced by hypervelocity impact. Some features suggestive of low velocity projectiles were observed but have been excluded from the analysis. Crystal surfaces are undersaturated with craters and have generally low densities of accretionary particles. The size frequency distributions for both the sunward and southward pointing surfaces are shown in Figure 1 and are very similar in shape. Both curves show a depletion in craters less than 0.10 μm in diameter, but this effect is most likely due to the limited resolution of the SEM. Scanning at highest resolution on smooth surfaces suggests that both distributions extend with a constant slope of ~ -2 to crater diameters $\lesssim 400$ Å. Our results are inconsistent with the work of Zook and Berg[2] who suggested that surfaces oriented normal to the ecliptic plane should be depleted in craters in the

MICROMETEORITES AND SOLAR FLARES

Hutcheon, I.D.

diameter interval 0.1 μm to 1.0 μm. The similarity in the size frequency distributions of craters produced by particles impacting from ecliptic and lunar South directions established here together with a study by Blanford et al.[3] of a North pointing surface, indicate that the micrometeoroid population is isotropic throughout interplanetary space in terms of size frequency distribution over the diameter range measured.

To evaluate the flux of hypervelocity particles in a given direction we measure the solar flare track profiles in the same crystals on whose surfaces we have observed craters. The magnitude of the track density at a given depth, when compared with our most recent lunar standard[4], enables us to determine the exposure age of a particular surface and to compute the micrometeorite flux. After their surfaces have been studied, the crystals are chipped out of their vugs, mounted and polished normal to the exposed surface, and etched to reveal the solar flare tracks. Samples are etched in a boiling solution of 3g NaOH:10g H_2O for plagioclase or 6g NaOH:5g H_2O for pyroxene. Tracks are counted on a plastic replica with SEM.

Our efforts, thus far, have concentrated on measuring the track profile in a plagioclase crystal from a South pointing vug of 71055. Over the depth interval measured, 2.5 μm to 180 μm, the track gradient is substantially flatter (slope of ~ -1) than gradients we have measured in uneroded crystals of unknown orientation. From the observations of microcraters and accretionary particles on its exposed surface we can exclude any significant amount of surface erosion. We are presently reassessing the exposure geometry to evaluate the effects of irradiation prior to opening of the vug, but cannot yet discount the possibility that this gradient reflects a true difference in the energy spectrum of solar particles impinging normal to the ecliptic. Measurements of track profiles in other South facing crystals are in progress to check this observation and will be reported. Pyroxene phenocrysts from sunward facing vugs of 74255 are also being etched to reveal the track gradient from solar particles in the ecliptic.

The determination of the flux of non-zodiacal particles is strongly dependent on the interpretation of the shape of the southward track density gradient. Until our analysis is completed, we can only estimate the ratio of ecliptic and non-ecliptic micrometeoroid fluxes by comparing the ratio of the density of 1.0 μm diameter craters to the solar flare track density at a depth of 10 μm for orthogonally oriented samples. Assuming the solar flare flux to be isotropic, we estimate that the production rate of 1.0 μm diameter craters on a South facing surface is lower by a factor of ~10 than the rate on a surface lying in the ecliptic.

Another probe of the physical characteristics of hypervelocity dust grains is the shape of the impact crater they produce. The parameter we use to quantify crater shapes is the circularity index, the ratio of the area bounded by the rim of the crater to the area of the smallest circle which just encloses the crater. We have measured crater circularities of more than 100 craters on each of two orthogonal surfaces and find no major differences between the ditribution of circularities of craters collected in the South pointing vugs and in the sunward facing vugs. There is some indication of a greater population of craters with circularity less than 0.5 for

MICROMETEORITES AND SOLAR FLARES

Hutcheon, I. D.

the non-ecliptic orientation. Extremely noncircular craters indicative, for instance, of needle-shaped interstellar dust grains are not observed. The number of common physical characteristics suggests that interplanetary particles of mass 10^{-13} g residing both in and out of the ecliptic plane originate from related sources and/or are subject to similar environments.

References

1. Roosen, R.G. (1971) Spatial distribution of interplanetary dust. In Physical Studies of Minor Planets, pp. 363-375. NASA SP-267.
2. Zook, H.A., and Berg, O.E. (1974) A Source for Hyperbolic Dust Particles. Preprint.
3. Blanford,G., Fruland, R.M., McKay,D.S., and Morrison, D.A. (1974) Lunar Surface Phenomena. Preprint.
4. Hutcheon, I.D., Macdougall, D., and Price, P.B. (1974) Proc. Fifth Lunar Sci. Conf., to be published.

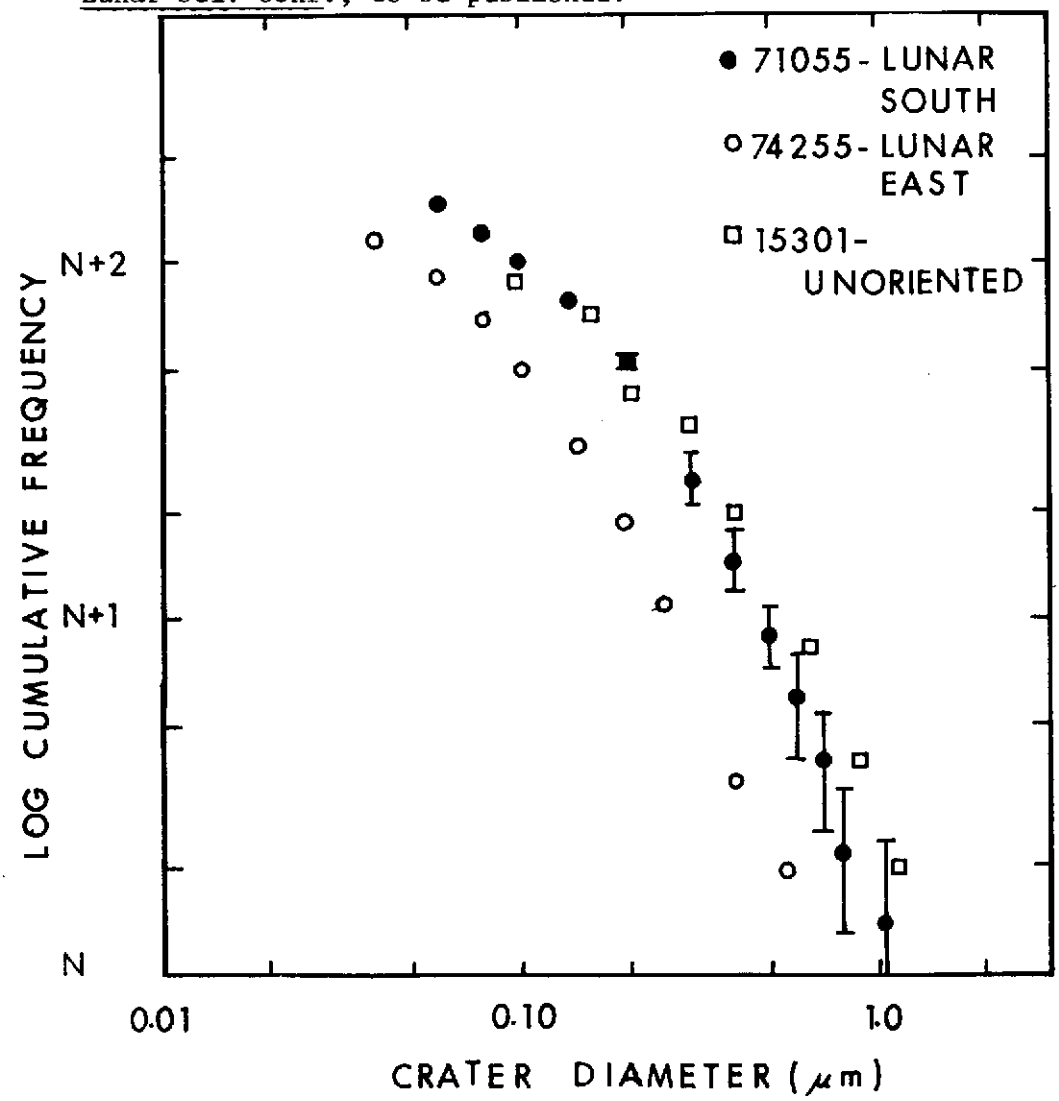

ELECTRET FORMATION ON THE LUNAR SURFACE--ADHESION AND CLUSTERING OF DIELECTRIC PARTICLES IN THE SPACE ENVIRONMENT;
Gustaf Arrhenius, Scripps Inst. of Oceanography, La Jolla, CA 92037

Exposure to space environment causes the lunar soil particles to adhere to each other forming grain clusters with low bulk density. The adhesion forces are electrostatic and due to persistent internal polarization. Dipole strengths are correlated with irradiation history, composition and density of structural discontinuities in the crystals.

Comparison of the electrostatic adhesion in top and bottom strata of the Apollo 12 double core where the age relationships are approximately known show that the adhesion, although perceptibly decayed, still persits after burial times estimated to be of the order of 10^7 years.

The phenonmenon of electret formation on the Moon relates to a number of other lunar processes but also to a number of general problems concerning the behavior of matter in space. Some of these are:

1. The turnover of the lunar regolith on a scale comparable with the size of the particles and of the observed sediment strata, and the relative importance at this scale of different driving mechanisms, primarily micrometeorite impact and electrostatic charging.

2. Possible lateral transport of lunar dust at a scale of meters and larger as proposed by Gold. Without such a process operating at a scale of at least 1-10 m, it is, as pointed out by Gold, difficult to understand the lack of throwout debris on rock surfaces and the disappearance from the soil surface of landing marks from rock projectiles.

3. The incipient aggregation of grains in Kepler orbits. It has long been a problem to explain how the planetary bodies in the solar system can have begun their embryonic growth from assemblages of orbiting particles (it is now well known [Spitzer, Kumar] that planetary bodies, in contrast to stars, are far too small to form by gravitational collapse of gas clouds). Although one now understands how low relative velocities can be obtained in orbiting many-body systems of particles, the mechanism for their ultimate cohesion has been unclear. The existance in the lunar dust of considerable electrostatic attractive interparticle forces due to radiation induced persistent internal polarization provides some quantitative insight into mechanisms possibly responsible for the primordial aggregation.

4. The nature of comets and meteor streams. Comets contain dust which we know from stream meteors to be partially aggregated into fluffy objects. Again, the way is unknown in which individual particles interact to build up such aggregates and possibly also larger bodies that exist in the cometary nucleus. This uncertainty applies also to the processes that work in the opposite direction leading to disaggregation and dispersion of particles. Guidance to understanding of these phenomena can be obtained by study of the surface related properties and interparticle forces in the lunar material.

THE LUNAR ELECTRIC POTENTIAL AND ITS PLASMA SHEATH EFFECTS (1), J. W. Freeman and M. E. Ibrahim, Dept. of Space Physics and Astronomy, Rice University, Houston, Texas 77001.

Any body immersed in a plasma or exposed to ultraviolet radiation acquires a charge on it's surface. The moon enjoys both of these environments. The magnitude and sign of the charge is determined by the balance of currents to the surface. Further, a plasma always acts to shield a net charge by establishing an ion or electron sheath of opposite polarity adjacent to the surface. Again, in the lunar case such sheaths have been observed. They form an important part of the lunar plasma environment. By measuring the positive ion fluxes under varying conditions of instrument potential relative to the lunar surface the ALSEP/SIDE provides data on both the lunar surface potential and the resulting ion sheaths.

The sign and magnitude of the lunar surface potential and the corresponding sheaths vary greatly with lunar local time and lunar position. Figure 1 illustrates the surface potential variation with solar zenith angle as measured by SIDE. We now summarize the conditions in various regions.

The Lunar Dayside In The Solar Wind or Magnetosheath: For all except large solar zenith angles the lunar surface potential is found to be positive and of the order of 10 volts (2). A new result published here for the first time is the indication of an asymmetry about zero zenith angle such that the potential increases to approximately +18 volts in the late lunar afternoon. See Figure 1. The general dayside positive potential arises from the ejection of photoelectrons from the lunar surface. Adjacent to this positive surface potential region is a compensating electron sheath. This sheath probably extends several meters above the lunar surface and contains electrons of number densities of the order of 10^3 electrons/cm^3 (3). These electrons (of solar wind origin and energy) have not been observed directly although Reasoner and Burke (4) have measured the analogous higher energy photoelectron sheath in the earth's high latitude geomagnetic tail. The electric field confined by this sheath is a few volts/meters and normal to the lunar surface.

Superimposed on and lying above this electron sheath is a more tenuous ionosphere consisting of the ionized ambient lunar atmosphere. These ions are promptly removed by the much weaker interplanetary electric field (5).

SURFACE POTENTIAL AND PLASMA SHEET

Freeman, J. W. and Ibrahim, M. E.

Terminator Region in the Solar Wind or Magnetosheath: As seen in figure 1 the lunar surface potential becomes negative as the terminator is approached from the day side (6). This negative surface potential is probably due to the flux of solar wind electrons which have access to the terminator. The potential reaches as much as a few hundred volts negative on the nightside near the terminator. In this region the compensating sheath is formed at least partly by positive ions. These ions are seen at the surface with energies comparable to the surface potential. They arise from ionization of the ambient atmosphere by the solar photon flux and solar wind which have access to the higher altitudes at the terminator. The shielding length or Debye length for this sheath is much larger than for the dayside electron sheath. The general surface electric field should be correspondingly lower, however, adjacent illuminated and shadowed areas characteristic of the terminator almost certainly give rise to very large local electric fields (7).

Dark Side in the Solar Wind or Magnetosheath: Plasma polarization and pressure effects limit direct solar wind electron travel to the night side of the moon however substantial negative potentials probably develop here also. The resulting ion sheath may consist of thermalized solar wind protons with a correspondingly large Debye length. Some evidence for the detection of this sheath may already exist. Schneider and Freeman (8) report the detection of solar wind energy positive ions on the far night side.

The Lunar Dayside in the Geomagnetic Tail: Burke and Reasoner have reported lunar surface potentials as high as +200 volts in the geomagnetic tail (4). SIDE data indicate potentials of about +10 volts are common in some regions in the tail. The SIDE result probably applies to the higher plasma density regions of the plasmasheet and boundary layer. An electron sheath consisting of photoelectrons and/or magnetotail electrons surrounds this dayside surface (4).

To summarize, in addition to the well known electron sheath on the lunar dayside, more tenuous but extensive positive ion sheaths exist adjacent to the negative terminator and night side. The terminator ions are supplied by ionization of the lunar atmosphere but the far night side ions probably originate from the solar wind.

SURFACE POTENTIAL AND PLASMA SHEET

Freeman, J. W. and Ibrahim, M. E.

REFERENCES

1. Research supported by NASA grant NAS9-5911
2. Freeman, J. W., M. A. Fenner, and H. K. Hills, Electric Potential of the Moon in the Solar Wind, J. Geophys. Res., 78, 4560, 1973.
3. Walbridge, Edward, Lunar Photoelectron Layer, J. Geophys. Res., 78, 3668, 1973.
4. Reasoner, D. L. and W. L. Burke, Characteristics of the Lunar Photoelectron Layer in the Geomagnetic Tail, J. Geophys. Res., 77, 6671, 1972.
5. Vondrak, Richard and John W. Freeman, The Lunar Ionosphere, This volume, 1974.
6. Lindeman, R. A., J. W. Freeman and R. Vondrak, Ions from the Lunar Ionosphere, Proc. Fourth Lunar Sci. Conf., Geochim. Cosmochim. Acta., Supplement 4, 3, 2889, 1973.
7. Criswell, David R., Lunar Dust Motion, Proc. Third. Lunar Sci. Conf., Geochim. Cosmochim Acta., Supplement 3, 3, 2671, 1972.
8. Schneider, Henry and John W. Freeman, Energetic Nighttime Lunar Ions, This volume, 1974. see also Freeman, J. W. Jr., Energetic Ion Bursts on the Nightside of the Moon, J. Geophys. Res., 77, 239, 1972.

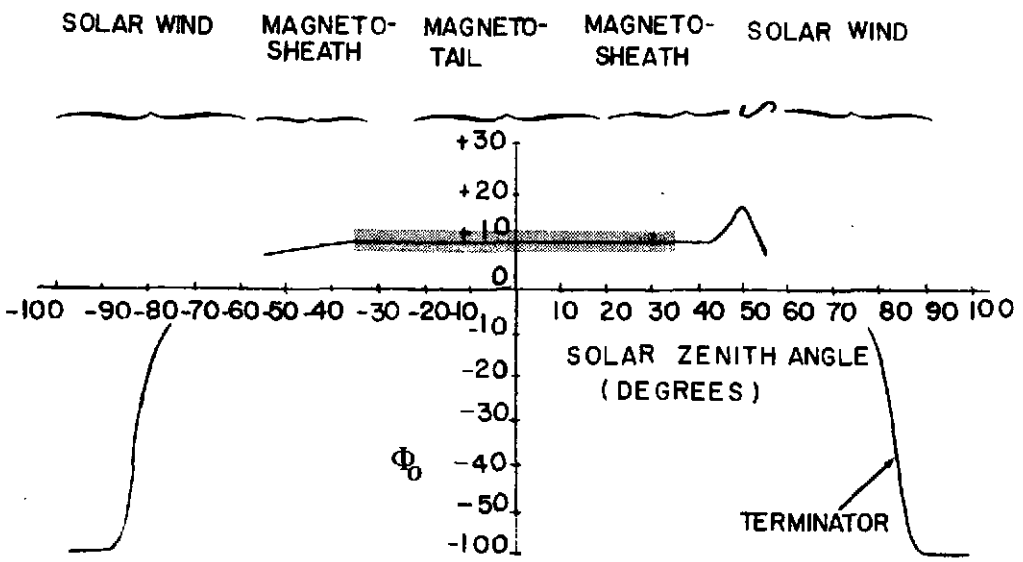

Φ_0 = LUNAR SURFACE POTENTIAL (VOLTS)

▒ = RANGE OF ERROR

(Figure 1)

ENERGETIC LUNAR NIGHTTIME ION EVENTS, Henry E. Schneider, John W. Freeman, Jr., Dept. of Space Physics and Astronomy, Rice Univ., Houston, Texas 77001

Freeman (1) has discussed a case wherein energetic ions were observed at the lunar surface during lunar night. This phenomena is observed regularly by the ALSEP/SIDE. This paper reports the preliminary findings of a detailed study begun on this subject.

The Rice University Suprathermal Ion Detector Experiment (SIDE) was deployed on the moon on Apollo missions 12, 14, and 15. Data is discussed in this paper only from the 14 and 15 instruments. The Apollo 12 instrument has been omitted because that data has not yet been incorporated in this study.

Both the 14 and 15 instruments give evidence of energetic ions during lunar night. These ions are observed all through the lunar night, but they occur most often 1 to 6 days before local sunrise (1 day = 12.2° of lunar rotation). A secondary activity peak is observed about 4 days after local sunset. Ions are observed on nearly every lunation. (Figure 1)

The ion events are most often less than 4 hours in duration and usually less than one hour. There are instances, however, when one event may last up to 20 hours. This type of event appears to be a superposition of a number of shorter events.

The energy spectra of the events vary from monoenergetic at 250 eV/q to 500 eV/q to fairly broad. The energy represented may range from 250 ev to 1500 ev/q. There is some indication that the peak energy of the events increases from 250 eV/q at sunset to 750 eV/q at about 3 days before sunrise and then decreases back to 250 eV/q 1 day before the sunrise terminator crossing.

Preliminary analysis of Explorer 35 magnetometer data from the time period February 1971 to June 1971 shows that there is some correlation between the occurance of an ion event and the direction of the interplanetary magnetic field (3). The counting rate seen by the Apollo 14 SIDE sharply increases where the field points in the ecliptic with longitude between 220° to 250° (solar equatorial units). This same longitude is correlated with counting rate all through the lunar night.

The characteristics of these events may be summarized as follows:

1. There is a preference for the events to occur 1 to 6 days prior to the sunrise terminator crossing in both the 14 and 15 instruments.
2. The events appear to show a lunar local time

dependence rather than a dependence on position in lunar orbit.

3. There is a preference for the longitude of the interplanetary magnetic field to lie in the range 220° - 250° when these ions are seen.
4. The ion energies are generally less than solar wind energies and the fluxes several orders of magnitude below that of the solar wind.

Item 2 above suggests that these ions are of solar wind origin. They are probably not the terrestrial bow shock protons seen often by SIDE at higher energies (2). We believe these ions to be solar wind ions deflected in some manner to the night side of the moon (4).

REFERENCES

1. Freeman, J. W., Jr., Energetic Ion Bursts on the Nightside of the Moon, J. Geophys. Res., 77, 239, 1972.
2. Benson, J. L., Observation of Bow Shock Protons at the Lunar Orbit, M.S. Thesis, Rice University, 1974.
3. We acknowledge the generous help from D. S. Colburn who supplied the Ames magnetometer data.
4. This research was supported by NASA contract NAS9-5911.

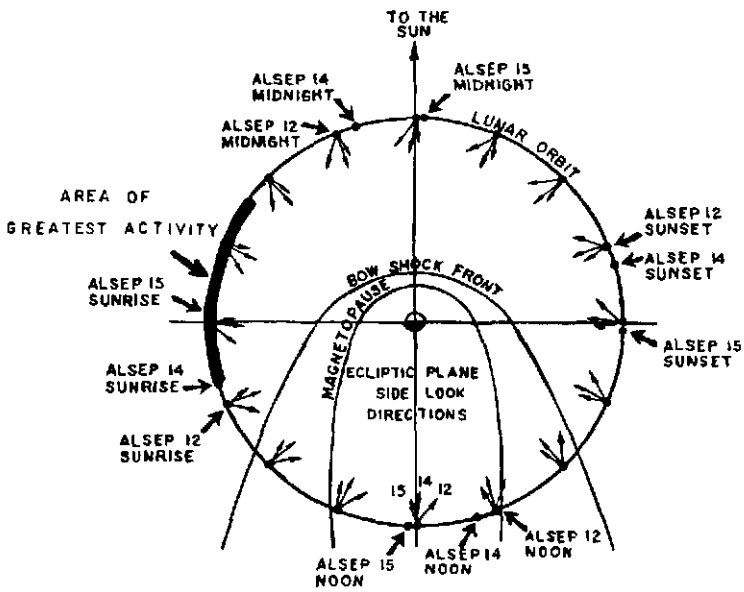

Figure 1

BOW SHOCK PROTONS IN THE LUNAR ENVIRONMENT, J. Benson, H. K. Hills, J. W. Freeman, Dept. of Space Physics and Astronomy, Rice University, Houston, Texas 77001, R. R. Vondrak, Radio Physics Laboratory, Stanford Research Institute, Menlo Park, Cal.

Protons from the earth's bow shock are observed by the Suprathermal Ion Detector Experiment (SIDE) in two regions of the lunar orbit. The dawn region begins at the dawn side bow shock crossing and ends ~5 days later and the dusk region begins at ~2 days prior to entering the dusk side magnetosheath and ends at the inbound bow shock crossing. Dusk and dawn refer to a terrestrial coordinate system. The dominant contribution to the ion spectra observed by the SIDE in these regions is from particles with energies between ~750 eV and 3500 eV. 3500 eV is the upper limit of the energy range of the detector, however particles with energies of greater than 3500 eV are known to exist in these regions (1).

Figure 1 shows typical time development of the SIDE count spectra for the two regions of the orbit in which the bow shock protons are observed. Note that the dusk side spectra show the onset of the flow coming at ~1.5 days before the magnetosheath and that the spectra get progressively softer as the moon approaches the bow shock. The dawn side spectra show a gradual hardening as the moon moves away from the bow shock and a cessation of the flow ~5 days after shock crossing. These examples of the ion spectra are "typical" and can vary considerably when interplanetary magnetic field and solar wind conditions change.

Figure 2 shows a single spectrum (20 minute average) for each of the two regions shown in Figure 1. These spectra were determined from data taken at ~1 day from the bow shock on either side of the magnetosphere. The differences in the dusk and dawn spectra shown here are typical. The dusk spectrum is harder than the dawn spectrum for the same distance from the bow shock. The fluxes shown on these graphs were determined by integrating over the portions of the spectrum that contained counts above background.

The asymmetry of the ion spectra observed in the dusk and dawn regions can be explained by considering the configuration of the interplanetary $\vec{B}$ field on the two sides of the magneto-

BOW SHOCK PROTONS

Benson, J. et al.

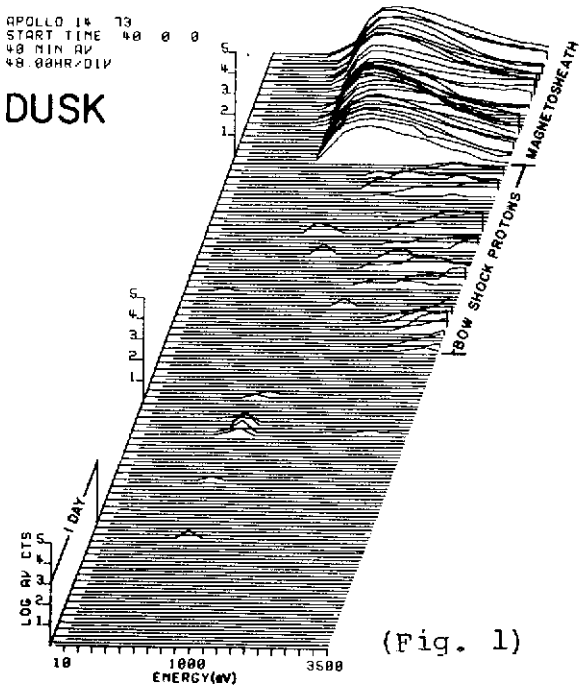

(Fig. 1)

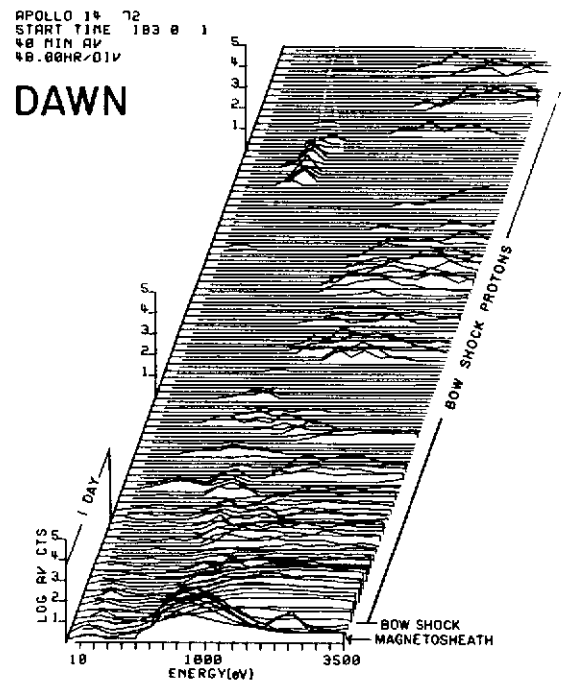

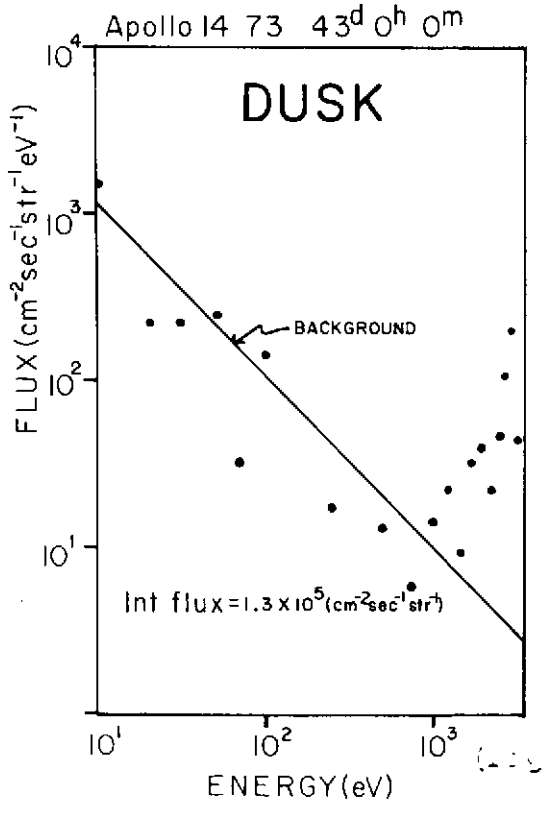

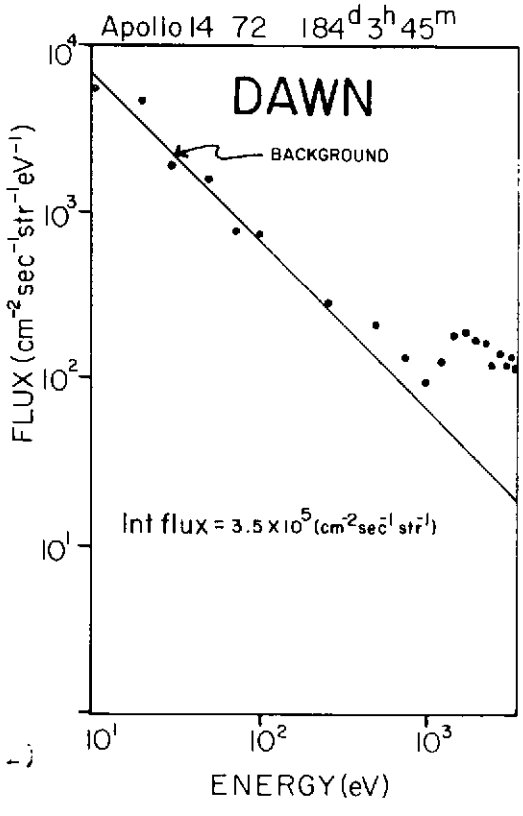

sphere. When $\vec{B}$ is at its average position, i.e. the garden hose angle, the field lines will contact the dawn side bow shock at a more normal angle of incidence than will the field lines on the dusk side. If it is assumed that the bow shock protons are released to the solar wind along interplanetary field lines, as originally suggested by Asbridge (2), then the ones released on the dusk side will be swept downwind much faster than those on the dawn side. A counterstreaming particle of a given energy can make it further in the sunward direction on the dawn side than on the dusk side which accounts for the fact that the flows are seen much further past the bow shock on the dawn side. The disappearance of lower energy particles from the spectra upstream is enhanced by the near parallel field line configuration on the dusk side. Hence the dusk spectra are harder than the dawn spectra at the same distance from the shock.

The observability of these bow shock protons at the lunar orbit was shown to be dependent on the latitude and longitude of the interplanetary $\vec{B}$ field by examining simultaneous data from SIDE and the Explorer 35 Ames magnetometer (3). Bow shock protons are most often observed when the solar ecliptic latitude of the field is near zero and when the solar ecliptic longitude of the field is such that the guiding center trajectory of the particle intercepts the moon.

REFERENCES

1. Lin, R. P., Meng, C. I., Anderson, K. A., 30 to 100 keV Protons Upstream from the Earth's Bow Shock, Journal of Geophysical Research, 79, 4, 489, 1974.

2. Asbridge, J. R., Bame, S. J., Strong, I. B., Outward Flow of Protons from the Earth's Bow Shock, Journal of Geophysical Research, 73, 5777, 1968.

3. Benson, J., Observation of Bow Shock Protons at the Lunar Orbit, M. S. Thesis, Rice Univ., Houston, Tx., 77001, 1974.

ACKNOWLEDGEMENTS

The authors would like to thank D. S. Colburn of the NASA Ames Research Center for providing the magnetic field data. This research was supported by NASA contract NAS9-5911.

FIRST OBSERVATION OF LOW ENERGY PROTONS IN THE GEOMAGNETIC TAIL AT LUNAR DISTANCES, D. A. Hardy and J. W. Freeman, Department of Space Physics and Astronomy, Rice University, Houston, Texas 77001.

The three Rice Suprathermal Ion Detector Experiments (SIDE) stationed on the lunar surface have detected a new region of plasma flow in the antisunward direction along the ordered field lines of the geomagnetic tail. This flow, similar to the "boundary layer" (Hones et al. 1972, Akasofu et al., 1973) and "plasma mantle" (Rosenbauer et al., 1974), observations made at smaller geocentric distances, has been found to possess the following characteristics:

1. The region of flow is encountered within the geomagnetic tail but exterior to the plasma sheet. The configuration and magnitude of the magnetic field during the event is indicative of the lobes of the geomagnetic tail with no consistent deviation in the field characteristics corresponding with the observation of the phenomenon.

2. The positive particles in the flowing plasma are primarily protons. This was ascertained by the observation of the proton peak in the positive ion mass analyzer of the Apollo 15 SIDE. Other constituents of the plasma have yet to be statistically verified.

3. The events occur over a wide spatial extent with continual observations of the particles over distances as great as ~17 R_e in the Y_{sm} direction and ~12 R_e in the Z_{sm} direction. The majority of the events are observed within a twelve R_e region bordering the magnetopause at the dawn and dusk sides of the magnetosphere.

4. The region in which the events are seen, appears to be of variable extent since the number of hours of observation of the particle flow within a tail passage varies drastically from lunation to lunation. Of the fifteen lunations studied the hours of observation varied between tail passages from approximately 2 hours to 43 hours.

5. The particles display a narrow differential flux spectrum peaked normally between 50 and 250 eV. The spectrum is generally stable over the duration of the event. Some cases of spectral variation in these events are seen to occur during transitions into or out of the plasma sheet or magnetosheath. A broadening of the spectrum and a shifting of the peak towards

higher energy are observed.

6. The flow possesses an integral flux only slightly below that of the magnetosheath. The following plasma parameters have been ascertained; integral flux between $.1 \times 10^7$ and 9×10^7 ions/cm^2-sec-ster, bulk velocity between 120 and 250 km/sec, temperatures in the ranges $.6 \times 10^5$ °K to 5×10^5 °K and number densities of the order .1 to 5/cm^3.

7. There appears to be a correlation between the extent of the tail passage over which the events are observed and the Kp averaged over these times. A higher average Kp is reflected in a higher incidence of encounters with the events.

8. The events are normally seen simultaneously by all three instruments. Preliminary analysis shows that the flow has an angular distribution extending over between 50 and 100 degrees.

It is proposed that the flow consists of particles which have entered through magnetic merging in the cusp of the magnetosphere. The particles are then convected towards the neutral plane by ExB drift. These could then be accelerated by a neutral line to provide the particles of the plasma sheet.

These particles constitute a heretofore undiscovered component of the lunar plasma environment.

REFERENCES

1. Hones, E. W., Jr., J. R. Asbridge, S. J. Bame, M. D. Montgomery, S. Singer, S.-I. Akasofu, Measurements of magnetotail plasma flow made with Vela 4B, J. Geophys. Res., 77, 28, 5503, 1972.

2. Akasofu, S.-I., E. W. Hones, Jr., S. J. Bame, J. R. Asbridge and A. T. Y. Lui, Magnetotail and boundary layer plasma at a geocentric distances of 18 R_e; Vela 5 and 6 observations, J. Geophys. Res., 78, 31, 7257, 1973.

3. Rosenbauer, H., H. Grunwaldt, M. D. Montgomery, G. Paschmen, and N. Sckopke, HEOS 2 plasma observations in the distant polar magnetosphere; The Plasma Mantle, subm. J. Geophys. Res., 1974.

A LUNAR SIGNATURE IN THE GEOMAGNETIC Ap INDEX.

K. Knott, ESTEC, Domeinweg, Noordwijk aan Zee, The Netherlands.

A great number of studies have been carried out in the past to decide whether or not a relationship exists between geomagnetic disturbances observed at the surface of the earth and the age of the moon. An excellent summary on what might be expected and what has been established can be found in a paper by Schneider (1967). The general conclusion of this summary is that the statistical volume is still too small to bring the noise level down low enough for a lunar signature to become detectable in the geomagnetic activity.

In the present study an attempt has been made to establish a relationship between the magnetic Ap-index (Rostocker, 1972) and the transition of the moon through the magnetosphere. Daily Ap-values from 1932 until 1972 compiled by Lenhart (1968) were used for this purpose. These data cover about 4 solar cycles - cycles 17, 18, 19 and 20, - of various degree of solar activity.

The interval from 1932 up to 1972 has been subdivided into lunar months with the day of full moon in the middle of these months. Ap-indexes of corresponding days in various lunar months have been added, the superposition resulting in an epochal histogramme. It is expected that solar influences - although predominant in intensity and often repeated with a periodicity close to that of the lunar phases - should level out in such diagrammes on a large enough statistical basis.

Epochal histogramms have been produced for different ranges of lunar ecliptic latitudes. A peak which is well above the statistical variations of the histogrammes appears for all cases near full moon, that is at the time when the moon encounters the tail of the earth's magnetosphere. For low ecliptic latitudes ($< 1^{\circ}$) the peak occurs at or shortly before the day of full moon. For higher latitudes the peak occurs one or two days after full moon.

It appears that the lunar signature in the various histogrammes is most pronounced for low lunar ecliptic latitudes. The rare occurrence of full moon at low latitudes, however, masks this effect in the histogrammes because statics get poor if the number of events is narrowed down. A peak near full moon is most pronounced in a histogramme covering lunar ecliptic latitudes less than 2.5° as this seems to be the best compromise between poor statistics and low ecliptic latitude.

Although a prominent peak near full moon exists in the histogramme covering the last four decades, the peak is less evident when the data are split up in individual histogrammes for the last four solar cycles. In particular, cycles of moderate solar activity (cycles 17 and 20) show

A LUNAR SIGNATURE

Knott, K.

less pronounced peaks than cycles of stronger solar activity (cycles 18 and 19). One very striking feature which has been detected is the apparent lack of a lunar signature in a histogram, which covers positive ecliptic lunar latitudes only, and a very pronounced peak in the histogram for negative latitudes.

The interpretation of the lunar influence on magnetospheric processes is given in two parts. The first one covers the appearance of a peak at or before full moon for events of small lunar ecliptic latitudes. It is argued that this peak is the result of the moons encounter with the plasma sheet.

The second process which impresses a lunar signature on geomagnetic data must be sought for a few days after full moon, that is during the period when the moon transverses the down magnetopause. An assymetry in terms of disturbance between the dawn and dusk magnetopause has been noted by Howe and Siscoe (1972) on the basis of Explorer 35 plasma measurements. It appears that in general the dawn side of the magnetopause somehow interacts more strongly with the solar wind than the dusk side. It seems, however, difficult to decide whether enhanced reconnection or whether diffusive or viscous interaction is taking place. The results of the present study indicate that the moon influences any such process.

References

Howe, H.C. and G.L.Siscoe (1972)
Magnetopause Motions at Lunar Distance Determined from the Explorer XXXV Plasma Experiment,Journ. Geophys. Res. 77, 6061.

Lenhart, K.G. (1968)
Geomagnetic and Solar Data for Use with Digital Computers, Transact. Am. Geophys. Union, 49, 463.

Rostocker, G. (1972)
Geomagnetic Indices, Rev. of Geophys. and Space Physics, 10, 935.

Schneider, O. (1967)
The Interaction of the Moon with the Earth Magnetosphere. Space Sc. Rev. 6, 655.

GASEOUS TRANSPORT ON THE MOON.* S. Jovanovic and G. W. Reed, Jr., Chemistry Division, Argonne National Laboratory, Argonne, Illinois 60439.

We have presented data supporting the transport of Hg (Jovanovic & Reed, 1973) and Br (Jovanovic & Reed, 1974) at the lunar surface in which the mobilizing agent is solar heating. We have also noted the general mobility of halogens on the basis of their hot water leachability and concluded that this mobile fraction is present as surface deposits in soils or soluble mineral phases in rocks.

These data may be reexamined in conjunction with results on heavy metals which occur terrestrially as volcanic sublimates. The metals to be discussed are Pb, Bi, Tl and Zn and their labile fractions in lunar soils are the amounts leached in 10 minutes with pH 5-6 HNO_3.

We have already discussed the transport, deposition and assimilation of ^{204}Pb with the agglutinate component in lunar soil (Allen et al., 1974). When the labile metal/labile halogen ratios in lunar soils are compared with the metal/halogen ratios found in terrestrial fumarolic gases, the lunar ratio is generally higher, in the case of metal/chloride by about 50 and in the case of metal/bromide by 5-10. The Bi/chloride ratio is an exception; the systems have essentially the same ratio. Possible explanation of these patterns are (a) low halogen contents on the moon, (b) the temperature at which the fumarolic gases were sampled (Mizutani, 1966, 1970) - the higher the temperature the higher the expected concentration of the metal, (c) the absence of these metals in the primary magmas and (d) the effect of H_2O, which may reverse the reaction leading to formation of the volatile metal halides. Other factors and combinations of the above may be decisive.

If the metals are volcanic, they may be considered to be juvenile. If little fractionation among the incompatible or dispersed elements since accumulation is assumed, then their concentrations and relative amounts may be compared with cosmic abundance (C.A.) data. The halogens exhibit the highest depletions although their ratios are close to C.A. ratios. The labile metal fractions are enhanced abundance-wise as may be expected if they are accumulating on surfaces; the residual metal is higher still by an order of magnitude in some cases. The labile metal ratios are also closer to C.A. ratios. Transport of metals and halogens to the surface, subsequent loss of some of each from the lunar surface by non-thermal acceleration and/or immobilization by incorporation into agglutinate phases produced by impact processes may account for the relationships observed.

*Work performed under the auspices of the USAEC and NASA.

GASEOUS TRANSPORT ON THE MOON

Jovanovic, S. and Reed, Jr., G. W.

References: Jovanovic, S., and Reed, G. W., Jr. (1973), Geochim. Cosmochim. Acta, Vol. 2, Supple 4, 1164; Jovanovic, S., and Reed, G. W., Jr. (1974), Abst. for Meteoritical Soc. Mtg., Los Angeles; Allen, R. O., et al. (1974), Geochim. Cosmochim. Acta, Vol. 2, Supple 5, in press; Mizutani, Y. (1966), Bull. Chem. Soc. Japan 39, 511; Mizutani, Y. (1970), Geochemical Jour. 4, 87.

SUNSET INTENSIFICATION OF LUNAR SURFACE ELECTRIC FIELDS; D. R. Criswell, The Lunar Science Institute, 3303 Nasa Road 1, Houston, Texas 77058.

Photoelectron ejection produces electric fields (ξ(v/cm)) and electric surface charge densities ($\sigma(\beta/cm^2) \simeq 5 \cdot 10^{9} \cdot \xi$) on fully sunlit surfaces of $\xi_o \simeq 1$ to 10 v/cm (1) & $\sigma_o \simeq 5 \cdot 10^{+9}$ to $^{+10}$ β/cm^2 and on partially illuminated surfaces in the terminator regions of $\xi_o \simeq 10^3$ v/cm & $\sigma_o \simeq 5 \cdot 10^{12}$ β/cm^2 (2,3). During the final stages ($\Delta t \simeq 4 \cdot 10^3$ seconds) of sunset the surplus charge (+Q) on isolated sunlit areas, resulting from photoelectron escape or accretion onto adjacent dark regions, is approximately conserved if external sources of discharging electrons are minimal. Contraction of the sunlit areas (A(cm^2)) will greatly increase $\sigma \sim +Q/A$ and therefore intensify $\xi \sim \sigma$.

Figure 1a depicts a partially illuminated surface during sunset. The highly conductive photoelectron cloud (total charge $-Q_1'$) over the sunlit area (A_1) creates an equipotential surface with surplus $+\sigma_1 = +Q_1/A$ on the surface. The dark area (a_1) is negatively charged (total charge $\sim -Q_1''$) by accretionary electrons from the photoelectron cloud which became spatially fixed due to the extreme electrical resistivity of the lunar materials. Ignoring leakage currents the inequality $+Q_1 \geq |-Q_1''|$ applies. In figure 1b the shadow has moved upward to encompass an area (ΔA)

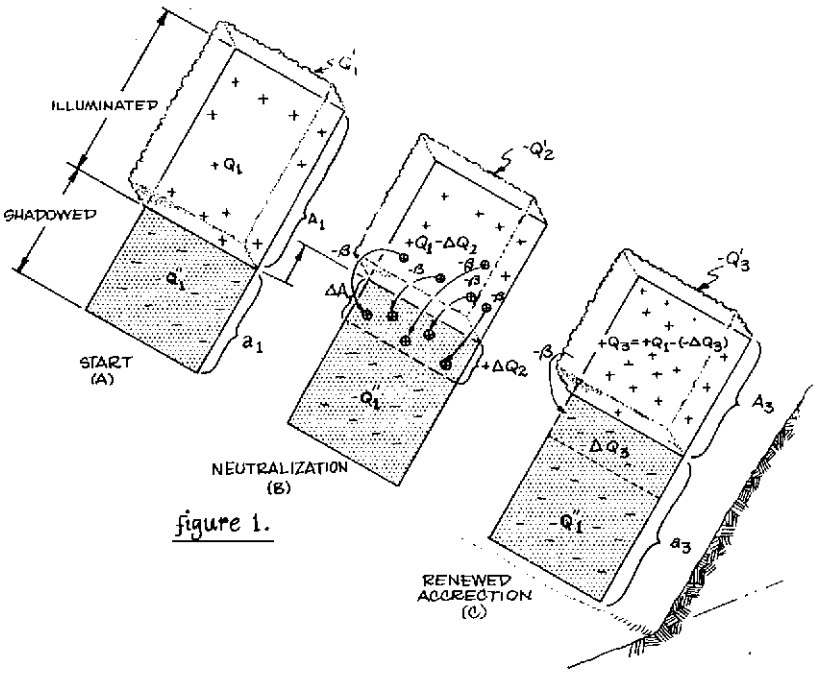

figure 1.

SUNSET INTENSIFICATION OF LUNAR SURFACE ELECTRIC FIELDS

Criswell, D. R.

of surplus positive charge $+\Delta Q_2 \simeq +\sigma_1 \cdot \Delta A$ and leaving $+Q_2 = +Q_1 - \sigma_1 \cdot \Delta A$ in the illuminated area. However, positively charged ΔA attracts photoelectrons and is neutralized by them. Each neutralizing photoelectron creates an equal surplus positive charge in the sunlit area. Thus, $+Q_2 = +Q_1$. Photoelectron accretion (figure 1c) on to ΔA will continue until the area is sufficiently negatively charged $(-\Delta Q_3)$ to repel all subsequent photoelectrons and $+Q_3 = Q_1 - (-\Delta Q_3)$ results. Because $A_3 < A_1$, $Q_3 \geq Q_1$, and $\xi \sim Q/A$ we have $\xi_3 > \xi_1$. What limits this process and prevents ξ from increasing indefinitely as A approaches zero?

Photoelectron emission from the adjacent dark areas would decrease +Q and -Q. The interplanetary ultraviolet background (4), primarily Lyman alpha, is $3 \cdot 10^8$ photons/cm^2-sec at the lunar surface. A photoelectron yield (5) of $5 \cdot 10^{-3}$ at 126.1 nm implies $\bar{f} \simeq 1.5 \cdot 10^5$ β/cm^2-sec. Let subscript "o" denote values at the start of the contraction phase. If $A_o > a_o$ then $\xi(v/cm) \simeq (\xi_o)(A_o/A)(\sigma_o - \frac{1}{2} \bar{f} \cdot \Delta t)$. Supercharging and field intensification will occur for $\sigma_o > \frac{1}{2} \bar{f} \cdot \Delta t \simeq 3 \cdot 10^8$ β/cm^2 or $\xi_o > \frac{1}{3}$ v/cm which is very likely to occur. Photoelectrons will also be evoked by light scattered from the directly illuminated regions to the eastern slopes of the local western surface and thence to the subadjacent dark areas. This flux should be no greater than $2 \cdot 10^2$ β/cm-sec $\cdot$ A/a at $4 \cdot 10^3$ seconds before sunset and will decrease as A decreases (2,5). Conduction currents (f_c) across the upward moving light/dark boundary will be also decrease +Q. An electrical conductivity (6) of the soil $\eta(250°K) \leq 10^{-17}$ mhos/cm implies $f_c \leq 60$ β/cm^2-sec $\cdot$ ξ and a characteristic decay time $\tau_c = \sigma/f_c \simeq 5 \cdot 10^{+9 \text{ to } +12} \cdot \xi/60 \cdot \xi \simeq 10^{+8 \text{ to } +11}$ sec $>> \Delta t \simeq 4 \cdot 10^3$ seconds. Solar wind electrons and protons are blocked from direct access to the sunset terminator (7). If $\xi_o \geq 1$ v/cm then these electron sources will not suppress the ξ intensification.

Levitation and transport of electrically charged grains of radius a(μ) discharges at the rate $f_d(\beta/cm^2\text{-sec}) \simeq 4.7\ a^{5/2} \cdot N(\text{grains/cm}^2)/\Delta t_d$ where N $\sim$ column density of grains, $\Delta t_d \sim$ grain dwell time in the column. For horizon-glows (2,8) $\Delta t_d \simeq 1$ sec, $N \simeq 10^{+2}$, $S \simeq 1$, $a \simeq 5\mu$ and $f_c \simeq 3 \cdot 10^4$ β/cm^2-sec which is a negligible discharge rate. Other inferred dust motions (Lunokhod sky background (9) and high altitude lunar dust (10) appear to produce even smaller discharge currents.

Contraction of positively charged sunlit areas during lunar sunset should produce intense but localized multipole electrostatic fields with $\xi > 10^4$ easily achievable. ξ(max) is not

SUNSET INTENSIFICATION OF LUNAR SURFACE ELECTRIC FIELDS

Criswell, D. R.

identified and may depend on the mechanical and electrical properties of lunar materials.

References

(1) Reasoner, D. L. and Burke, W. J. (1972) Characteristics of the lunar photoelectron layer in the geomagnetic tail, J. Geophys. Res. 77, p. 6671-6687.

(2) Criswell, David R. (1972) Lunar dust motion, Proc. Third Lunar Science Conf., Suppl. 3, Geochim. et Cosmochim. Acta, vol. 3, pp. 2671-2680, MIT Press.

(3) Criswell, D. R. (1973) Horizon-glow and the motion of lunar dust, in "The Proc. Symp. on Photon and Particle Interactions with Surfaces in Space", ed. R. Grard, D. Reidel Publ.

(4) Fastie, W. G., Feldman, P. D., Henry, R. C., Moos, H. W., Barth, C. A., Thomas, G. E., Lillie, C. F. and Donahue, T. M. (1973) 23. Ultraviolet Spectrometer Experiment, Apollo 17 Preliminary Science Report, NASA SP-330.

(5) Feuerbacher, B., Anderegg, M., Fitton, B., Laude, L. D., Willis, R. F. and Grard, R. J. L. (1972) Photoemission from lunar surface fines and the lunar photoelectron sheath, Proc. Third Lunar Science Conf., Suppl. 3, Geochim. et Cosmochim. Acta, vol. 3, pp. 2639-2653, MIT Press.

(6) Olhoeft, G. R., Frisillo, A. L., and Strangway, D. W. (1972) Frequency and temperature dependence of the electrical properties of a soil sample from Apollo-15, The Apollo-15 Lunar Samples, ed. J. W. Chamberlain and C. Watkins, Lunar Science Inst., p. 477-481.

(7) Snyder, C. W., Clay, D. R., and Neugebauer, M. (1970) 5. The Solar-Wind Spectrometer Experiment, Apollo 12 Preliminary Science Report, NASA SP-235.

(8) Rennilson, J. J. and Criswell, D. R. (1974) Surveyor observations of lunar horizon-glow, The Moon, vol. 10, p. 121-142.

(9) Severny, A. B., Terez, E. I. and Zvereva, A. M. (1973) Preliminary results obtained with an astrophotometer installed on Lunokhod-II, COSPAR-Konstanz-25 May-5 June.

(10) McCoy, J. E. and Criswell, D. R. (1974) Evidence for a high altitude distribution of lunar dust, Proc. Fifth Lunar Science Conf., Suppl. 5, Geochim. et Cosmochim. Acta, vol. 3, pp. 2991-3005, Pergamon.

LUNAR PHOTOELECTRON LAYER DYNAMICS; Edward Walbridge, Department of Systems Engineering, University of Illinois at Chicago Circle, Box 4348, Chicago, Illinois 60680.

Possible waves and oscillations in the lunar photoelectron layer (PEL) are investigated. The lunar PEL is a sea of hot (~ 15,000°k) photoelectrons extending to a height of about 2 meters above the lunar surface. It is of interest to determine whether a disturbance of the PEL at some point on the moon's sunlit surface will cause a series of ripples to spread through the layer. The steady state PEL is reviewed as a basis for discussing PEL motions. Magnetic fields are neglected, so that there are four possible wave modes to consider. The propagation through the PEL of the two electromagnetic modes is discussed, as is the interaction of an incident electromagnetic wave with the PEL. It is concluded that, for such an incident wave, the intensity of the partial reflection will be too small for detection. Positive-ion waves, the third mode, are dismissed and plasma waves are considered at length. It is concluded that vertical plasma oscillations will be strongly Landau damped since the PEL is too shallow to permit vertical wavelengths that are long compared to the Debye length. Horizontally propagating plasma waves are also strongly damped but by a different mechanism, viz. electrons storing the wave's kinetic energy are continually reabsorbed at the lunar surface. Hence there are no propagating waves in the PEL other than electromagnetic.

However there is a type of oscillation which appears to be new, is not fully understood, and which may not be strongly damped. With these oscillations, termed flight-time oscillations, the height of the PEL fluctuates as does the electric field, the electric field being always directed vertically upward. The physical basis for these oscillations is what might be called a flight-time resonance. The real part, ω_f, of the frequency of flight-time oscillations is found to be slightly greater than the plasma frequency. These oscillations are analagous to the height oscillations of the vertical jet of water in a city park water fountain. If flight-time oscillations are not much damped then it would be simplest to interpret them as plasma oscillations continually driven by the upwelling photoelectron stream. A possible laboratory investigation of these oscillations is discussed. For the surfaces of the moon and the planet mercury ω_f is found to be respectively $\sim 4 \times 10^6$ and $\sim 10^7$ radians/sec. The PEL's of those surfaces may be in a state of continual vertical "quivering" due to flight-time oscillations, or may be quiescent.

MANIFESTATIONS OF NON-METEORITIC REDISTRIBUTION OF LUNAR DUST; D. R. Criswell, The Lunar Science Institute, 3303 NASA Road 1, Houston, Texas 77058.

Surveyor observations of horizon-glow (1,2), Lunokhod-II detection of a post-sunset brightness of the lunar sky (3), astronaut observations of streamers associated with sunrise and sunsets as seen from lunar orbit (4), and preliminary results from the Apollo-17 "Lunar Ejecta and Meteoroid" Detector (O. Berg, private communication) strongly indicate a continuing circulation of the smallest size fraction of lunar fines about the surface. Micrometeorite bombardment cannot disturb sufficient volumes of material nor supply sufficient energy to secondary ejecta to explain these phenomena. Electrostatic transport and possibly other presently unidentified mechanisms must be operative. In any case, there should be evidence of the preferential disturbance and transport of the smallest size fraction of the soils. The lunar sample literature will be reviewed in this context with particular emphasis on radiation track production, concentrations of solar gases, and volatile distributions as a function of grain size. The influence of surface iron in photoelectron production and electrostatic transport will be noted and related to optical observations of surface albedo variations.

(1) Criswell D. R. (1972) Lunar dust motion, Proc. Third Lunar Science Conf., Geochim. et Cosmochim Acta, Suppl. 3, Vol. 3, pp. 2671-2680, MIT Press.
(2) Rennilson J. J. and Criswell D. R. (1974) Surveyor Observations of lunar horizon-glow, The Moon, vol. 10, pp. 121-142.
(3) Severny A. B., Terez E. I. and Zvereva A. M. (1973) Preliminary results obtained with an astrophotometer installed on Lunokhod-II, COSPAR-Konstanz-25 May-5 June.
(4) McCoy J. E. and Criswell D. R. (1974) Evidence for a high altitude distribution of lunar dust, Proc. Fifth Lunar Science Conf., Geochim. et Cosmochim. Acta, Suppl. 5, Vol. 3, pp. 2991-3005, Pergamon.

ADDITIONAL ASTRONAUT OBSERVATIONS OF POSSIBLE LIGHT SCATTERING BY LUNAR DUST ATMOSPHERE, by J. E. McCoy and D. R. Criswell.

It would appear that the Apollo crews in lunar orbit have observed several instances of solar light scattering by a transient lunar dust "atmosphere" over the terminator regions (1). The crew of Apollo 17, in particular, recorded sketches of the appearance of solar corona zodiacal light as it appeared to them above the lunar horizon while approaching orbital sunrise. These sketches included distinct streamer features which displayed time variations on the scale of seconds to minutes, incompatable with features of the solar corona. Evaluation of various possible sources of such light distribution lead to the conclusion that they were produced by light scattering from a population of small particulates above the lunar terminator, extending back to encompass the shadow boundary. The angular extent of the streamer indicated that the light scattering particles extended from the lunar surface to the altitude of the spacecraft. Although apparently observed by some of the other Apollo crews as well, the Apollo 17 observations were the only ones documented sufficiently to provide a basis for reasonable interpretation.

Additional documentation of the occurrence and variability of such streamers is available from the air-to-ground voice transcriptions (2) and onboard tapes of crew comments (3). Two periods of orbital sunset were observed with specific comment on the streamers which seems relevant to the question of size and variability.

The first is on orbit 61, H. H. Schmitt (LMP) makes the following comments: "In lieu of the solar corona photography I watched---Gene and I both watched it set and there are two bands which I can still see now---a zodiacal light, I guess, going out symmetrically on either side of the plane in the ecliptic and they make an angle between themselves of about, let's say, 70° to 80°. I can still---knowing they are there---I can still pick up the bands, streamers, I guess would be a better word. And last night when I watched one set there was a strong linear streamer going out---of maybe three or four or five diameters---I will have to get my directions straight. Well, I'll figure out which side of the ecliptic it was. That was not nearly so strong when I looked this time---now partly---that may be dark adaptation, I don't know, but I will try to keep track of that one. But those two streamers today are about an equal strength and they are still visible as zodiacal light."

The next day he makes the following remarks on orbit 72: "Just had a good view of the sunset and the corona and there are two strong bright streamers just right at sunset, one parallel to the plane of the ecliptic and the other--oh, maybe 10° to the south of the plane. And they form two of the major longer duller streamers that are streaming out of the sun now. There are some

other linear streamers that are still visible, but those are the major ones. Once you get out to the position of Mars, they all have about the same intensity---which is very low---the pattern is distinctly different from the one I believe I mentioned to you yesterday. ---It was right at sunset, at any rate. Still have a very strong glow visible at the sunset point. And that glow---the general glow visible to me now---and, of course, I am not very well light adapted---dark adapted---but extends about to a position---oh, let's see,---about the same distance from the sun as the apparent distance of Venus---between Venus and Mars right now. Well, let me---let me start over on that. The apparent distance from Venus to Mars is about the same distance as from Mars to the limit of the strong solar glow."

These observations indicate the angular extent of the streamers from the sun to exceed that of Mars at this time (33°). This extent is now applicable to features visible for some time after sunset. The complete change in location and configuration of the major streamers present from day to day, while not completely impossible for coronal features as in the case of the sunrise streamers sketched by Cernan and Evans (1), seems more compatable with the idea of determination by some projection of features of the changing lunar terminator as it moves at the rate of 12° per day.

References:

(1) McCoy, J. E. and Criswell, D. R., (1974), Evidence for a high altitude distribution of lunar dust, *Proc. Fifth Lunar Science Conf., Geochimica et Cosmochimica Acta, Suppl. 5, vol. 3, pp. 2991-3005*, Pergamon.

(2) *Apollo 17 Technical Air-to-Ground Voice Transcription, v. 1*, MSC-07629, December 1972.

(3) *Apollo 17 C. M. Onboard Voice Transcription Document*, MSC-07633, 1973.

ON THE FORMATION OF A MAGNETIC BOUNDARY LAYER AT THE LUNAR LIMB, Héctor Pérez de Tejada, Instituto de Geofísica, UNAM, México 20, D.F.

The behavior of the solar wind at the lunar limb has been previously examined by means of a simplified magnetogasdynamic analog consisting of a collision-dominated plasma flow streaming over a non-conducting semi-infinite flat solid surface in the presence of a magnetic field aligned to the flow direction. For cases in which the freestream temperature is higher than the surface temperature, the analysis of the problem indicates that as a consequence of viscothermal interactions between the streaming flow and the surface, the magnetic field intensity in the vicinity of the surface may exhibit values above the freestream level. This result suggests the presence at the lunar limb of a low-intensity magnetic field perturbation with magnitudes smaller than those of the selenographic-correlated magnetic increases detected both in the lunar wake and at the lunar terminator. The quantitative estimates and functional dependences of the predicted magnetic perturbations are found to be compatible with some experimental observations of the magnetic penumbral increases of the moon's wake.

The reality of the proposed magnetogasdynamic configuration relies on the assumption that the solar wind flow reacts collectively across distances comparable to the typical proton gyroradius and presumes the operation of adequate coupling processes between the solar wind particles and particles of lunar origin. Within the framework provided by these assumptions, substantial understanding of the behavior of the density, velocity, and magnetic field of the solar wind at the lunar limb can be obtained by applying conventional formulations of viscothermal boundary layer theories. A very useful result available from such theories is the approximate conservation of the total (thermal plus magnetic) pressure for cases in which the flow streams over a semi-infinite flat surface and exhibits very large values of the magnetic Reynolds number. This condition can be conveniently given as:

$$\hat{P} + \epsilon \hat{B}_x^2 = 1 + \epsilon \qquad (1)$$

MAGNETIC BOUNDARY LAYER

Pérez de Tejada, Héctor

where $\hat{P}$ denotes the normalized thermal pressure of the flow, $\hat{B}_x$ the normalized magnetic field intensity along the direction of motion of the incident flow (x direction), and ϵ the ratio of the magnetic to the thermal pressure in the undisturbed flow. The implications of this expression in relation to the continuum -fluid interpretation of the solar wind flow at the lunar limb indicate that for cases in which the imposed magnetic field is aligned to the flow direction the resulting magnetic field perturbation at the surface can be determined by combining equation (1) with the equation of state of an ideal gas and the relation:

$$\hat{B}_x = \hat{\rho}\,\hat{V}_x \qquad (2)$$

which is a solution of the induction equation of a perfectly conducting magnetic field-aligned magnetogasdynamic flow ($\hat{\rho}$ and $\hat{V}_x$ denote the normalized density and parallel component of the velocity vector).

For orientations of the magnetic field other than along the direction of motion, the simple coupling between the velocity, density and magnetic fields given by relation (2) is no longer valid, and thus the arguments pointed out for the behavior of the magnetic field at the surface do not apply. For these cases, it is in general necessary to refer directly to the solution of the complete set of differential equations that describes the problem. Nevertheless, we can still assess some general characteristics of the resulting magnetic geometry within the interaction region if additional restrictions are imposed on the problem. For example, under the assumption that the velocity of the flow is left essentially unaltered by the viscous mechanism (as appears to be the case for the solar wind-lunar limb interaction process), the velocity profile remains uniform (to first approximation) across the imposed temperature boundary layer. Under these conditions, the velocity field is modified only by the parallel stratification of streamlines that results from the induced non-uniform density distribution across the thermal boundary layer.

MAGNETIC BOUNDARY LAYER

Pérez de Tejada, H.

The effects that the stratification of streamlines produces on the configuration of a magnetic field frozen to the fluid particles can now be inferred from a simple geometrical inspection. When the magnetic field vector is parallel to the velocity vector, considerations of conservation of mass and magnetic flux indicate that an analagous stratification of magnetic field lines must also take place (this situation is conveniently expressed by relation 2). Thus, as indicated before, the magnetic field intensity will not be uniform across the temperature boundary layer, but should reproduce the variations exhibited by the density profile, which is in turn determined from a self-consistent solution satisfying equation 1. For the particular case in which the freestream temperature is higher than the surface temperature, the density of the flow and hence the magnetic field intensity near the surface will be enhanced with respect to their freestream values. The corresponding magnetic geometry may be characterized by a situation in which the density of magnetic field lines is higher in the vicinity of the surface than in the freestream flow.

When the imposed magnetic field is perpendicular to the flow direction, any transverse displacement of streamlines within the temperature boundary layer does not alter the distribution of magnetic field lines; that is, as the fluid particles are forced to move toward or away from the surface in response to the corresponding pressure distribution across the temperature boundary layer, the density of magnetic field lines remains unaltered and the magnetic field intensity keeps its freestream value. In these conditions no appreciable perturbation of the magnetic field intensity comparable to that of the aligned case can be predicted from the pure thermal interaction between the flow and the surface. When the magnetic field vector is oriented at a certain angle with respect to the velocity vector of the undisturbed flow, the transverse displacement of streamlines will result in a parallel rearrangement of magnetic lines of force which will give rise to a magnetic field perturbation less accentuated than that expected for the magnetic field-aligned case.

PRESENT AND PAST SOLAR WIND AND SECONDARY ION BOMBARDMENT OF THE MOON. Geiss J., Physikalisches Institut, University of Bern, Sidlerstrasse 5, 3012 Bern, Switzerland.

The solar wind (SW) ion flux reaches the lunar surface without much perturbation (1). The average proton flux is about $2.7 \times 10^8 cm^{-2} sec^{-1}$, other elements appear to be present in roughly solar abundance proportions (2, 3, 4). The influx on the moon depends not only on latitude, but also on longitude, because of the shielding effect of the tail of the earth's magnetosphere (minimum influx in the region of the zero meridian).

SW particles implanted in lunar surface material are recognized by the inverse relation of their abundance to grain size, by etching experiments or by a depth sensitive activation technique. In this way, noble gases, H, N and C of SW origin have been identified (cf. 5-12). Thus there exists imprinted in lunar material a historical record of the solar wind with great potential for studying the solar wind flux and composition in the past, and the history of the sun in general. For such studies it is important to ascertain what percentage of these "surface correlated" volatile elements is of SW origin. Competing sources could be (a) comets, (b) lunar fumaroles, (c) interstellar gas, and (d) ions which are produced in the lunar atmosphere by solar UV and SW charge exchange and are subsequently accelerated through the $\underline{V} \times \underline{B}$-force induced by the solar wind. The latter effect is particularly critical, because it produces a grain-surface implantation similar to the solar wind. The $\underline{V} \times \underline{B}$-mechanism has been studied in detail by Manka and Michel (13, 14). Quantitative predictions are seriously hampered by the difficulty to assess the effective trapping efficiencies in lunar surface material of low energy ions ($E < 1$ keV). Nevertheless, some estimates on the rates of implantation are made in this paper, based on trapping probabilities determined in the laboratory, and on densities, composition and distribution of the lunar atmosphere (15, 16). The estimates for implantation rates at lower latitudes ($\vartheta \lesssim 35^o$) presented here are based on the following model assumptions: Uniform temperature of 300 K; surface density n_o for $-50^o \leq \vartheta \leq 50^o$ is a function of the longitude alone; average solar wind conditions are V = 400 km/sec and $B_\perp = 4\gamma$; trochoidal trajectories for heavier singly charged ions are approximated by straight lines. The situation at the subsolar meridian (for a solar wind sector with negative B direction) is shown in figure 1, assuming an effective trapping efficiency $\eta = 1$ for $E > 600$ eV and $\eta = 0$ for $E < 600$ eV. It is evident from this figure tht the number of ions lost is much larger than the number which is trapped. Integration of the appropriate equations (cf. 13, 14) for Ar^{40} and comparison with the solar wind Ar^{36} influx leads to the $Ar^{40}_{tr}/Ar^{36}_{SW}$ ratios presented in table 1.

PRESENT AND PAST SOLAR WIND

Geiss, J.

Taking into account some loss due to elevated temperatures and saturation, we estimate that the Ar^{40}, observed in present lunar atmosphere, gives

$$\left(Ar^{40}_{tr}/Ar^{36}_{SW}\right)_{\text{effective today}} = 0.1 \text{ to } 0.2$$

Although single grains or spherules may occasionally contain such low $(Ar^{40}/Ar^{36})_{tr}$ ratios (21), much higher ratios, i.e. values between about 0.4 and 8, are observed in lunar fines and breccias (cf. 22-24, 6). The ratios vary with location on the lunar surface as well as with depth (cf. 23-27) but no clear systematic increase with depth has been found. Possible reasons for the high observed $(Ar^{40}/Ar^{36})_{tr}$ are that in the past (generally or at times)

(a) Ar^{40} production was higher

(b) Outgassing produced by lunar volcanism and impact was stronger

(c) $\underline{V}x\underline{B}$ in the solar wind was stronger

or

(d) there are additional mechanisms of Ar^{40} implantation.

(c) would explain the indicated correlation (4) between $(He^4/He^3)_{tr}$ and $(Ar^{40}/Ar^{36})_{tr}$ since a stronger solar wind flow would enhance the $\underline{V}x\underline{B}$-acceleration of Ar^{40} and at the same time could yield higher He^4/He^3 ratios in the solar wind.

A possibility for (d) would be the potassium destillation mechanism proposed by the Zurich group (28).

From table 1 and the observed $Ar^{36}/Ar^{40} \sim 0.1$ in the lunar atmosphere (15) it is evident that (at least today) recycling of SW argon amounts to only a few percent or less. For Neon recycling is similarly insignificant and also for Kr and Xe, unless the heavy noble gas ions have much higher trapping probabilities at low energies than the lighter noble gases.

The He^4/He^3 ratio in the lunar atmosphere ought to be much higher than in the solar wind because of (a) the faster escape of He^3 and (b) the addition of radiogenic He^4. However, the recycling factor for He is so small that the surface correlated He should be representative of the retained SW gas. Thus the observed difference of He^4/He^3 in fines and breccias (29, 30) appears to be a real solar wind effect (cf. 30).

PRESENT AND PAST SOLAR WIND

Geiss, J.

Recycling of SW carbon and nitrogen may be more significant, because trapping or sticking efficiency at low energies may be high. This could contribute to the observed excess of C and N over the noble gases, but by only a factor of less than 2.

The densities of nitrogen and carbon compounds in the present lunar atmosphere appear to be so low (16) that (at least at present) the contribution of $\underline{V}x\underline{B}$-implantation to the observed N and C concentrations in lunar fines is negligible. This observation supports the generally held conviction that the N in fines is essentially solar wind nitrogen, validating two conclusions advanced before:

- N^{15}/N^{14} in solar surface material is essentially not different from the N^{15}/N^{14} in the solar nebula. This places severe constraints on models of solar structure and evolution which involve slow mixing (cf. 31).
- The total amounts of solar wind gases (particularly N) in the regolith columns penetrated by deep drilling at the Apollo 15, 16 and 17 landing sites are so large that higher solar wind fluxes in the past (as compared to the present flux) must be suspected (4).

The author thanks O. Eugster and Ch. Filleux for discussions. This work was in part supported by the Swiss National Science Foundation (Grant NF 2.080.73).

REFERENCES: "Proc. LSC" refers to the Proceedings of the Lunar Science Conferences, Geochimica et Cosmochimica Acta Supplements.

(1) D.R. Clay, B.E. Goldstein, M. Neugebauer, and C.W. Snyder, Apollo 15 Prelim. Sci. Rep. NASA sp-289, p. 10-1, 1972.
(2) S.J. Bame, J.R. Asbridge, A.J. Hundhausen, and M.D. Montgomery, J. Geophys. Res. 75, 6360, 1970.
(3) J. Geiss, F. Bühler, H. Cerutti, P. Eberhardt, and Ch. Filleux, Apollo 16 Prelim. Sci. Rep. NASA SP-315, p 14-1, 1972.
(4) J. Geiss, Proc. 13th International Cosmic Ray Conference, University of Denver, Colorado, 5, 3375, 1973.
(5) P. Eberhardt, J. Geiss, H. Graf, N. Grögler, U. Krähenbühl, H. Schwaller, J. Schwarzmüller, and A. Stettler, Proc. LSC 1, 1037, 1970.
(6) H. Hintenberger and H.W. Weber, Proc. LSC 4, 2003, 1973.
(7) S. Epstein and H.P. Taylor, Proc. LSC 3, 1429, 1972.
(8) D.A. Leich, T.A. Tombrello, and D.S. Burnett, Lunar Science V, Lunar Science Institute, p. 444, 1974.

PRESENT AND PAST SOLAR WIND

Geiss, J.

(9) P.H. Cadogan, G. Eglinton, J.N. M. Firth, J.R. Maxwell, B.J. Mays and C.T. Pillinger, Proc. LSC 3, 2069, 1972.
(10) O. Müller, Proc. LSC 3, 2059, 1972.
(11) P.S. Goel and P.K. Kothary, Proc. LSC 3, 2041, 1972.
(12) J.W. Smith, I.R. Kaplan, and C. Petrowski, Proc. LSC 4, 1651, 1973.
(13) R.H. Manka and F.C. Michel, Science 169, 278, 1970.
(14) R.H. Manka, Lunar Atmosphere and Ionosphere, Ph.D. Thesis, Rice University Houston, 1972.
(15) R.R. Hodges, J.H. Hoffman, F.S. Johnson, and D.E. Evans, Proc. LSC 4, 2855, 1973.
(16) J.H. Hoffman, R.R. Hodges and F.S. Johnson, Proc. LSC 4, 2865, 1973.
(17) J. Meister, An Experiment for the Determination of the Composition in the Solar Wind: Trapping in Aluminium of Low Energy Noble Gas Ions, Ph. D. Thesis, University of Bern, 1969.
(18) W. Stettler, University of Bern, unpublished data.
(19) H. Cerutti, Determination of Argon in the Solar Wind from Analyses of the Apollo SWC Foils, Ph.D. Thesis, University of Bern, 1974.
(20) Ch. Filleux, Trapping in Al_2O_3 of Low Energy Noble Gas Ions, Master Thesis, University of Bern, 1971.
(21) T. Kirsten, F. Steinbrunn and J. Zähringer, Proc. LSC 2, 1651, 1971.
(22) D. Heymann and A. Yaniv, Proc. LSC 1, 1261, 1970.
(23) A. Yaniv and D. Heymann, Proc. LSC 3, 1967, 1972.
(24) H. Hintenberger, H.W. Weber, and L. Schultz, Lunar Science V, Lunar Science Institute, p. 334, 1974.
(25) D.D. Bogard and L.E. Nyquist, Proc. LSC 4, 1975, 1973.
(26) W. Hübner, D. Heymann, and T. Kirsten, Proc. LSC 4, 2021, 1973.
(27) O. Eugster, P. Eberhardt, J. Geiss, N. Grögler and M.D. Mendia, Geochim. Cosmochim. Acta 37, 1991, 1973.
(28) H. Baur, U. Frick, H. Funk, L. Schultz and P. Signer, Proc. LSC 3, 1947, 1972.
(29) H. Hintenberger, H.W. Weber, and N. Takaoka, Proc. LSC 2, 1607.
(30) P. Eberhardt, J. Geiss, H. Graf, N. Grögler, M.D. Mendia, M. Mörgeli, H. Schwaller, A. Stettler, U. Krähenbühl, and H.R. von Gunten, Proc. LSC 3, 1821, 1972.
(31) P. Bochsler and J. Geiss, Solar Physics 32, 3, 1973

PRESENT AND PAST SOLAR WIND

Geiss, J.

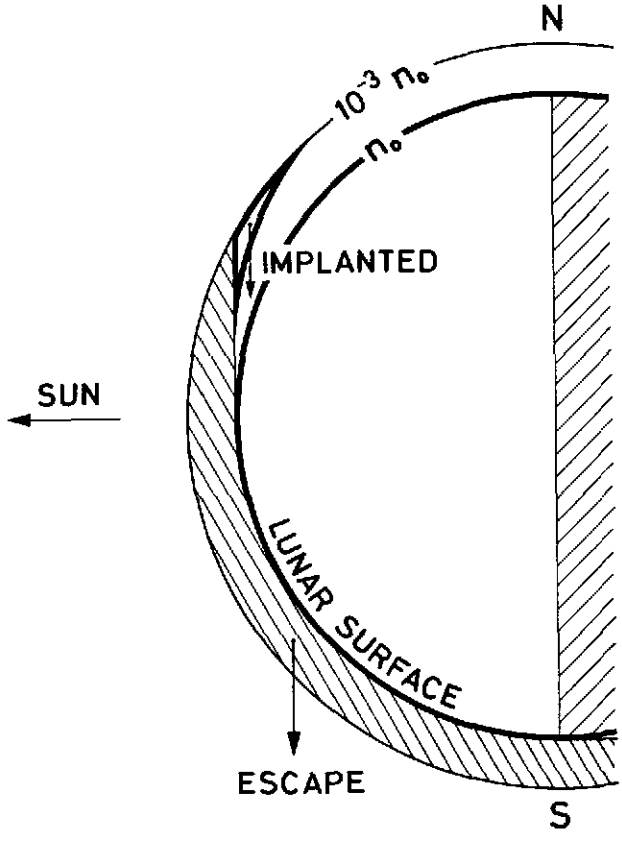

Figure 1:

Lunar argon atmosphere, assuming an uniform scale heigth corresponding to 300 K. Argon ions produced in the southern shaded area by solar UV or SW charge exchange escape from the moon. Ions created in the quasi-triangle of the northern hemisphere are implanted in lunar surfac material, if $\eta = 1$ for $E > 600$ eV and $\eta = 0$ for $E < 600$ eV is assumed as the effective trapping efficiency.

Trapping probability η	$Ar^{40}_{tr}/Ar^{36}_{SW}$
Aluminium, experimental (17, 18, 19)	0.4
$\eta = 1$ for $E > 600$ eV, $\eta = 0$ for $E < 600$ eV	0.2
Al_2O_3 (anodized Al) (20, 18)	0.2

Table 1:
Calculated $Ar^{40}_{tr}/Ar^{36}_{SW}$ ratios for an assumed and two measured trapping probabilities $\eta(E)$, valid for lower latitudes.

A COSMIC DUST EXPERIMENT ON THE MOON, EARLY RESULTS:

Otto E. Berg, Goddard Space Flight Center, Greenbelt, Maryland 20771

A 3-axis cosmic dust experiment placed on the lunar surface by the Apollo 17 crew is registering impact parameters of cosmic dust and lunar ejecta. 1,117 events were recorded in 8 months. The data show an interesting particle event rate increase associated with the passage of the terminators at the experiment site. During sunrise the particles move eastward with an event rate which is 100 times the normal rate. During sunset, the particle movement is westward with an event rate which is 15 times the normal rate. A preliminary, plausible explanation for the phenomenon is electrostatic levitation. Particle fluxes derived from each of the three sensor systems are within an order of magnitude in agreement with those obtained from two similar experiments in heliocentric orbits--Pioneers 8 and 9 (4×10^{-4} m^{-2} sec^{-1} $(2\ sr)^{-1}$) . The preliminary data indicate little evidence of lunar ejecta with speeds in excess of 0.8 km sec^{-1} (the speed threshold sensitivity for plasma detectors).

TOPIC INDEX

I. LARGE SCALE INTERACTIONS--OBSERVATIONS AND THEORIES

II. SURFACE MAGNETIC AND ELECTRIC FIELDS--ANCIENT AND PRESENT DAY

V. DISTURBANCE AND TRANSPORT OF LUNAR SURFACE MATERIALS

Page

VI. FUTURE LUNAR EXPLORATION

Page

VII. GEOCHEMISTRY/EXPERIMENTAL TECHNIQUES

Page

Sample Number Index*

*Pagination refers to first page of paper in which sample number is cited.

Author Index*

---

*Pagination refers to first page of paper in which author is cited.

SUBJECT INDEX*

*Pagination refers to first page of paper in which subject is cited.

THE MOON'S ANCIENT MAGNETIC FIELD AND LUNAR PREHISTORY, C.P. Sonett, Department of Planetary Sciences and Lunar and Planetary Laboratory, University of Arizona, Tucson, Arizona, 85721.

Recent evidence from the Apollo program shows that lunar material is magnetized. The general view that this magnetization is thermoremanent is supported by the most recent measurements which indicate paleofields in basalts at 3.95 aeons of 1.2 oersteds decreasing to 0.33 oe. at 3.6 aeons (1). Breccias are also magnetic, but the problem of their magnetization appears more complex than for the crystaline rocks. Direct measurement of magnetic fields on the floor of Procellarum, Hadley, Fra Mauro and Cayley (2) indicate values ranging from threshold (several gamma) upwards to more than 300 gamma. Satellite determinations of the surface field show values typically smaller than 1 gamma for the radial component, indicating that very localized sources cannot be the seat of these fields. However regional magnetization, perhaps associated with fractured basement rock of regular magnetization, is present (3). These measurements are concentrated near the lunar equator over a limited range of longitude. Explorer 35 shows inferentially, by measurement of limb shock waves, that magnetization is suppressed over maria (4). The somewhat limited statistics infer that the magnetization is restricted to the equatorial regions.

With the extended evidence of paleomagnetism in meteorites, including carbonaceous chondrites, the cosmogonic view that the protosolar nebula and the accretional period were associated with a strong overall solar system field is strengthened. This field may be a fragment of the original galactic field, a nascent solar field originating in a dynamo, or some combination of the two. Hide has proposed that impact magnetization could be the source of at least part of the lunar field, since no overall dipole moment has been detected (5), (6), (3). Srnka (private communication) recently carried out experiments at Culham showing the generation of 35 gauss fields with hypervelocity impacts. However the dwell time for such fields must be exceedingly short. If regional magnetization exists on the Moon, the source field for imprinting magnetization must last sufficiently long for the material to pass through a range of blocking temperatures. Since the time constant for cooling a sphere is 1 second for an object with radius of 1 cm, this rises to (0)700 years for 1 km. Thus, impact seems ruled out for regional magnetism, but could be important on the regolith and generally in modifying previously imprinted fields. That the lunar source field was the Earth's magnetosphere is unlikely. Using a reasonable tidal Q for Earth, the time of immersion in the magnetosphere is extremely short. Increasing the Earth's dipole moment by one order does not alleviate the problem, because in view of the thermal time constants this time is too short for regional magnetization to be acquired.

An obvious source of magnetization for the Moon would be an internal dynamo. But arguments incorporating mean density and moment of inertia show that the Moon could not possess an Fe core larger than about 350 km radius; for FeS this increases to about 500 km. Levy (7) has argued that

THE MOON'S ANCIENT MAGNETIC FIELD AND LUNAR PREHISTORY

Sonett, C. P.

this rules out a lunar dynamo even for a rotation speed equal to breakup, but Runcorn points out (private communication) that when scaled between Earth and Jupiter, Levy's analogy fails since both planets are apparently endowed with self-excited dynamos. If the Moon were endowed with planetary spin at its birth, it was likely spin damped by tidal forces in the past, probably via Earth capture. But Earth data seems to rule out capture subsequent to 3.2 aeons ago, which appears to be the date of the most recent magnetization. Since the highlands appear magnetized a dynamo source field should have operated from nearly the time of accumulation of the Moon. Although the requirement for early differentiation and dynamo action can be met, it is far more difficult to retain high lunar spin in the period after 3.2 aeons ago, unless some drastic revision takes place in the current outlook upon the Earth-Moon dynamical history(8). Because of the difficulty in providing for a late dynamo, maria magnetization seems to require that a two stage magnetization has taken place (9).

The presence of a primordial or early solar field is sufficient for imprinting magnetization in both meteorites and lunar material (10). A high solar spin with the field a mixture of dipolar and quadrupolar (the latter provides a steady component in the plane of the ecliptic) is needed. This also assumes that the geometry follows the present epoch spiral. Both a primordial field and early dynamo suggest the Urey-Runcorn model. The primordial moon's core acquires an isothermal remanence. This field is later recorded in the crust as the latter cools through its blocking temperature range. The core IRM eventually vanishes via long period heating. Whether isothermal remanence can be of sufficient strength to supply the source field for the late maria magnetization remains unresolved.

Controversy surrounds details of the collapse of the protosolar cloud, but the classical view is that even if the electrical conductivity had been low, a substantial magnetic field would have been captured from the galactic background and carried inwards (11). Whether this is important as a source field for the primeval Sun is not understood, but a strong field seems to be required to reduce angular momentum partitioned to the cloud from the galactic rotation. If the early field or spin were too large, collapse of the protosolar cloud would tend to be inhibited, but a residue of each is still vital for spinning up the Sun and for eventually braking its rotation.

Acknowledgment

This work was supported by NASA grants NSG 7020 and NGR 03-002-370.

References

(1) Stephenson A., Collinson D.W. and Runcorn S.K. (1974) in Proc. Fifth Lunar Sci. Conf., Pergammon Press, in press.

(2) Dyal P., Parkin C.W., Daily W.D. (1973) Surface magnetometer experiments: internal lunar properties, in Proc. Fourth Lunar Sci. Conf. Geochim. Cosmochim. Acta, 3, 2925.

THE MOON'S ANCIENT MAGNETIC FIELD AND LUNAR PREHISTORY

Sonett, C. P.

(3) Russell C.T., Coleman P.J. Jr., Lichtenstein B.R., Schubert G. and Sharp L.R. (1973) Subsatellite measurements of the lunar magnetic field, Proc. Fourth Lunar Sci. Conf. Suppl. 4, Geochim. Cosmochim. Acta, 3, 2833.
(4) Sonett C.P., Mihalov J.D. (1972) Lunar fossil magnetism and perturbations of the solar wind, J. Geophys. Res. 77, 588.
(5) Sonett C.P., Colburn D.S. and Currie R.G. (1967) The intrinsic magnetic field of the Moon, J. Geophys. Res. 72, 5503.
(6) Behannon K.W. (1968) Intrinsic magnetic properties of the lunar body, J. Geophys. Res. 73, 7257.
(7) Levy E.H. (1972) Magnetic dynamo in the Moon: a comparison with the Earth, Science 178, 52.
(8) Sonett C.P. and Runcorn S.K. (1973) Electromagnetic evidence concerning the lunar interior and its evolution, The Moon 8, 308.
(9) Runcorn S.K. and Urey H.C. (1973) A new theory of lunar magnetism, Science 180, 636.
(10) Sonett C.P. (1974) Evidence of a primordial solar wind, Proc. Third Solar Wind Conf., in press.
(11) Hoyle, F. (1960) On the origin of the solar nebula, Q.J.R.A.S. 1, 28.

THE MOON AS A HYDROMAGNETIC ANTENNA, J.K. Chao and C.P. Sonett, Lunar and Planetary Laboratory, University of Arizona, Tucson, Arizona 85721.

While bathed in the solar wind the Moon displays an intense electromagnetic induction excited by fluctuations of the interplanetary magnetic field. These fluctuations are both convected and propagated disturbances. A detailed distinction between these mechanisms is not required for lunar induction as both appear as time variations of the field in the frame co-moving with the Moon. However, a secondary distinction does arise since all such disturbances are characterized by wave normal surfaces which define the wave normal vector, $\underline{k}$.

The inductive signal arising from the flow of eddy currents in the lunar interior has been studied in the frequency range from less than 10^{-4} Hz to 4×10^{-2} Hz (Sonett et al., 1972), the latter being defined as the value of frequency for which quantization noise in Explorer 35 magnetometer signals rises to an unacceptable level. Explorer 35 data is used to obtain a normalized value of the field components on the lunar surface. Division of the lunar signal by that found at Explorer 35 defines an empirical transfer function, A. Values of A range from nearly unity at the low frequency limit to a peak value of over 3 with increasing frequency, finally decreasing with further frequency increase.

The formal similarity of lunar induction (equivalent to the transverse electric (TE) mode in electromagnetic theory) to Mie scattering has previously been pointed out by Sonett and Colburn (1974). The case of the Moon corresponds to a very lossy object electrically, and therefore its response differs strongly from an optically transparent one. The similarity to Mie scattering arises from consideration of the wave number spectrum of the interplanetary magnetic field which corresponds to wavelengths encompassing the scale size of the Moon. At low frequency the excitation corresponds to Rayleigh pseudoscattering while at intermediate and high frequency to Mie pseudoscattering.(The term pseudoscattering occurs since most, if not all the induced radiation is confined to the lunar interior by the dynamic pressure of the solar wind.)

Because of the relation to Mie scattering, an angular dependence of the lunar response (transfer function) is expected, together with a dependence upon the apparent phase velocity of the incident wave field in the solar wind. This has been experimentally detected in the response of the Lunar Surface Magnetometer (LSM) and is indicated in a preliminary way in earlier publications. In this paper we provide calculations upwards to approximately the Nyquist frequency of the LSM. Calculations have been made for both varying phase velocity, $\underline{v}_p$, and scattering angle, θ. The latter is defined in the conventional sense as the central angle, centered in the Moon between the direction of $\underline{k}$ and the position of the LSM on the lunar surface. The upper frequency limit is established by computational limits associated with the radial equation. A two layer model is used for the Moon consisting

THE MOON AS A HYDROMAGNETIC ANTENNA

Chao, J. K. and Sonett, C. P.

of a core of conductivity, $\sigma_c = 4 \times 10^{-4}$ Hz, surrounded by a non-conducting shell.

Strong dipolar response at low frequency (Rayleigh limit) is present. Near to and above the principal maximum, higher orders become important. At high frequency the transfer function can decrease to below unity because of the strong phase shift of the excited radiation compared to the forcing function(Figure 1). The behavior of the phase function depends strongly upon the signal frequency. Below the peak amplitude corresponding primarily to dipole radiation, the phase function is relatively stable with modest phase variations. The phase, passing through several complete cycles, rapidly changes at high frequency (Figure 2). The transfer function amplitude, A, is smallest for $\theta = 180^\circ$. As θ is diminished, the peak amplitude increases until for $\theta = 90^\circ$, $A \to \infty$, because the normal component of the forcing function vanishes.

There are well known difficulties in inverting the lunar response into a high resolution profile of the interior electrical conductivity. However, these difficulties become assets for the inverse problem of obtaining information on θ and $\underline{v}_p$, i.e. the sensitivity of θ and $\underline{v}_p$ to interior model variations is small. For this reason the Moon can serve as an ideal hydromagnetic antenna for probing the angular and spatial spectrum of the $\underline{k}$ vector field of the solar wind.

Acknowledgment

This work was supported under NASA Grants NSG-7020 and NGR 03-002-370.

References

(1) Sonett C.P., Smith B.F., Colburn, D.S., Schubert G. and Schwartz K., (1972) The induced magnetic field of the Moon: conductivity profiles and inferred temperature, in Proc. Third Lunar Sci. Conf. Geochim. Cosmochim Acta, Suppl. 3, p. 2309.

(2) Sonett C.P. and Colburn D.S.(1974) Mie scattering of the interplanetary magnetic field by the whole Moon, in Planets, Stars and Nebulae Studied with Photopolarimetry, ed. T. Gehrels, Univ. of Ariz. Press, p. 419.

THE MOON AS A HYDROMAGNETIC ANTENNA

Chao, J. K. and Sonett, C. P.

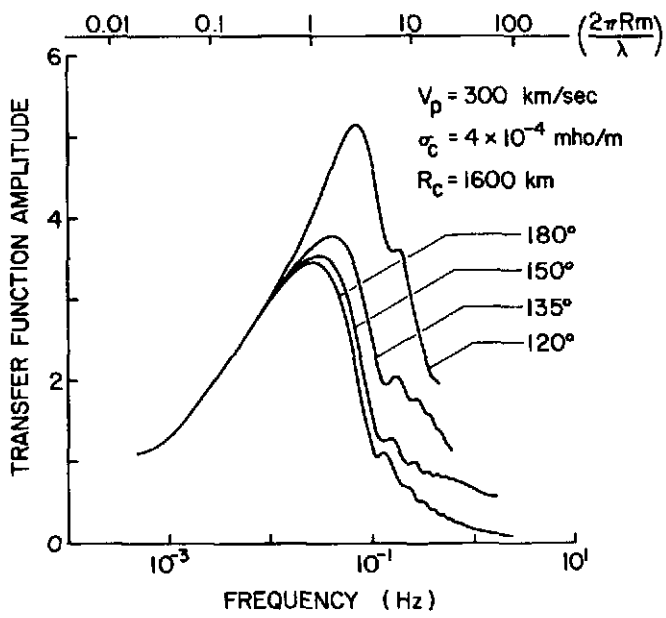

Fig. 1. Tangential transfer functions for a two layer Moon with core conductivity, σ_c=4x10^{-4} mho/m and a non-conducting shell corresponding to the "best" two layer model of Sonett et al.(1972). The phase velocity assumed for the calculation is v_p=300 km/sec. Below about 10^{-2} Hz only the magnetic dipole contributes significantly. This graph demonstrates the result of high frequency induction with the introduction of a multiplicity of higher order magnetic dipoles. θ is the scattering angle defined as the central angle with origin at the center of the Moon and angle measured between the position of the observer and the wave normal vector, $\underline{k}$, of the incoming radiation.

Fig. 2. Showing the transfer function amplitude and phase for scattering angle, θ = 150° and v_p = 300 km/sec.

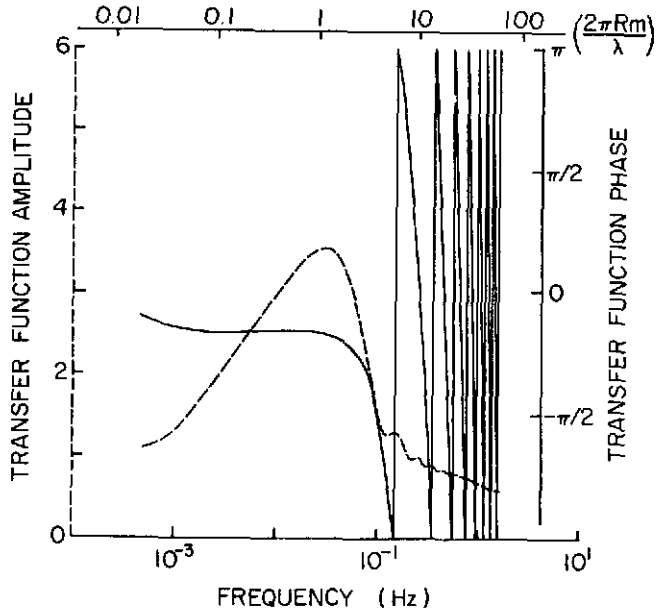

THE RECORD OF SOLAR AND GALACTIC RADIATIONS IN THE ANCIENT REGOLITH; Robert M. Walker, Washington Univ., Laboratory for Space Physics, St. Louis, Missouri 63130

Lunar surface rocks have been used to investigate the record of galactic protons and heavy particles for times up to 50 million years. Because of erosion the record of solar flare particles extends over the shorter time span of less than 10 million years. The bulk of the data indicates the time constancy of both times of radiations, although at least one anomaly exists. In principle, studies of lunar soil columns and portions of ancient regolith, as perserved in lunar and meteoritic breccias, can be used to decipher the history of these radiations back to the early stage of the solar system. The paper summarizes the current incomplete state of our knowledge based on present experimental data and also discusses projected new experimental approaches to the problem. An attempt is made to pose key questions whose answers are critical to understanding the early history of the sun and the moon.

PHOTOEMISSION ELECTRONOSPHERE AS A SOURCE OF MERCURY'S MAGNETIC FIELD; E. H. Walker, Aberdeen Proving Ground, Aberdeen, Md., 21005, and A. J. Fennelly, Physics and Astronomy Dept., Western Kentucky University, Bowling Green, Ky., 42101.

The characteristics of Mercury's magnetic field have been reported elsewhere (1). Main characteristics are the peak observed fields of 98 gammas at closest approach (altitude 704 km) and the derived magnetic moment that is located 0.47 R_M (radius of Mercury) from the center of the planet. The dipole is oriented within 20° of the ecliptic pole being slightly tilted. We show that the field strength observed and the offset position of the dipole are consistent with the idea of an induced magnetic field arising from the presence of a layer of photoelectrons and an electronosphere (2,3). Furthermore, the magnetic field is the residual field arising from peak solar winds (storm) interactions with the highly conductive photoemission electronosphere of Mercury which prevents rapid leakage or decay of the magnetic field. At times of strong solar wind (storm conditions and solar flares) the solar wind presses nearly to the planet's surface. As flare conditions subside, the electronosphere, together with its magnetic field, expands against the reduced pressure of the solar wind and the interplanetary magnetic field to give rise to the magnetopause observed by Mariner-10.

We also show that the reason for Mercury's exhibiting a fully developed electronosphere with a strong embedded magnetic field, while the moon - so apparently similar in many ways to Mercury (1) - does not, lies principally in the higher photon flux to the surface of Mercury thereby giving rise to a higher screening field on Mercury. This causes a change in the electric potential energy of the electronospheric field varying as the 4th power of the distance of the planet from the sun. As a result, the moon's field is not sufficiently strong (electric field pressure) to resist the solar wind, while Mercury's field can resist the solar wind pressure, presenting the conditions necessary for the field build-up in response to the flare activity.

General characteristics of the photoemission-induced electronosphere. The electric potential at the surface (3) of the moon results from the balance of the flux of solar wind ions and electrons to the surface with the photoelectrons emitted from the surface. Under ordinary conditions the potential is $\varphi = 4.4$ volts and the electric field $E_o \simeq 3.4$ volts/meter at the sub-solar point of the moon. The electric field at the surface is given by (3) $E_o = en_o/\varepsilon_o$, while $n_o = 2N_\nu\gamma/\varphi_o$ with $v_o = \sqrt{2U/n_e}$ or $\sqrt{3kT/m_e}$. For Mercury we would expect to obtain, from the similarity of the two, an increased photon flux N_ν about 20 volts for the potential and 16 volts/meter for the field. In order for the electronosphere to support its own magnetic field, the electric field which lies at the base of the interaction must be strong enough to resist the magnetic field pressure, the solar wind gas pressure, and the gravitational field of the planet. This may be formulated (4) as $p + B^2/8\pi + \int \rho_m\, g\, dr < \int \rho_e\, \varphi\, dr$. By standard manipulations (4) and the change of units we re-express this as $\rho_e v_t^2/2 + e^2/2\mu_o + \varepsilon_o(m_e/e)^2\, g^2/2 < \varepsilon_o E_o^2/2$. An equality sign indicates stable equilibrium. In what follows we may neglect gravitational terms in the equations and determine the satisfaction of the implied criteria for the moon and for Mercury. The magnetic field within the electronosphere may be obtained from any one of a number of equations (4): $B^2 = (\rho/j_t)dE_t/dt$ or $B^2 = -\eta\nabla p/d_D\eta$.

PHOTOEMISSION ELECTRONOSPHERE AS A SOURCE OF MERCURY'S MAGNETIC FIELD

Walker, E. H. et al.

For the moon at the sub-solar point $v_t = 400$ km/sec, $\rho_e = 8.35 \cdot 10^{-21}$ kg/m^3, $B = 6\gamma$, $E_o \approx 3.4$ V/m or less. We find that $\frac{1}{2} \epsilon_o E_o^2 = 5.12 \cdot 10^{-11}$ J/m^3 and $\frac{1}{2} \rho_e v_t^2 + B^2/2\mu_o = 6.82 \cdot 10^{-10}$. For the moon at latitude 70° these numbers become $v_t = 137$ km/sec, $E_o \approx 2.8$ volts/m and we find out that the righthand side of the equation is $4.0 \cdot 10^{-11}$ J/m^3 while the lefthand side is $9.24 \cdot 10^{-11}$. For Mercury at the sub-solar point these numbers are $v_t = 600$ km/sec, $\rho_e = 2.84 \cdot 10^{-20}$ kg/m^3, $d = 17\gamma$, and $E_o = 16$V/m. Right is $1.13 \cdot 10^{-9}$ J/m^3 & left is $5.23 \cdot 10^{-9}$. For each of these three cases we see that the righthand side is not greater than the lefthand side and so the electric field cannot be supported against the pressure of the solar wind. For Mercury at latitude 60° however these numbers are $v_t = 205$ km/sec, $E_o \approx 13$V/m and the righthand side reads $7.56 \cdot 10^{-10}$ J/n while the lefthandside reads $7.14 \cdot 10^{-10}$. Here the criterion is satisfied and we see that under normal conditions the solar wind is not strong enough to collapse the electronosphere of Mercury. Therefore, toward the edge of the illuminated face of Mercury a buildup of the magnetic field can beget a region that supports the interplanetary medium. Once a magnetic field arising from currents in the electronosphere forms the charging mechanism is drastically altered. For evidence of this see reference (5) where values of the lunar potential and the electric field in the tail of the earth's magnetosphere are $\varphi = 200$V, $E_o = 20$V/m. On Mercury these values would go to about $\varphi = 1000$V, $E_o = 100$V/m. Therefore, for Mercury - even at the sub-solar point with the magnetic field embedded in the electronosphere - we find using the equation $\frac{1}{2} \rho_e v_t^2 + B_i^2/2\mu_o \leq \frac{1}{2} \epsilon_o E_o^2$ (at surface) is satisfied since $5.23 \cdot 10^{-9}$ is less than or equal to $4.43 \cdot 10^{-8}$ J/m^3. This electric field corresponds to $B_i \approx 330\gamma$.

Characteristic time for loss of magnetic field. Spitzer (4) gives the equation for the time τ required for the dissipation of a magnetic field embedded in a plasma: $\tau \simeq 4\pi L^2/\eta \simeq 5 \cdot 10^{-13} T^{3/2} \cdot L^2$-sec where L is the characteristic length of the plasma in cm and T is the plasma temperature (Spitzer gives $2 \cdot 10^{-13}$ ~ this value is for an electron plasma). For 10ev electrons ($T = 10^5$ K) and the characteristic length $L = (2\pi R_N^2 \lambda)^{1/3}$ where λ is the electronospheric sheath thickness.

From Bettinger and Walker (6) and Walker (7) we find the shield sheath σ is $\sigma = \lambda/h = 1.17 \xi_s^{1/2}$ where h (Debye length) $= [\epsilon_o \, kT/e^2 \, n_o]^{1/2}$ and $\lambda = 1.17 \, h(\varphi_o/kT)^{1/2}(R_M/h)^{1/3}$. We find for $\varphi_o = 200$V, $E_o = 20$V/m that $\lambda = 573$ meters and $L = 2.77 \cdot 10^5$ meters so that $\tau = 1.215 \cdot 10^{10}$ sec = 387 years. We see therefore that the field will be retained. The expression for τ involves η - the resistivity. An improved value of τ would take into account the effect of resistivity that takes account of the currents (forming the magnetic field of the electronosphere) and their energy loss each time an electron is lost to the surface. This is not the total energy of the electron but only that energy in the direction as required to maintain the field current. Note also that the field would reflect the inducing conditions occurring under peak solar storm conditions. Note in the references that are given in reference (1) that there are similarities between this situation and the situation for planets with ionospheres. This applies therefore to fields induced in planets with ionospheres and may be applicable also to other cases particularly as to the predicted position of the magnetic dipole.

Position and orientation of field. The dipole must arise from currents

induced in the electronosphere which is located on the hemisphere facing the sun. This means that the dipole has been moved away from the center of the planet and towards the sun. With the values given above we find that the dipole is displaced almost to 0.5 R_M which is fairly close to the reported value of 0.47 R_M in reference (1). As to the orientation, ideally a current flowing in a hemispherical shell will have a pole at the center of the hemisphere to minimize the current density. However to maximize the resistance to the passage of the interplanetary field and to the solar wind the poles should fall on the edge of the hemisphere according to Lenz' Law. The competition of these two factors produces magnetic fields which are about of equal intensity with dipoles oriented in the ecliptic plane and with the ecliptic axis giving an orientation to the field which is tilted to about latitude 45°. This also is about equal to the tilt that was reported in reference (1).

Magnetopause. We can find from the strength of the field at the surface what the approximate height of the magnetopause should be. Using a dipole approximation with the value of B_o at the surface is equal to 330 gammas we find that the magnetic field pressure of the dipole field is approximately equal to the pressure exerted by the plasma in the solar wind at a distance that could range from 1150 km to about 11000 km. A median value calculated for the conditions approximately during encounter (see reference 1) is about 3400 meters or 3.4 km. Thus we see that the hypothesis of a photoemission electronosphere as a source of Mercury's magnetic field gives rise to all the observed features reported by the magnetometer experiments in Mariner-10 during encounter (1). It is known that Jupiter's magnetic field has a dipole which is offset about 0.1 R_J north of the equatorial plane and about 0.2 R_J toward longitude 170° and also that the field is tilted at an inclination of about 15°. We would like to speculate that perhaps some small part of Jupiter's magnetic field is due to a magnetic field of this type arising in its ionosphere while of course the bulk of the field is probably some type of a core field and is involved in the large amounts of radio emissions in the radiation belt of Jupiter (8).

References

1. Ness, N. F., Behannon, K. W., Lepping, R. P., Whang, Y. C., Schatten, K. H. (1974), Science, 185, 151; also see Science, 185, pp. 141-180.
2. Singer, S. F., and Walker, E. H. (1962), Icarus, 1, 112.
3. Walker, E. H. (1973), in Photon and Particle Interactions with Surfaces in Space, pp. 521-544, D. Reidel.
4. Spitzer, L., Jr. (1965), Physics of Fully Ionized Gases, Wiley-Interscience, New York.
5. Reasoner, D. L., Burke, W. J. (1973), in Photon and Particle Interactions with Surfaces in Space, p. 369, D. Reidel.
6. Bettinger, R. T. and Walker, E. H. (1965), Phys. Fluids, 8, 748.
7. Walker, E. H. (1973), in Photon and Particle Interactions with Surfaces in Space, pp. 73-89, D. Reidel.
8. Smith, E. J., Davis, L., Jr., Jones, D. P., Colburn, D. S., Coleman, T. J., Jr., Dyal, P., and Sonett, C. P. (1974), Science, 183, 305-306.